

# Local mechanical properties of tissue engineered heart valves

**Citation for published version (APA):**

Cox, M. A. J. (2009). *Local mechanical properties of tissue engineered heart valves*. [Phd Thesis 1 (Research TU/e / Graduation TU/e), Biomedical Engineering]. Technische Universiteit Eindhoven.  
<https://doi.org/10.6100/IR642606>

**DOI:**

[10.6100/IR642606](https://doi.org/10.6100/IR642606)

**Document status and date:**

Published: 01/01/2009

**Document Version:**

Publisher's PDF, also known as Version of Record (includes final page, issue and volume numbers)

**Please check the document version of this publication:**

- A submitted manuscript is the version of the article upon submission and before peer-review. There can be important differences between the submitted version and the official published version of record. People interested in the research are advised to contact the author for the final version of the publication, or visit the DOI to the publisher's website.
- The final author version and the galley proof are versions of the publication after peer review.
- The final published version features the final layout of the paper including the volume, issue and page numbers.

[Link to publication](#)

**General rights**

Copyright and moral rights for the publications made accessible in the public portal are retained by the authors and/or other copyright owners and it is a condition of accessing publications that users recognise and abide by the legal requirements associated with these rights.

- Users may download and print one copy of any publication from the public portal for the purpose of private study or research.
- You may not further distribute the material or use it for any profit-making activity or commercial gain
- You may freely distribute the URL identifying the publication in the public portal.

If the publication is distributed under the terms of Article 25fa of the Dutch Copyright Act, indicated by the "Taverne" license above, please follow below link for the End User Agreement:

[www.tue.nl/taverne](http://www.tue.nl/taverne)

**Take down policy**

If you believe that this document breaches copyright please contact us at:

[openaccess@tue.nl](mailto:openaccess@tue.nl)

providing details and we will investigate your claim.

# Local mechanical properties of tissue engineered heart valves

Martijn A.J. Cox



# Local mechanical properties of tissue engineered heart valves

PROEFSCHRIFT

ter verkrijging van de graad van doctor aan de  
Technische Universiteit Eindhoven, op gezag van de  
Rector Magnificus, prof.dr.ir. C.J. van Duijn, voor een  
commissie aangewezen door het College voor  
Promoties in het openbaar te verdedigen  
op dinsdag 2 juni 2009 om 16.00 uur

door

Martijn Antonius Johannes Cox

geboren te Budel-Dorplein

Dit proefschrift is goedgekeurd door de promotor:

prof.dr.ir. F.P.T. Baaijens

Copromotor:

dr. C.V.C. Bouten

This research is supported by the Dutch Technology Foundation STW, applied science division of NWO and the Technology Program of the Ministry of Economic Affairs.

Financial support by the Netherlands Heart Foundation for the publication of this thesis is gratefully acknowledged.

A catalogue record is available from the Eindhoven University of Technology Library

ISBN: 978-90-386-1781-7

Reproduction: Universiteitsdrukkerij Technische Universiteit Eindhoven

© Copyright 2009, Martijn A.J. Cox

All rights reserved. No part of this publication may be reproduced, stored in a retrieval system, or transmitted, in any form or by any means, electronic, mechanical, photocopying, recording or otherwise, without the prior written permission from the copyright owner.

---

## Summary

---

Annually 6000 children are born in Europe alone with a defected heart valve, thus needing a heart valve replacement. As clinically available replacement heart valves consist of non-living materials, they lack the ability to grow with the patient. Therefore several re-operations are necessary during the patient's lifetime to replace the valve with a larger one.

Tissue engineering offers a promising alternative for existing heart valve replacement strategies. Heart valve tissue engineering focuses on the production of a living heart valve, created with the patient's own cells. Therefore, the valve has the capacity to grow, repair and remodel with the growing demands of the patient. In short, the patient's cells are seeded *in vitro* on a biodegradable mold in the shape of a heart valve. After that, the thus obtained construct is placed in a bioreactor, where mechanical and biochemical conditioning protocols are used to stimulate tissue development. After several weeks in the bioreactor, the biodegradable mold is replaced by tissue produced by the patient's own cells. The tissue engineered heart valve is then ready for implantation back into the patient.

One of the most important challenges in heart valve tissue engineering is to create a valve that is strong enough to withstand the high pressures that occur *in vivo* in the human body. The mechanical strength of the native heart valve is largely determined by a highly organized network of collagen fibers. Researchers at the Eindhoven University of Technology have successfully used mathematical remodeling algorithms to predict the native collagen fiber architecture as a result of local stresses in the valve during the diastolic loading phase of the cardiac cycle, i.e. when the heart valve is closed. Based on these results a Diastolic Pulse Duplicator (DPD) has been created, which enables mimicking of diastolic pressures during *in vitro* heart valve tissue engineering in a bioreactor. With the DPD indeed strong tissue engineered heart valves have been created, which *in vitro* showed the capacity to withstand the high pressures relevant for *in vivo* survival. Although this is an important step, it remains unclear if, and to what extent, tissue engineered heart valves develop towards a native-like collagen fiber architecture.

The aim in the current thesis is to answer this question by measuring the local fiber architecture in native and tissue engineered heart valves. As currently existing mechanical characterization methods do not allow for a full characterization of the local fiber mechanics, a new method is

developed and validated. In this innovative approach spherical indentation is applied in combination with confocal imaging of the tissue deformation. Subsequently, a computational model is fitted to the experimental results using parameter estimation. As a result the local fiber architecture as well as the local tissue mechanics are obtained.

Application of this method to native and tissue engineered heart valves indicated that tissue engineered heart valves indeed develop towards the native valve fiber architecture, although organization and alignment are more pronounced in native valves. The most important difference between native and current tissue engineered valves is that tissue engineered valves appear to be an order of magnitude stiffer in the *in vivo* strain regime. Based on experimental observations presented in this thesis, this is hypothesized to be caused by a difference in the unloaded configuration of the individual collagen fibers.

Although the new mechanical characterization method is developed specifically for measuring the local mechanical properties of heart valves, it should be emphasized that the method can be used for mechanical characterization of planar soft biological tissues in general.

---

# Contents

---

<b>Summary</b>	<b>v</b>
<b>1 Introduction</b>	<b>1</b>
1.1 Anatomy and function of the aortic valve . . . . .	2
1.1.1 The heart . . . . .	2
1.1.2 The aortic valve . . . . .	2
1.1.3 Aortic valve replacement . . . . .	3
1.2 Tissue engineering . . . . .	4
1.3 Aortic valve mechanics . . . . .	6
1.3.1 Mechanical characterization . . . . .	6
1.3.2 Constitutive modeling . . . . .	7
1.4 Rationale and outline of this thesis . . . . .	8
1.4.1 Rationale . . . . .	8
1.4.2 Outline . . . . .	10
<b>2 Computational Feasibility</b>	<b>11</b>
2.1 Introduction . . . . .	12
2.2 Materials and methods . . . . .	13
2.2.1 Geometry and boundary conditions . . . . .	14
2.2.2 Constitutive model . . . . .	15
2.2.3 Finite element implementation . . . . .	17
2.2.4 Parameter estimation . . . . .	17
2.2.5 Simulated experiments . . . . .	19
2.3 Results . . . . .	20
2.3.1 Feasibility of spherical indentation . . . . .	20



2.3.2	Simulation A . . . . .	22
2.3.3	Simulation B . . . . .	24
2.4	Discussion . . . . .	26
<b>3</b>	<b>Experimental validation: small deformations and isotropy</b>	<b>31</b>
3.1	Introduction . . . . .	32
3.2	Materials and methods . . . . .	33
3.2.1	Experimental set-up . . . . .	33
3.2.2	JKR theory . . . . .	34
3.2.3	Finite element model . . . . .	35
3.3	Results . . . . .	36
3.4	Discussion . . . . .	39
<b>4</b>	<b>Experimental validation: large deformations and anisotropy</b>	<b>41</b>
4.1	Introduction . . . . .	42
4.2	Materials and methods . . . . .	43
4.2.1	Experiments . . . . .	43
4.2.2	Numerical model . . . . .	44
4.2.3	Parameter estimation . . . . .	46
4.3	Results . . . . .	47
4.3.1	PDMS rubbers . . . . .	47
4.3.2	TE constructs . . . . .	47
4.4	Discussion . . . . .	50
<b>5</b>	<b>Application: mechanical characterization of Bio-Artificial Muscle</b>	<b>55</b>
5.1	Introduction . . . . .	56
5.2	Materials and methods . . . . .	57
5.2.1	Bio-Artificial Muscle . . . . .	57
5.2.2	Indentation tests . . . . .	57
5.2.3	FE model . . . . .	57
5.2.4	Parameter estimation . . . . .	59
5.2.5	Compression test simulation . . . . .	59
5.3	Results . . . . .	59
5.3.1	Compression test simulation . . . . .	61
5.4	Discussion . . . . .	64
<b>6</b>	<b>Tissue engineered heart valves develop native-like structural properties <i>in vitro</i></b>	<b>67</b>

---

6.1	Introduction . . . . .	68
6.2	Materials and methods . . . . .	70
6.2.1	Tissue engineered heart valves . . . . .	70
6.2.2	Determination of local fiber distribution and fiber mechanics . . . . .	71
6.3	Results . . . . .	75
6.3.1	Indentation test and Digital Image Correlation . . . . .	75
6.3.2	Parameter estimation . . . . .	75
6.3.3	Estimated fiber distribution and fiber mechanics . . . . .	76
6.4	Discussion . . . . .	78
<b>7</b>	<b>Local structural mechanics of aortic, pulmonary and tissue-engineered heart valves</b>	<b>83</b>
7.1	Introduction . . . . .	84
7.2	Materials and methods . . . . .	86
7.2.1	Native and tissue engineered heart valves . . . . .	86
7.2.2	Local structural mechanics . . . . .	86
7.3	Results . . . . .	90
7.3.1	Indentation test and Digital Image Correlation . . . . .	90
7.3.2	Parameter estimation . . . . .	92
7.3.3	Structural fiber mechanics . . . . .	92
7.4	Discussion . . . . .	93
<b>8</b>	<b>General discussion</b>	<b>97</b>
8.1	Summary and conclusions . . . . .	98
8.2	Scope and limitations of the developed method . . . . .	99
8.3	Recommendations . . . . .	101
	<b>References</b>	<b>114</b>
	<b>Samenvatting</b>	<b>115</b>
	<b>Dankwoord</b>	<b>117</b>
	<b>Curriculum vitae</b>	<b>119</b>



---

## Introduction

---

*This thesis aims to elucidate and quantify the relationship between global mechanical properties and local structural tissue development in tissue engineered heart valves. To this end, a novel method is developed for the local and structural mechanical characterization of tissue engineered and native heart valves using spherical indentation combined with confocal imaging. With this method, local structural mechanics of tissue engineered heart valves, subjected to different mechanical conditioning protocols, are compared to local structural mechanics of native heart valves. Although heart valves are the main topic of this thesis, it should be emphasized that the developed method applies to the local mechanical characterization of planar soft biological tissues in general. The current chapter provides some background to the scientific problem with an introduction on heart valves and heart valve tissue engineering and mechanical characterization of biological tissues.*

## 1.1 Anatomy and function of the aortic valve

### 1.1.1 The heart

Day after day, our hearts pump over 7000 liters of blood through our body, beating about 3.7 billion cycles over a lifetime, while weighting a mere 500 grams. Clearly, nature's design of our heart is an impressive accomplishment from an engineering point of view. The heart contains two pumps: the left heart, which pumps oxygen-rich blood through our circulatory system, and the right heart, which pumps oxygen-deprived blood through our lungs. Both pumps contain two pulsatile compartments: the atrium and the ventricle. While the ventricles function as the main pumps, the atria allow efficient filling of the ventricles. To propel blood in the right direction and prevent back-flow, four one-way valves are built into the heart design: the tricuspid valve, the pulmonary valve, the mitral valve and the aortic valve. Especially interesting is the design of the aortic valve, which is situated between the left ventricle and the aorta (Fig. 1.1).

### 1.1.2 The aortic valve

The aortic valve is a largely passive structure, although some active cellular components are present. The valve consists of three semi-lunar leaflets of less than 1 mm in thickness. Still it is able to withstand the repetitive high pressures that occur *in vivo*. As illustrated in Fig. 1.2, loading of the aortic valve is highest during diastole, when the difference between aortic and left ventricular pressure approximates 13 kPa even in rest. To meet these performance requirements, the aortic valve leaflets have developed into highly specialized and organized structures. Like most biological tissues, the leaflet consists of cells surrounded by an extracellular matrix (ECM). The ECM mainly consists of collagen, elastin and glycosaminoglycans (GAGs). Collagen fibers have the main load-bearing function, while elastin helps the collagen fibers to function, e.g. by providing elastic recoil to the valve leaflets. The negatively charged GAGs attract water from the surroundings, thus forming a gel-like structure in which the fiber components are embedded. GAGs provide the heart valve tissue with compressive stiffness. Macroscopically, the aortic valve leaflet is a three-layered structure (Fig. 1.3a). The fibrosa layer, which can be found at the interface with the aorta, is composed predominantly of a highly organized network of collagen fibers (Fig. 1.3b, Thubrikar (1990)). This fiber network, with parallel collagen bundles running from the commissures towards a more branched network in the belly region, is considered the strongest and stiffest part of the aortic valve leaflet. The ventricularis layer, located at the ventricular side, mainly consists of a radially oriented network of elastin fibers (Scott and Vesely, 1995, 1996). The ventricularis main function is to keep the fibrosa under compression when the valve is opened. When the valve closes, initial stiffness is provided by the ventricularis, which is taken over by the fibrosa as soon as the collagen network becomes stretched. Finally, the middle - spongiosa - layer mainly consists of GAGs and loosely arranged collagen fibers. The spongiosa forms the connection between fibrosa and ventricularis through

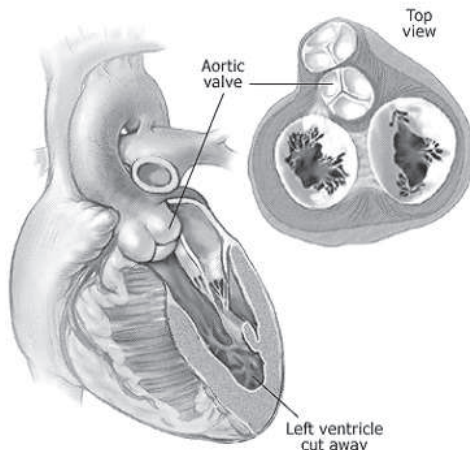


**Figure 1.1:** Schematic picture of the anatomy of the heart, with the left ventricle cut away, showing the aortic valve (left) and a top view of a heart cross section (right), showing the trileaflet shape of the aortic valve.

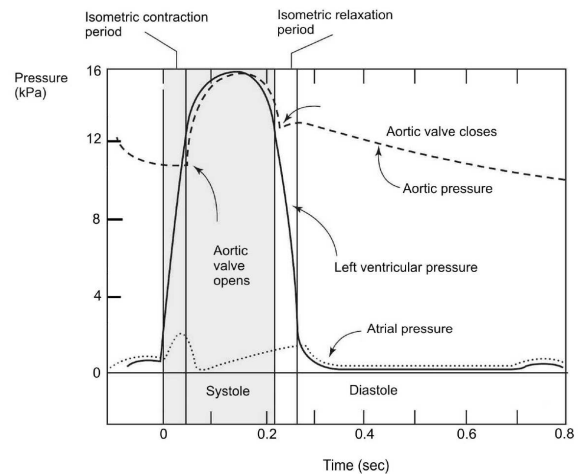


**Figure 1.2:** Blood pressures during the cardiac cycle. At end-systole, left ventricular pressure drops rapidly, thus causing the aortic valve to close at begin-diastole. During the diastolic phase, pressure differences over the aortic valve are maximal, approximating 13 kPa even during rest.

loosely arranged elastin and collagen fibers, and serves to absorb compressive forces and shear stresses (Schoen and Levy, 1999).

### 1.1.3 Aortic valve replacement

Despite its ingenious design, the aortic valve is more prone to insufficiency problems compared to the other heart valves. Besides due to congenital defects, heart valves can also be affected due to e.g., aging, inherited conditions, lifestyle, infection or rheumatic fever. In case of severe insufficiency, the heart valve is usually replaced with a valve prosthesis. In 2003, 290.000 heart valves were replaced worldwide, with an expected increase to 850.000 by the year 2050 (Yacoub and Takkenberg, 2005). Current valve prostheses are either mechanical or bioprosthetic valves. Mechanical valve prostheses have demonstrated life-long durability, but also require life-long anti-coagulation therapy, associated with impaired mobility and a substantial risk of spontaneous embolism and bleeding. For bioprosthetic valves anti-coagulation therapy is most often not necessary which is why these have become more popular in recent years. Bioprosthetic valves are valves obtained from animals or donor patients. An issue with bioprosthetic valves is the limited durability, often necessitating another valve replacement after 10 to 15 years. Therefore, mechanical prostheses are currently used to treat patients under 60 years, while for patients over 65 years, or with a life expectancy of less than 10 years, or at risk of life-threatening bleeding, tissue prostheses are chosen. A special case of a bioprosthetic valve is the pulmonary autograft. In the so-called Ross procedure, the patient's pulmonary valve is transferred to the aortic position, while a replacement valve is used at the pulmonary site (Ross,

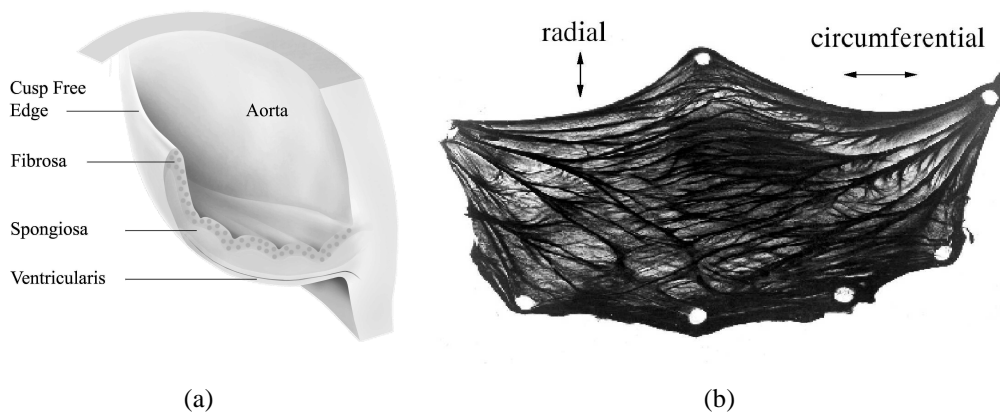


**Figure 1.3:** a) Schematic drawing of the typical three layered structure of the native aortic leaflet (adapted from Mol et al. (2004)) and b) Microscopy image of a native porcine aortic leaflet showing a highly organized collagen fiber network (adapted from Sauren (1981)).

1967). Apart from the Ross-valve, all current valve substitutes are unable to grow, repair and remodel in response to environmental changes. As a result, patients with a replacement valve suffer from an increased risk of co-indications and a reduced life expectancy due to suboptimal valve substitutes (Yacoub and Takkenberg, 2005). For children with congenital defects the situation is even worse. Currently, several re-operations are necessary to replace their valve prostheses with a larger one, as current prostheses can not adapt to the growing demands of the patient from childhood to adolescence. The exception is again the Ross procedure, although long term studies indicate that the pulmonary valve can not adapt sufficiently to the aortic environment either (Carr-White et al., 2001; Klieverik et al., 2007; Takkenberg et al., 2009).

## 1.2 Tissue engineering

Tissue engineering offers a promising strategy towards overcoming the shortfalls of current heart valve substitutes. The goal of tissue engineering is to create living heart valves, based on the patient's own cells, which do have the capacity to grow repair and remodel (Schoen and Levy, 1999; Rabkin and Schoen, 2002; Haverich, 2004; Mol and Hoerstrup, 2004; Vara et al., 2005). Several approaches have been used to tissue engineer heart valves, mainly differing with respect to the scaffold material, which could be either biologic, synthetic, or a decellularized valve from an animal or human donor. With their Synergraft<sup>TM</sup> decellularization technology, the US based company Cryolife has been responsible for both the largest success and failure of heart valve tissue engineering. Early clinical results with decellularized porcine valves, which were reseeded with the patient's own cells, were dismal (Simon et al., 2003). An unexpected severe immune response to the porcine tissue led to valve failure and clinical studies were aborted prematurely. However, using the same technology with donor patient valves, currently over 300 patients have received a new pulmonary heart valve, with an average follow-up of

4.0 years (www.cryolife.com, visited early 2009). An obvious disadvantage of this approach is that still a donor valve is needed. Furthermore, contradiction exists in literature on whether full recellularization and growth potential is possible with these scaffolds (Elkins et al., 2001; Bechtel et al., 2003; Stamm and Steinhoff, 2006). In the *in vitro* tissue engineering approach a full autologous solution is pursued. Cells from the patient are seeded into a scaffold that is designed either from synthetic (biodegradable) (Shinoka et al., 1995; Hoerstrup et al., 2000) or biological materials (Jockenhoevel et al., 2001; Neidert et al., 2002). Subsequently, the cells are stimulated in a bioreactor to produce extracellular matrix. As a result, a living autologous tissue is obtained that can be implanted back into the patient (Fig. 1.4). Hoerstrup et al. (2000)

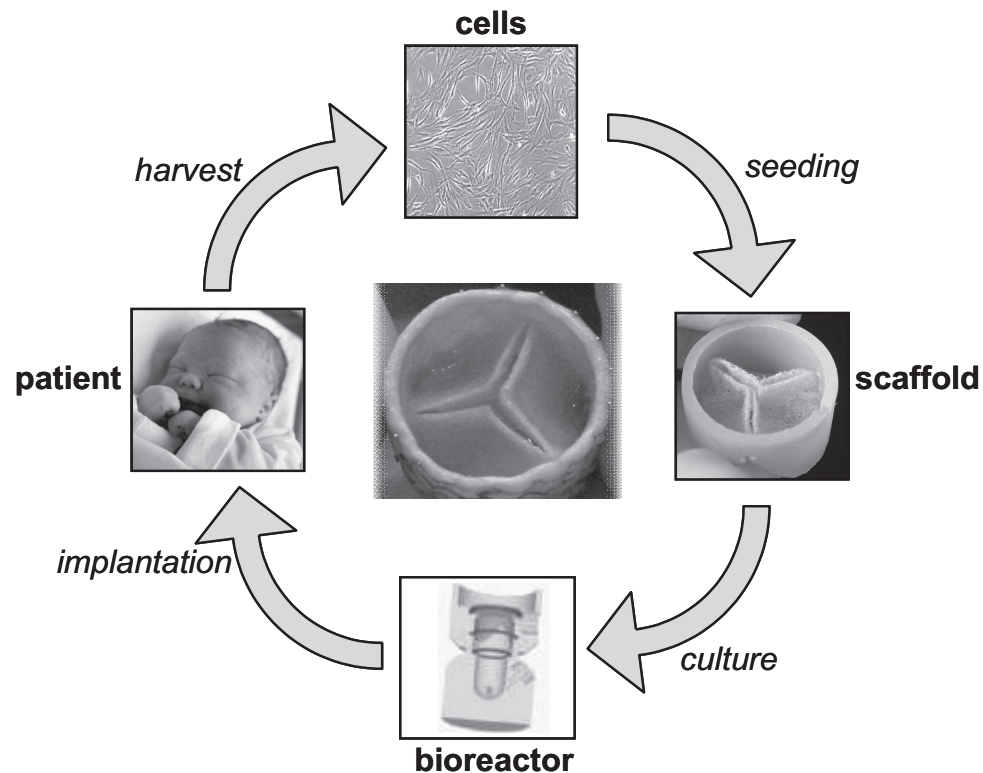


**Figure 1.4:** Visualization of the *in vitro* tissue engineering paradigm: Cells are harvested from the patient and expanded *in vitro*. Subsequently, cells are seeded on a biodegradable scaffold in the shape of a heart valve. The thus obtained construct is placed in a bioreactor, where it is subjected to mechanical and biochemical stimuli to induce extracellular matrix production. After 4 weeks of tissue culture, the tissue engineered heart valve (central image) is ready for implantation back into the patient.

reported successful implantations of tissue engineered pulmonary valves in lambs, with a maximal follow-up of 20 weeks. After 20 weeks, mechanical properties were comparable to native tissue. To stimulate tissue development a pulse duplicator, or flow bioreactor, was used, thus mimicking the opening and closing behavior of the heart valve during the cardiac cycle. Taking this biomimetic concept a step further, Mol et al. (2005a) realized that the loading of the aortic valve mainly takes place during the diastolic phase of the cardiac cycle, i.e. when the valve is closed. Therefore, they designed a diastolic pulse duplicator (DPD), or a strain bioreactor, thus



mimicking the *in vivo* environment during diastole. With the DPD, human heart valves were engineered that demonstrated *in vitro* the capability to withstand the high systemic pressures that occur at the aortic position (Mol et al., 2006). Although these results feed the hypothesis that mechanical conditioning stimulates the development of strong heart valves, the underlying mechanisms of the apparent relationship between global mechanical conditioning and the development of local tissue structure are still poorly understood. To elucidate these mechanisms researchers have been using rectangular tissue engineered constructs as a model system. Among others it was found that large strains are beneficial for developing strong tissue (Mol et al., 2003), and that not only collagen content, but also collagen cross-links play an important role in tissue strength and maturity (Balguid et al., 2007). Furthermore, intermittent loading (Rubbens et al., 2008) and hypoxia (Balguid et al., 2009) appear to have a positive influence on tissue development.

## 1.3 Aortic valve mechanics

### 1.3.1 Mechanical characterization

One of the most important challenges in heart valve tissue engineering is to create a heart valve that is capable of withstanding the high *in vivo* pressures, especially those at the aortic site. An important benchmark for the desired mechanical properties of tissue engineered heart valves is provided by the native aortic valve. Luckily, the aortic valve mechanics have been subject of extensive study ever since the first prosthetic heart valve replacements several decades ago. Pioneering work on aortic valve mechanics was performed by Clark (1973), with uniaxial tensile tests on human aortic valve leaflets in circumferential and radial direction. Leaflets were found to be stiffer in circumferential than in radial direction, which in retrospect can be explained by the anisotropic nature of the collagen fiber network in the fibrosa (Fig. 1.3b). Furthermore the leaflets' tensile behavior is characterized by an initial expansion at low stress, followed by a sharp transition region after which stiffening occurs. This feeds the argument that the initial stiffness of the tissue is provided by an elastin network, after which the collagen fibers take over. In addition to the work of Clark (1973) it was found that the aortic valves clearly demonstrate viscoelastic behavior, i.e. stress/strain relaxation and hysteresis, (e.g. Sauren et al. (1983); Carew et al. (2000)), although tensile behavior appears to be independent of strain rate (Kunzelman and Cochran, 1992). Vesely and Noseworthy (1992) used uniaxial tests to measure the mechanical properties of the fibrosa and ventricularis separately. The same group found that when the contribution of elastin to the valve mechanics is disrupted, the valve leaflets distend and become stiffer and less extensible in radial direction (Adamczyk et al., 2000; Lee et al., 2001).

For a full characterization of the in-plane mechanical behavior of biological tissues, biaxial tests need to be performed, as uniaxial tensile tests do not allow coupling between material axes (Fung, 1973; Chew et al., 1986; May-Newman and Yin, 1995; Billiar and Sacks, 2000b).

The most complete mechanical characterization of the aortic heart valve has been performed by the group of Sacks, who tested porcine aortic valves (PAV) using a range of biaxial testing regimes and set-ups (Sacks et al., 1998; Sacks, 1999; Billiar and Sacks, 2000b,a). Additionally, they used small angle light scattering (SALS) to measure local collagen fiber direction and dispersity (Billiar and Sacks, 1997). By mapping SALS results onto local strain fields during equibiaxial tension of PAV they found that local maximal strain is perpendicular to the local collagen orientation, thus indicating that collagen fibers are stiffer than the surrounding tissue and influence mechanical behavior accordingly (Billiar and Sacks, 2000b).

### 1.3.2 Constitutive modeling

Especially for biaxial tensile tests, interpretation of and comparison between experimental results is not straightforward. To this end, constitutive models have been used to provide a mathematical description for the mechanical behavior. Often, the tissue stress is related to the tissue strain using a set of material parameters, thus providing an objective tool for comparing different experiments. Important pioneering work on the constitutive modeling of biological tissue was performed by Fung (1973), who introduced a generalized strain energy density function for biological tissues. Although this type of modeling allows the correct description of the multiaxial relationship between stresses and strain in biological tissues, the model tends to be overparameterized (Chew et al., 1986). Furthermore, Fung-type models are phenomenological in nature, and therefore, interpretation of the material parameters is not straightforward. To increase insight in the underlying mechanisms of material behavior, structural models should be used. The first and probably most complete approach was given by Lanir (1983). In his approach, total strain energy is considered to be the sum of the individual fiber strain energies. Fibers are assumed to be one-dimensional and linear elastic, with zero compressive and bending stiffness. The characteristic non-linear behavior is obtained by a fiber recruitment law, in which fiber straightening (recruitment) is governed by a gamma distribution. Billiar and Sacks (2000a) modified this model by replacing the mathematically complex fiber recruitment law by a single exponential fiber law to incorporate non-linear behavior. Furthermore, fiber distribution was modeled to be Gaussian. The resulting model contained only a handful of easily interpretable *structural* parameters. With this model, the strong axial coupling phenomena, including negative strains, that were observed during biaxial tests of aortic valve leaflets were successfully explained by collagen fiber reorientation. Building further on this, Holzapfel et al. (2000) used the rule of mixtures to separate collagen fiber mechanics from the mechanical behavior of the cells and remaining extracellular matrix. With this model, the mechanical behavior of arteries was described successfully. A next step in structural modeling was provided by Driessen et al. (2008) who used remodeling algorithms to *predict* the fiber architecture of native heart valves and blood vessels based on *in vivo* loading conditions. The material parameters obtained by Billiar and Sacks (2000a) were used in a constitutive model adapted from Holzapfel et al. (2000). By assuming that fibers align in between principal strain direction, Driessen et al. (2008) qualitatively predicted the collagen fiber distribution in the aortic valve (Fig. 1.3b) based on the

tissue strains during *diastolic* loading of the leaflets.

## 1.4 Rationale and outline of this thesis

### 1.4.1 Rationale

The remodeling results of Driessen et al. (2008) provide further support to the hypothesis that by mimicking diastolic loading *in vitro* in a bioreactor, tissue engineered heart valves are stimulated to develop towards native tissue structure. However, important experimental proof for this theory is still missing. First of all, although the results of Billiar and Sacks (2000b,a) provided important insight into the structural behavior of the aortic valve, they are still limited in the sense that biaxial tests are nonlocal and material behavior therefore represent a weighted average of the tissue mechanics, while the aortic valve structure is strongly inhomogeneous. As an effect the observed mechanical characteristics are only representative for the central belly region of the aortic valve. An important modeling assumption of Driessen et al. (2008) is that the intrinsic mechanical properties of the collagen fibers are homogenous over the entire leaflet, and thus the differences between e.g., belly and commissures are entirely contributed to the fiber distribution. However, macroscopically clear structural differences can be observed, e.g., bundle diameter is larger in the commissures than in the belly (Fig. 1.3). Therefore, local measurement of tissue structural mechanics is needed to test this assumption. Secondly, a profound mechanical characterization of tissue engineered heart valves is still missing. Mechanical testing thus far has largely been limited to two orthogonal uniaxial tensile tests. This way, it was demonstrated that TEHV are stiffer in circumferential than in radial direction, which also holds for native heart valve leaflets (Mol et al., 2006). Driessen et al. (2007) even successfully applied their structural model to describe these orthogonal tensile tests. However, they also argue that e.g., biaxial testing is needed for a full characterization of the tissue mechanics. Finally, it is unknown whether the local tissue structure develops towards native values. Although TEHV seem reasonably homogeneous from a macroscopic view, microscopically a trend towards the native inhomogeneous structure is desired and expected based on the remodeling algorithm of Driessen et al. (2008). Again, local structural and mechanical characterization is necessary for elucidating the underlying structure-function principles.

The *objective* of this thesis is to provide experimental proof and quantification for some of the model assumptions and hypotheses of Driessen et al. (2008). It is hypothesized that by mimicking diastolic loads *in vitro* in a bioreactor, tissue engineered heart valves can be stimulated to develop towards native valve local structural properties. To quantify the relation between global mechanical conditioning and local structural tissue development, local structural mechanics of native and tissue engineered heart valves will be characterized and compared. The tissue engineered valves will be subjected to different mechanical conditioning protocols. For this purpose a mechanical characterization method is required that 1) allows local characterization of the tis-

sue mechanics, 2) is able to capture the full in-plane mechanical behavior of biological tissues and 3) incorporates fiber structure and mechanics directly into the experimental set-up *and* in the resulting material model. The most commonly used method for full mechanical characterization is biaxial testing. Although this could be combined with imaging of fiber structure and local strain field (e.g., Billiar and Sacks (2000b)), the minimal sample size needed is too large to allow local characterization, and thus material parameters represent average material properties of the central test region. Especially for the commissural region this will provide difficulties. Therefore, biaxial testing does not meet all our requirements. To the best of our knowledge, only one study has aimed at mechanical characterization of the commissural region by measuring flexural rigidity (Mirnajafi et al., 2006). Flexural stiffness tests could qualify as a local measurement, and e.g. using three-point bending (Merryman et al., 2006) in combination with confocal imaging would also provide information on fiber structure. However, bending tests will not provide sufficient information for a full characterization of the in-plane tissue mechanics.

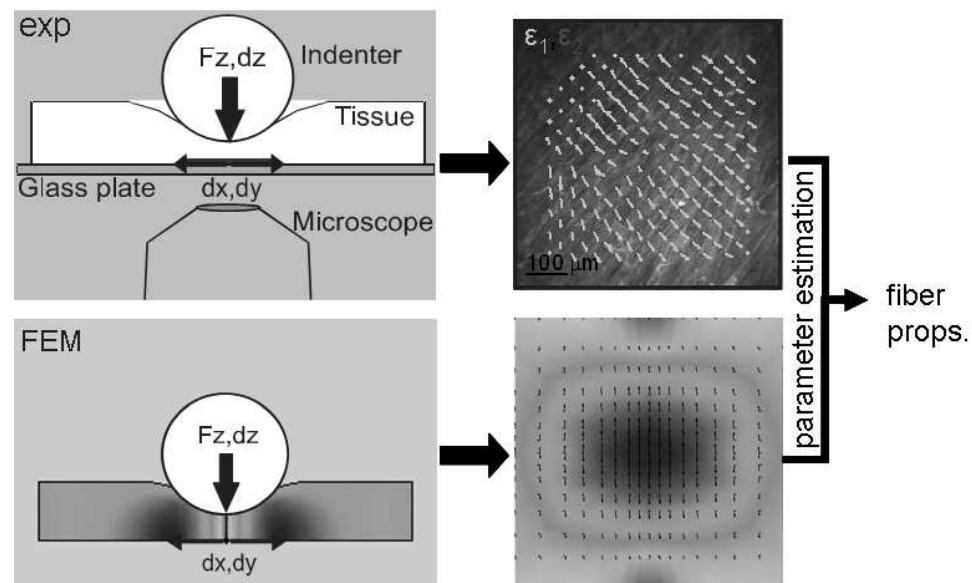


**Figure 1.5:** Spherical indentations are combined with confocal imaging and Digital Image Correlation (DIC) to measure deformations during the indentation test. A Finite Element (FE) analysis is inversely coupled to these results using parameter estimation. As a result, the local structural mechanical behavior is characterized.

Therefore in this work a novel method is developed for the mechanical characterization of planar soft biological tissues, in which indentation tests are performed, combined with confocal imaging (Fig. 1.5). An indentation device is mounted on top of an inverted microscope, with the test tissue laid flat on a base plate. The tissue is stained with a fluorescent collagen probe to allow visualization of the collagen fibers. The indentation test is performed using a small spherical indenter; indentation force and confocal images of the tissue at the base plate are recorded during the indentation test. After that, Digital Image Correlation (DIC) is used to

quantify in-plane deformations from these images, without any prior assumptions on the collagen fiber distribution. In addition, a dedicated finite element (FE) analysis of the indentation test is performed, using the structural constitutive model of Driessen et al. (2008). Parameter estimation is used to couple the FE results to the experimental data. The resulting material parameters represent the local fiber structure and fiber mechanics.

As the indenter size is small compared to global tissue dimensions, this method qualifies as a local measurement. Furthermore, confocal imaging allows visualization of the collagen fibers. Since fibers are stiffer than the surrounding tissue, deformation perpendicular to the main fiber direction is largest when indentation is performed. Therefore, local tissue anisotropy can be quantified as well. It should be emphasized that the fiber structure is not determined directly from the confocal images. Instead, it follows from the local deformation field. Thus, the estimated fiber structure is *directly coupled* to the local tissue mechanics.

### 1.4.2 Outline

First, the novel mechanical characterization method needs to be developed and tested. To this end a computational feasibility is performed in Chapter 2. The FE model is fitted to simulated experimental results to investigate if the full in-plane mechanical behavior of soft biological indeed can be captured using only one indentation test. Next, experimental validation is needed. Therefore, in Chapter 3 indentation tests are performed on linear elastic rubbers. Results from the FE analysis are compared to analytical solutions, assuming small deformations and isotropic material behavior. For a full experimental validation, uniaxial tensile tests and indentation tests on elastic rubbers are correlated in Chapter 4. Furthermore, indentation tests are performed on tissue engineered constructs. The tissue constructs are subjected to equibiaxial or uniaxial mechanical constraining during culture to create isotropic and anisotropic fiber structural properties, respectively. Thus, Chapter 4 aims at experimental validation for large deformations and anisotropic material behavior. Although the indentation approach is developed for characterization of heart valves, it is applicable for planar soft biological tissues in general. This versatility is demonstrated in Chapter 5, where the mechanical properties of Bioartificial Muscle (BAM) tissues cultured with and without cells are investigated. The main objective of this thesis is subject of Chapter 6 and 7. In Chapter 6, local structural mechanical properties are determined for tissue engineered heart valves, which are cultured using different loading protocols. Thereafter, Chapter 7 aims at the local structural mechanics of native (ovine) aortic and pulmonary leaflets. The obtained results are compared to the TEHV results of Chapter 6. Finally, in Chapter 8, the main findings are summarized and a discussion is provided on the scope and limitations of the proposed method, followed by some future perspectives.

It needs to be remarked that Chapters 2 to 6 are based on separate papers and therefore, overlap and repetition will occur in these chapters.

---

# Computational Feasibility

---

*In this chapter, the feasibility of a spherical indentation test combined with confocal imaging for the local mechanical characterization of planar soft biological tissues. The aortic heart valve is chosen as a typical example. A finite element model of the aortic valve leaflet is fitted to simulated experimental data using parameter estimation.*

The content of this chapter is based on:

Cox, M.A.J., Driessen, N.J.B., Bouten, C.V.C., and Baaijens, F.P.T. *Mechanical characterization of anisotropic planar biological soft tissues using large indentation: A computational feasibility study*. J. Biomech. Eng., 128(3):428-436, 2006.

## 2.1 Introduction

In the fast growing field of tissue engineering, knowledge and control of the tissue's mechanical properties is an important issue. This includes the desired target properties of the native tissue, as well as the properties of developing tissue engineered constructs. The typical highly nonlinear and anisotropic behavior of soft tissues (Clark, 1973; Lanir and Fung, 1974b; Humphrey, 2002) puts high demands on their mechanical characterization. Therefore, sophisticated experimental techniques need to be developed to determine these (local) mechanical properties. The current study focuses on a method for characterization of planar biological tissues, such as skin and mitral valve or aortic heart valve leaflet material. Traditionally, mechanical testing of planar biological tissues is performed by (multi)axial tensile testing. Clark (1973) performed uniaxial tensile testing of the aortic leaflet, while Ghista and Rao (1973) investigated tensile properties of the mitral valve. Lanir and Fung (1974a,b) performed biaxial tensile tests on rabbit skin. Vito (1980) greatly reduced the interspecimen variability seen in biaxial testing of planar tissues by aligning the testing axes with the material axes. Billiar and Sacks (1997) used small-angle light scattering (SALS) to quantify collagen fiber distribution during biaxial testing. The interested reader is referred to some extended reviews on the mechanical testing of planar biological materials (Sacks, 2000; Sacks and Sun, 2003). Uniaxial tensile tests do not provide sufficient information to fully map the anisotropic material behavior (Fung, 1973; Chew et al., 1986; May-Newman and Yin, 1995; Billiar and Sacks, 2000a), although one study by Lanir et al. (1996) suggested the combination of two separate perpendicular uniaxial tests, performed in a biaxial test set-up. Biaxial tensile experiments are difficult to perform, and boundary effects limit the test region to a small central portion of the tissue (Nielsen et al., 1991). In addition, for both cases, material parameters are found as an average for the whole test sample, while material properties of biological structures are likely to be inhomogeneous. To the authors' knowledge in only one study biaxial testing data were used to determine local mechanical properties (Nielsen et al., 2002). However, this study was limited to inhomogeneous elastic membranes.

To overcome some of the beforementioned limitations indentation tests may be used. Indentation experiments can be performed relatively easy and when the indenter size is small relative to tissue dimensions, material properties can be determined locally. Indentation tests were used before to mechanically characterize biological soft tissues (Gow and Vaishnav, 1975; Hori and Mockros, 1976; Gow et al., 1983; Zheng and Mak, 1996; Lundkvist et al., 1997; Han et al., 2003; Ebenstein and Pruitt, 2004). However, mostly, infinitesimal deformations and linear elasticity were assumed. In that case Hertz-contact is applicable, which yields an analytical solution for the force-depth relationship (Hertz, 1881). In some special cases analytical solutions even include nonlinear material properties (Green and Zerna, 1968; Humphrey et al., 1991) and/or finite layer thickness (Hayes et al., 1972; Matthewson, 1981). Costa and Yin (1999) showed that for finite indentations of nonlinear materials the infinitesimal strain theory is no longer valid. Some combined numerical-experimental work assuming geometrical nonlinearity was done by the group of Sato, who estimated local elastic moduli of blood vessels using pipette aspiration

(Aoki et al., 1997; Ohashi et al., 1997), which is an approach comparable to indentation tests. Recently, combining biaxial stretching with aspiration by a rectangular-shaped pipette, they found incremental elastic moduli in three different directions for porcine thoracic aorta (Ohashi et al., 2005). A recent computational study by Bischoff (2004) proved the feasibility of using asymmetric indenters to reveal anisotropy from the force-depth curve in biological soft tissues, assuming geometrical and material nonlinearity. However, to reveal anisotropy, results from numerous cylindrical indentation tests needed to be combined.

In our study, a computational analysis is performed on the feasibility of spherical indentation tests using large deformations. We hypothesize that the local collagen fiber distribution and mechanical properties can be obtained from *one single* indentation test, using combined analysis of local tissue deformations and the indentation force at various indentation depths. In further addition to Bischoff (2004), parameter estimation is used to fit the computational model to artificially generated experimental data. This provides further justification of the feasibility of the proposed experimental set-up. A fiber-reinforced nonlinear constitutive model based on the work by Holzapfel et al. (2000) is adopted. Modifications as proposed by van Oijen (2003) and Driessen et al. (2005b) include fiber volume fraction and a discrete fiber distribution function. Experimental results by Billiar and Sacks (2000b) on native porcine aortic valve leaflets are used to obtain material parameters and artificially generate experimental data. Parameter fitting is carried out with a Gauss-Newton estimation algorithm. The simulated experimental data make it possible to test the accuracy of the estimation algorithm under well-defined conditions. Finally, noise is added to the measurement data to test the algorithm's robustness for more realistic experimental data.

## 2.2 Materials and methods

It is expected that the method proposed in this study applies to planar soft biological tissues in general. However, as a typical example, we chose to model indentation tests on aortic leaflet tissue. To withstand diastolic pressures, the aortic valve leaflets have developed a well-organized collagen fiber architecture (Fig. 2.1). As a result of this, the leaflets exhibit highly nonlinear, anisotropic and inhomogeneous mechanical behavior (Billiar and Sacks, 2000b). An aortic leaflet consists of three functional layers, the fibrosa, the ventricularis and the spongiosa. The fibrosa, at the aortic side of the leaflet, consists mainly of a dense circumferentially aligned collagen fiber network. The ventricularis is largely composed of radially aligned elastin fibers. The fibrosa and ventricularis are connected through the spongiosa, which contains loosely arranged collagen and is abundant in glycosaminoglycans. The layered structure of the leaflet was not taken into account in the computational model.



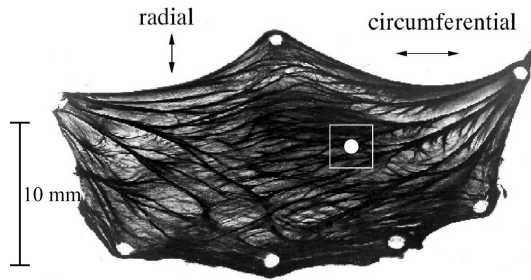


**Figure 2.1:** Microscopy image of a porcine aortic valve leaflet, showing large collagen fiber bundles (modified from Sauren (1981), with permission). The white square and circle illustrate the dimensions of the modeled tissue sample and indenter, respectively.

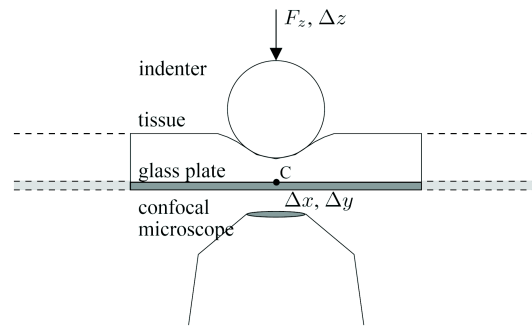


**Figure 2.2:** schematic view of the simulated set-up. Spherical indentation tests are performed on top of an inverted confocal microscope.

### 2.2.1 Geometry and boundary conditions

A hypothetical experiment was modeled where the aortic leaflet tissue rests on a rigid glass surface that, for instance, can be mounted on an inverted confocal laser scanning microscope (CLSM). Indentation would be applied by a rigid sphere (Fig. 2.2). Furthermore, we assumed that the indentation force could be measured by the indentation device, and that in plane deformations at the transition between the tissue and the glass surface could be obtained from the confocal microscope. Digital Image Correlation (DIC) would be used to obtain deformation gradient data from the confocal images (Sutton et al., 1983). Under these assumptions a number of indentation experiments were simulated. A three-dimensional model of the leaflet was considered. Under symmetry assumptions a quarter tissue block was modeled (Fig. 2.3). For local characterization of mechanical properties the indenter radius should be small relative to the overall tissue dimensions. In addition, for continuum mechanics to be applicable the indenter radius should be large relative to the tissue's microstructure dimensions, e.g., the diameter of the collagen fiber bundles ( $\sim 100 \mu m$ ). Therefore, the indenter radius was chosen equal to the tissue thickness of 0.5 mm. In preliminary computational studies no significant stresses and strains were observed at a distance greater than three times the indenter radius from the indentation site. Therefore, a  $1.5 \times 1.5 \times 0.5 \text{ mm}^3$  part of the aortic leaflet was modeled. The relative dimensions of the model with respect to the complete leaflet are illustrated in Fig. 2.1. In the block of tissue, material properties were assumed to be uniform. Contact between indenter and tissue as well as between tissue and glass surface was assumed to be frictionless. The indentation was applied in vertical direction in 60 steps of 0.05 mm, yielding a maximal global indentation of 0.30 mm or 60%.

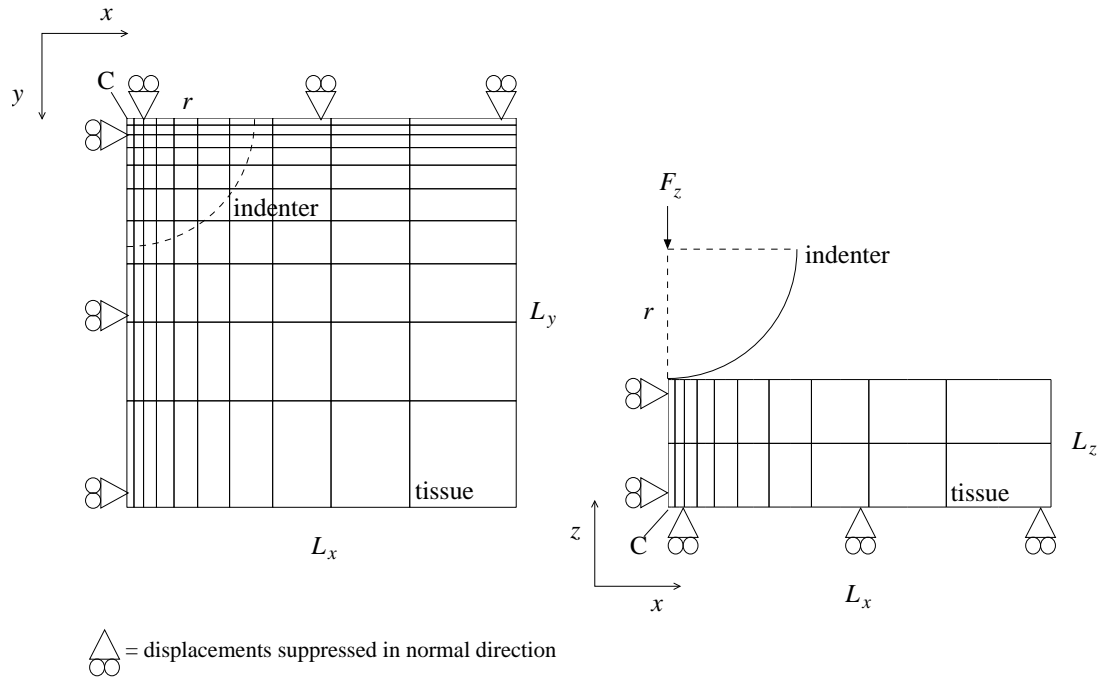


**Figure 2.3:** Top view (left) and front view (right) of the 3D model, showing indenter and boundary conditions.

## 2.2.2 Constitutive model

In the absence of inertia and body forces, the balance of momentum was given by

$$\vec{\nabla} \cdot \boldsymbol{\sigma} = \vec{0}, \quad (2.1)$$

where  $\boldsymbol{\sigma}$  represents the Cauchy stress. Conservation of mass was preserved by the incompressibility condition

$$J - 1 = 0, \quad (2.2)$$

with  $J = V/V_0 = \det(\mathbf{F})$ .  $V$  and  $V_0$  denote the volume in current and reference configuration, respectively and  $\mathbf{F}$  is the deformation gradient tensor. The Cauchy stress  $\boldsymbol{\sigma}$  consisted of the hydrostatic pressure  $p$  and the extra stress  $\boldsymbol{\tau}$ ,

$$\boldsymbol{\sigma} = -p\mathbf{I} + \boldsymbol{\tau}, \quad (2.3)$$

where  $\mathbf{I}$  represents the unity tensor. According to the constitutive model for incompressible fiber-reinforced materials by Holzapfel et al. (2000), the extra stress  $\boldsymbol{\tau}$  was split into an isotropic matrix part and an anisotropic fiber part. The fiber stress  $\boldsymbol{\psi}_f$  represents the stress contribution of the collagen fibers and is only working in fiber direction  $\vec{e}_f$ , i.e., the bending stiffness of the fibers was assumed to be equal to zero. The matrix stress  $\hat{\boldsymbol{\tau}}$  represents the stress contributions of all components except the fibers. Two modifications were made to the theory by Holzapfel et al. (2000). Firstly, the rule of mixtures was applied to account for fiber volume fraction  $\phi_f$  (van Oijen, 2003), and secondly, a modification was made to incorporate multiple fiber directions

(Driessen et al., 2005b). Assuming no interactions between the fiber layers, this yields for the extra stress  $\tau$ ,

$$\tau = \hat{\tau} + \sum_{i=1}^{N_f} \phi_f^i \left[ \psi_f^i - \vec{e}_f^i \cdot \hat{\tau} \cdot \vec{e}_f^i \right] \vec{e}_f^i \vec{e}_f^i, \quad (2.4)$$

where  $N_f$  was defined as the total number of fiber directions. The multiple fiber directions were used to incorporate the angular fiber distribution found in aortic valve leaflets (Billiar and Sacks, 2000b). The matrix behavior was described with an incompressible Neo-Hookean model,

$$\hat{\tau} = G(\mathbf{B} - \mathbf{I}), \quad (2.5)$$

where  $G$  is the shear modulus. The left Cauchy-Green deformation tensor  $\mathbf{B}$  is given by  $\mathbf{B} = \mathbf{F} \cdot \mathbf{F}^T$ . The typical nonlinear behavior of the collagen fibers was modeled by assuming an exponential relationship between the fiber stress  $\psi_f^i$  and fiber stretch  $\lambda_f^i$  (Billiar and Sacks, 2000a; Driessen et al., 2005b):

$$\psi_f^i = k_1 \lambda_f^i \left[ e^{k_2 (\lambda_f^i)^2 - 1} - 1 \right]. \quad (2.6)$$

In Eq. (2.6),  $k_1$  is a stress-like parameter and  $k_2$  is a dimensionless parameter. It was assumed that fibers are unable to withstand compressive forces. Therefore Eq. (2.6) only holds when  $\lambda_f^i$  is greater than or equal to unity. Otherwise fibers are not stretched and fiber stress equals zero. Assuming affine deformations, the deformed fiber direction  $\vec{e}_f^i$  was calculated from the fiber direction in undeformed reference configuration  $\vec{e}_{f_0}^i$ ,

$$\vec{e}_f^i = \frac{1}{\lambda_f^i} \mathbf{F} \cdot \vec{e}_{f_0}^i, \quad (2.7)$$

and the fiber stretch was given by

$$\lambda_f^i = \|\mathbf{F} \cdot \vec{e}_{f_0}^i\| = \sqrt{\vec{e}_{f_0}^i \cdot \mathbf{C} \cdot \vec{e}_{f_0}^i}. \quad (2.8)$$

The right Cauchy-green deformation tensor is given by  $\mathbf{C} = \mathbf{F}^T \cdot \mathbf{F}$ . It was assumed that fibers were distributed in the leaflet plane. The fiber directions in the undeformed configuration are then represented by

$$\vec{e}_{f_0}^i(\gamma^i) = \cos(\gamma^i) \vec{v}_1 + \sin(\gamma^i) \vec{v}_2, \quad (2.9)$$

where  $\vec{v}_1$  and  $\vec{v}_2$  span the fiber plane and the angle  $\gamma^i$  is defined with respect to  $\vec{v}_1$ . In this study,  $\vec{v}_1$  and  $\vec{v}_2$  were chosen equal to  $\vec{e}_x$  and  $\vec{e}_y$ , respectively. A discretized Gaussian distribution function was used for the fiber volume fraction:

$$\phi_f^i(\gamma^i) = A \exp \left[ \frac{-(\gamma^i - \mu)^2}{2\sigma^2} \right]. \quad (2.10)$$

In Eq. (2.10),  $\gamma^i$  was defined from 1 to 180 degrees, with a resolution of 1 degree. Mean and standard deviation were represented by  $\mu$  and  $\sigma$ , respectively.  $A$  is a constant that forces the total fiber volume fraction to equal  $\phi_{tot}$ :

$$A = \frac{\phi_{tot}}{\sum_{i=1}^{N_f} \exp \left[ \frac{-(\gamma^i - \mu)^2}{2\sigma^2} \right]}. \quad (2.11)$$

### 2.2.3 Finite element implementation

The finite element package SEPRAN was used for solving the balance equations (Segal, 1984). The exact implementation was derived from van Oijen (2003). The aortic valve was meshed with  $10 \times 10 \times 2 = 200$  elements. Mesh refinement was applied in both  $x$  and  $y$  direction; the elements at the site of indentation were fifteen times smaller than the largest elements in both directions (Fig. 2.3). In a preliminary study, increasing the total number of elements did not induce significant changes in the numerical results. The element type is a 27-node Taylor-Hood tri-quadratic brick using continuous pressure interpolation. To ensure that the Babuska-Brezzi condition was matched, pressure interpolation (linear) was one order lower than the interpolation for displacements (quadratic). An updated Lagrangian formulation was adopted and incompressibility was accounted for by applying a mixed formulation.

### 2.2.4 Parameter estimation

To estimate material parameters from experimental data, a mixed numerical experimental method was used (Hendriks et al., 1990; Oomens et al., 1993; Meuwissen, 1998; Meuwissen et al., 1998). The estimation algorithm was implemented according to Meuwissen (1998). Measurements (indentation force and in plane deformations as a function of indentation depth) were stored in a column  $\underline{m} = [m_1, \dots, m_N]^T$ , where  $N$  is the number of measurement points. The material parameters were stored in a column  $\underline{\theta} = [\theta_1, \dots, \theta_P]^T$ , where  $P$  is the number of parameters. The finite element model was used to calculate the response  $\underline{h}$  corresponding to a given set of parameters  $\underline{\theta}$  and input  $\underline{u}$ . The input  $\underline{u}$  may for example consist of prescribed forces and/or displacements.  $\underline{m}$  was related to  $\underline{\theta}$  according to

$$\underline{m} = \underline{h}(\underline{u}, \underline{\theta}) + \underline{\xi}, \quad (2.12)$$

where  $\underline{\xi}$  is an error column. The error column  $\underline{\xi}$  may consist of measurement errors and modeling errors. A more detailed discussion on this is beyond the scope of this study, the interested reader is referred to Meuwissen (1998). The estimation algorithm aims at minimizing the difference between  $\underline{h}(\underline{u}, \underline{\theta})$  and  $\underline{m}$ . A quadratic objective function  $J(\underline{\theta})$  was defined to quantify the goodness of fit,

$$J(\underline{\theta}) = [\underline{m} - \underline{h}(\underline{u}, \underline{\theta})]^T \underline{V} [\underline{m} - \underline{h}(\underline{u}, \underline{\theta})], \quad (2.13)$$

where  $\underline{V}$  is a positive definite symmetric weighing matrix. For  $J(\underline{\theta})$  to be a (local) minimum, the first derivative of  $J(\underline{\theta})$  with respect to  $\underline{\theta}$  should be equal to zero, and in addition, the second derivative of  $J(\underline{\theta})$  needs to be positive definite. Setting the first derivative of  $J(\underline{\theta})$  equal to zero yields,

$$\underline{H}^T(\underline{u}, \underline{\theta}) \underline{V} [\underline{m} - \underline{h}(\underline{u}, \underline{\theta})] = \underline{0}, \quad (2.14)$$

in which the sensitivity matrix  $\underline{H}(\underline{u}, \underline{\theta})$  is given by

$$\underline{H}(\underline{u}, \underline{\theta}) = \frac{\partial \underline{h}(\underline{u}, \underline{\theta})}{\partial \underline{\theta}}. \quad (2.15)$$

Since, in general,  $\underline{h}(\underline{u}, \underline{\theta})$  is nonlinear in  $\underline{\theta}$ , Eq. (2.14) needs to be solved iteratively. Using a first order linearization of  $\underline{\theta}$ , the following iterative scheme was obtained (Meuwissen, 1998),

$$\begin{aligned}\underline{\theta}^{(i+1)} &= \underline{\theta}^{(i)} + \delta \underline{\theta}^{(i)}, \\ \delta \underline{\theta}^{(i)} &= \underline{K}^{(i-1)} \underline{H}^{(i)T} \underline{V} \left[ \underline{m} - \underline{h}^{(i)} \right], \\ \underline{K}^{(i)} &= \underline{H}^{(i)T} \underline{V} \underline{H}^{(i)}.\end{aligned}\quad (2.16)$$

In Eq. (2.16),  $i$  denotes the iteration number and  $\underline{h}^{(i)}$  and  $\underline{H}^{(i)}$  are shorthand notations for  $\underline{h}(\underline{u}, \underline{\theta}^{(i)})$  and  $\underline{H}(\underline{u}, \underline{\theta}^{(i)})$ , respectively. Furthermore,  $\delta \underline{\theta}^{(i)}$  was assumed to be small and the following two approximations were used,

$$\begin{aligned}\underline{h}(\underline{\theta}^{(i)} + \delta \underline{\theta}^{(i)}) &\approx \underline{h}^{(i)} + \underline{H}^{(i)} \delta \underline{\theta}^{(i)}, \\ \underline{H}(\underline{\theta}^{(i)} + \delta \underline{\theta}^{(i)}) &\approx \underline{H}^{(i)}.\end{aligned}\quad (2.17)$$

The iterative scheme in Eq. (2.16) is known as the Gauss-Newton linearization equation. In the neighborhood of the optimal solution, quadratic convergence is reached. However, when initial parameter estimates are poor, convergence is worse and even divergence may occur. Although several modifications to this scheme have been proposed (Bard, 1974), the presented scheme was chosen for its ease of implementation and fast near-optimum convergence. The iterative procedure was continued until parameter changes were smaller than a critical value:

$$\sqrt{\delta \underline{\theta}^{(i)T} \delta \underline{\theta}^{(i)}} < \delta_{\theta}, \quad (2.18)$$

where  $\delta_{\theta}$  was set to  $10^{-3}$  and  $\delta \underline{\theta}^{(i)T}$  was defined as

$$\begin{aligned}\delta \underline{\theta}^{(i)T} &= \left[ \delta \bar{\theta}_1^{(i)}, \dots, \delta \bar{\theta}_P^{(i)} \right], \\ \delta \bar{\theta}_j^{(i)} &= \left| \delta \theta_j^{(i)} \right| / \left| \theta_j^{(i)} \right|, \quad j = 1, \dots, P.\end{aligned}\quad (2.19)$$

To increase robustness farther away from the optimal solution, an extra constraint was put on  $\delta \theta_j^{(i)}$ : as long as  $|\delta \theta_j^{(i)}| > |\theta_j^{(i)}|$ ,  $\delta \theta_j^{(i)} = \delta \theta_j^{(i)} / 2$ .

In Eq. (2.16),  $\underline{H}^{(i)}$  needs to be determined for each parameter set  $\underline{\theta}^{(i)}$ . In this study, a forward finite difference scheme was adopted, in which small perturbations of each separate parameter were used to determine  $\underline{H}^{(i)}$ .

$$H_{kj}^{(i)} \approx \frac{h_k(\underline{\theta}^{(i)} + \Delta \theta_j \underline{e}_j) - h_k(\underline{\theta}^{(i)})}{\Delta \theta_j}, \quad (2.20)$$

where  $\underline{e}_j$  is a column of length  $P$  of which the  $j^{\text{th}}$  entry equals one while all others are set to zero and  $\Delta \theta_j$  is a small variation of parameter  $j$ . With this scheme, no adjustments to the finite element code were needed.  $\Delta \theta_j$  was chosen according to

$$\begin{aligned}\Delta \theta_j &= \Delta_{rel} \theta_j^{(i)} \quad \text{if } \Delta_{rel} \theta_j^{(i)} > \Delta_{abs}, \\ &= \Delta_{abs} \quad \text{if } \Delta_{rel} \theta_j^{(i)} \leq \Delta_{abs},\end{aligned}\quad (2.21)$$

where  $\Delta_{rel}$  was set to  $10^{-3}$  and  $\Delta_{abs}$  to  $10^{-3}\theta_j^{(0)}$ . In the estimation runs, normally distributed noise was added to the measurement data. The randomness of the noise causes a certain randomization in the final parameter estimates. To test the accuracy of the parameter estimates, the errors of the final parameter estimates were compared to the estimated standard deviation for each parameter, which was given by the square root of the corresponding diagonal term in the approximate covariance matrix of the parameters  $\underline{P}$ :

$$\underline{P} = \underline{K}^{-1} \underline{H}^T \underline{V} \underline{\psi} \underline{V} \underline{H} \underline{K}^{-1}. \quad (2.22)$$

In Eq. (2.22),  $\underline{\psi}$  is the covariance matrix of the measurement noise. In case of uncorrelated noise,  $\underline{\psi}$  is a diagonal matrix with the square of the standard deviations of the measurement noise at its diagonal terms. By normalizing Eq. (2.22) with its diagonal terms, the correlation matrix  $\underline{R}$  is obtained. The elements of  $\underline{R}$  are given by

$$R_{ij} = P_{ij} (P_{ii} P_{jj})^{-1/2}, \quad i, j = 1, \dots, P. \quad (2.23)$$

The diagonal terms of  $\underline{R}$  are all unity, while the off-diagonal terms are in the interval  $[-1, 1]$ . The off-diagonal terms are a measure for the correlation between the different parameters. When the absolute value of an off-diagonal term is close to 1, the estimates are highly correlated, which often indicates a poor experimental design or an overparameterized model. Another check of the quality of the model fit was performed by examination of the residual errors  $\xi$  in Eq. (2.12). The relative standard deviation of the residual errors should be comparable to the relative standard deviation of the applied measurement noise. The relative standard deviation of the displacement and force residual errors was estimated according to

$$\hat{s}_{res} = \sqrt{\frac{1}{N} \sum_{i=1}^N \left( \frac{m_i - h_i}{m_i} \right)^2}. \quad (2.24)$$

## 2.2.5 Simulated experiments

To generate experimental results, a simulation was run with fiber material parameters as found for the aortic leaflet by Billiar and Sacks (2000b), who performed biaxial tensile tests on native porcine aortic valves. This corresponds to  $k_1 = 0.7$  kPa and  $k_2 = 9.9$  (Driessen et al., 2005b). Mean and standard deviation for the fiber distribution function were  $\mu = 0^\circ$  and  $\sigma = 10.7^\circ$ . Total fiber volume fraction  $\phi_{tot}$  was set to 0.5 (Li et al., 2001). The matrix shear modulus  $G$  was set to 10 kPa (Driessen et al., 2005b). Two indentation tests were considered in the parameter estimation: simulation A and B. In simulation A, the fiber distribution  $\sigma$  was assumed to be known a priori, for example from SALS measurements. As measurement data  $\underline{m}$ , the indentation force as a function of indentation depth was chosen. The indentation force was normalized by dividing by the mean indentation force. The estimation algorithm was used to fit the matrix shear modulus  $G$  and the fiber parameters  $k_1$  and  $k_2$ . Other parameters were assumed to be known. In first instance, parameter estimation was carried out without adding extra noise to

the experimental data. This way, the original parameters should be found exactly by the estimation algorithm. Secondly, noise was added to the experimental data to test the estimation for its robustness. Measurement noise was assumed to be normally distributed with a standard deviation of 5% relative to the measurement data. In simulation B, the fiber distribution  $\sigma$  was added as an extra parameter in the estimation process. To be able to fit the fiber distribution, information is needed on the material anisotropy. Therefore, first and second principal strain as a function of indentation depth, in the center of indentation, at the transition between tissue and glass surface (indicated by  $C$  in Fig. 2.2 and Fig. 2.3), were added to the measurement data. Like the indentation force, first and second principal strain were normalized by dividing by their respective means. Again, the estimation algorithm was applied with and without noise, normally distributed with a standard deviation of 5%, relative to the measurement data.

Due to the highly nonlinear material behavior the absolute difference between measurement data and model fit increases with increasing indentation depths. Accordingly, the value of the objective function  $J$  (Eq. (2.13)) is dominated by data at the highest indentation depths. To compensate for this, the weighing matrix  $\underline{V}$  was used to impose weighing factors inversely proportional to the square of the measurement data points.  $\underline{V}$  was defined as a diagonal matrix, the diagonal elements were given by

$$V(i, i) = \frac{1}{m(i)^2}, \quad i = 1, \dots, N. \quad (2.25)$$

This way, all data points equally contribute to the objective function  $J$ . A remark should be made that the weighing matrix  $\underline{V}$  may also be used to weigh the data points based on their expected measurement errors, if statistical information on the errors is available.

## 2.3 Results

### 2.3.1 Feasibility of spherical indentation

To illustrate the feasibility of spherical indentation in revealing material anisotropy and non-linearity, simulations were carried out for various fiber distributions. Figure 2.4 shows the indentation force (middle row) and principal stretches (bottom row) as a function of indentation depth, for three different fiber distributions (top row): a single fiber direction (left column,  $\mu = 0^\circ$ ,  $\sigma \rightarrow 0^\circ$ ), fiber distribution as found for the native porcine valve by Billiar and Sacks (2000a,b) (middle column,  $\mu = 0^\circ$ ,  $\sigma = 10.7^\circ$ ) and a uniform fiber distribution (right column,  $\mu = 0^\circ$ ,  $\sigma \rightarrow \infty^\circ$ ). In Fig. 2.4, the first and second principal stretch are always parallel and perpendicular to the main fiber direction, respectively. Stretches are measured at the transition between tissue and glass plate in the center of indentation  $C$  (Fig. 2.2 and Fig. 2.3). For the uniaxial fiber distribution, deformation perpendicular to the fiber direction was much higher, since the matrix material was weaker than the fibers. As a result, fiber deformations were relatively small, and thus the force needed for the indentation was relatively small as well. Note that the maximal principal fiber stretch almost equaled 2, for the uniaxial as well as the native valve

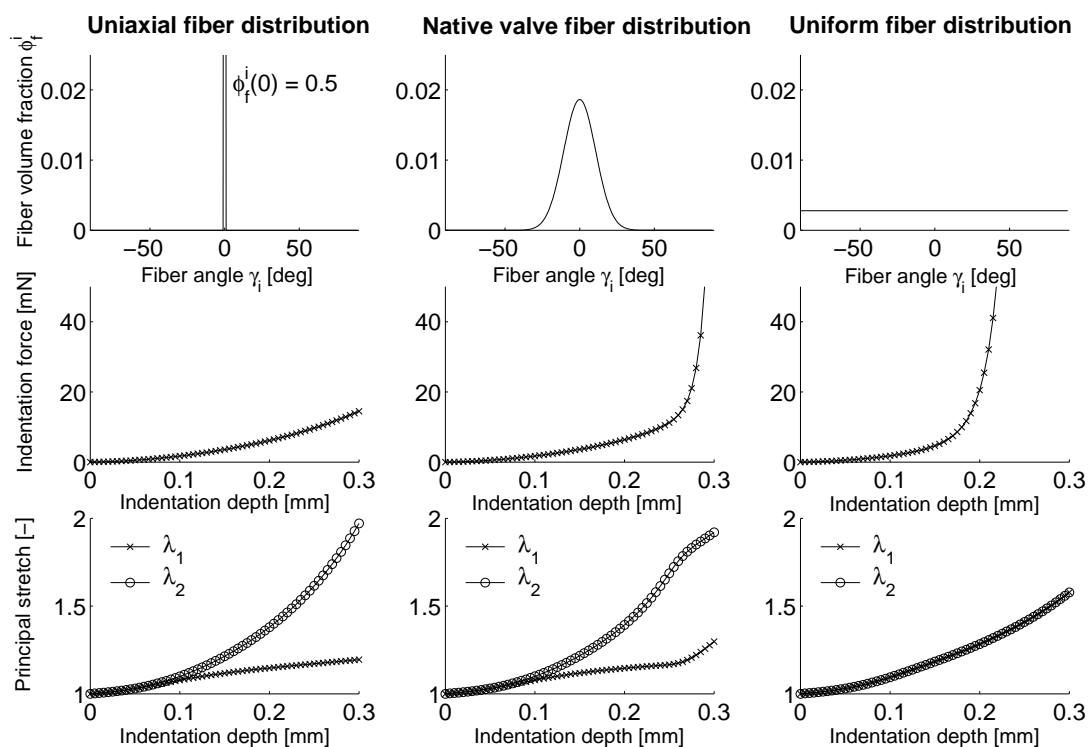


**Figure 2.4:** Indentation force (middle row) and first ( $\lambda_1$ ) and second ( $\lambda_2$ ) principal stretches (bottom row) as a function of indentation depth, for three different fiber distributions (top row): a single fiber direction (left column,  $\mu = 0^\circ$ ,  $\sigma \rightarrow 0^\circ$ ), native valve fiber distribution (Billiar and Sacks, 2000a,b) (middle column,  $\mu = 0^\circ$ ,  $\sigma = 10.7^\circ$ ) and a uniform fiber distribution (right column,  $\mu = 0^\circ$ ,  $\sigma \rightarrow \infty^\circ$ ).



fiber distribution, pointing out the very large deformations that were found locally. When a native valve fiber distribution was assumed, deformations perpendicular to the main fiber were again larger than in the parallel direction. At an indentation of approximately 50% (0.25 mm), a sudden change in slope was visible for the stretch-indentation curves. Comparable phenomena of so-called ‘collagen locking’, were observed by Driessen et al. (2005a), in simulations of the aortic valve leaflet during pressurization, and by Billiar and Sacks (2000b), in biaxial tensile testing of the aortic valve leaflet. The larger deformations perpendicular to the main fiber direction caused a broadening of the angular fiber distribution (Fig. 2.5a). However, the changes in slope were mainly caused by a redistribution of the fiber stress. Figure 2.5b shows the relative contribution of fibers in all directions to the total fiber stress. At smaller indentations, the fiber stress was mainly carried by fibers in the main fiber direction. Starting at approximately 0.22 mm indentation, this shifted to fibers more perpendicular to the main fiber direction. The absolute value of the fiber stress was increasing in all directions, thus the redistribution of the fiber stress was caused by a large increase in fiber stress in directions more perpendicular to the main fiber direction. This increase explains the sharp transition in the indentation force curve (Fig. 2.4). In the uniform distribution, obviously no differences between the first and second

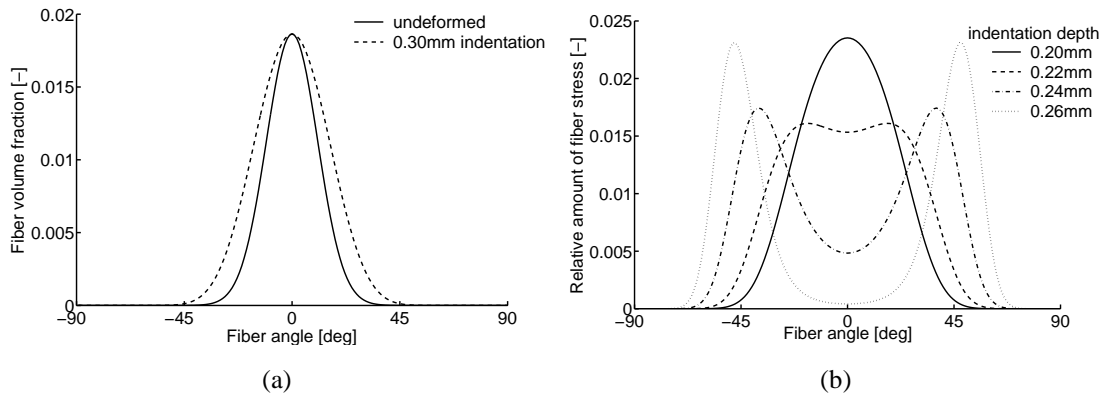


**Figure 2.5:** a) Angular fiber distribution in the undeformed configuration (solid line) and at 0.30 mm indentation (dashed line); b) Relative fiber stress distribution at four levels of indentation: 0.20 mm (solid line), 0.22 mm (dashed line), 0.24 mm (dash-dotted line) and 0.26 mm (dotted line).

principal stretches were observed. The indentation force was even higher than in the native valve simulation. Relatively many fibers were stretched, which resulted in a large increase in stiffness and therefore a large increase in indentation force.

### 2.3.2 Simulation A

In simulation A, matrix shear modulus  $G$  and fiber parameters  $k_1$  and  $k_2$  were estimated from the force-indentation curve. Results for the 0% and 5% noise case are summarized in Table 2.1. When no noise was added to the measurement data, the exact parameter values were found within 8 iterations. After adding noise to the experimental data, 10 iterations were needed be-

**Table 2.1:** Initial and final parameter estimates for the 0% and 5% noise simulation A. In the 5% noise case, the error and estimated standard deviation per parameter are given as well. All parameters are scaled with respect to the exact parameter value that was used in the generation of the experimental data.

Parameter	Initial Estimate	0% Noise	5% Noise		
		Final Estimate	Final Estimate	Error	Estimated Standard Deviation
$G^*$	0.50	1.000	1.018	0.018	0.023
$k_1^*$	2.00	1.000	0.809	0.191	0.223
$k_2^*$	0.50	1.000	1.018	0.018	0.025

fore the convergence criterion was matched. The measurement data were fit very well (Fig. 2.6). The randomness of the noise made that parameters were not found exactly. The estimated stan-

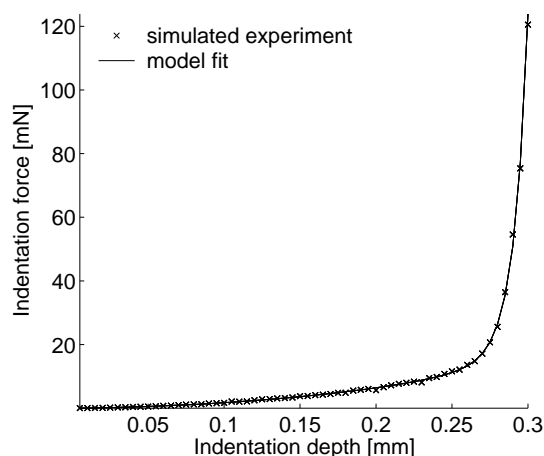


**Figure 2.6:** Indentation forces as a function of indentation depth for simulation A. The experimental data (cross) is fit very well by the model (solid line).

dard deviations of the parameters in Table 2.1 are the diagonal terms of the estimated covariance matrix  $\underline{P}$ , obtained from Eq. (2.22). The errors in the parameter estimates coincided well with the estimated standard deviations.

The residual errors in the experimental data were evaluated according to Eq. (2.24). The standard deviation of the noise was 5% relative to the measurement data. This should coincide with the mean relative standard deviation of the residual errors  $\hat{\delta}_{res}$ . For simulation A,  $\hat{\delta}_{res}$  equaled 0.077, which was in agreement with the standard deviation of the applied noise. Simulations were repeated for several initial parameter sets; the final estimates were in the expected range in all cases. The correlation matrix  $\underline{R}$  (Eq. (2.23)) was used to quantify the correlation between the different parameter estimates. Table 2.2 shows that the magnitude of the correlation number was higher than 0.90 for all parameters, which means that the parameters were highly corre-

lated. This may indicate that the model is overparameterized for this experimental design. Even though the exact parameters were found within the variation expected from the applied noise, this is an important aspect to take into account.

**Table 2.2:** Correlation between the different parameters for simulation A.

	$G$	$k_1$	$k_2$
$G$	1.000	-0.939	0.927
$k_1$	-0.939	1.000	-0.995
$k_2$	0.927	-0.995	1.000

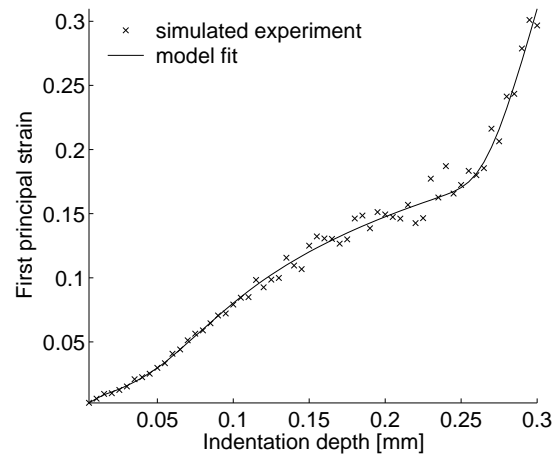
### 2.3.3 Simulation B

In simulation B, first and second principal strain at the center of indentation, as well as indentation force were used for the parameter estimation, thus yielding a total of  $3 \times 60 = 180$  measurement points. Initial and final parameter estimates are given in Table 2.3. For 0% noise,

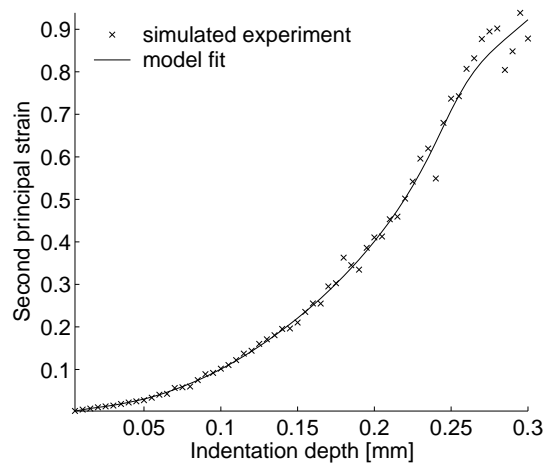
**Table 2.3:** Initial and final parameter estimates for the 0% and 5% noise simulation B. In the 5% noise case, the error and estimated standard deviation per parameter are given after 20 iterations. All parameters are scaled with respect to the exact parameter value that was used to generate the experimental data.

Parameter	Initial Estimate	0% Noise	5% Noise		
		Final Estimate	Final Estimate	Error	Estimated Standard Deviation
$G^*$	0.50	1.000	0.991	0.009	0.007
$k_1^*$	2.00	1.000	0.973	0.027	0.037
$k_2^*$	0.50	1.000	1.007	0.007	0.014
$\sigma^*$	2.00	1.000	1.000	0.000	0.012

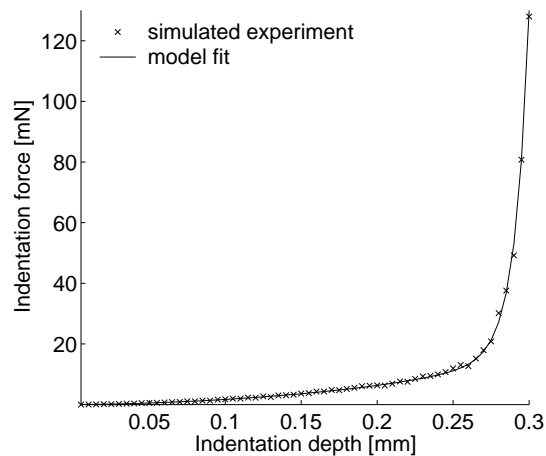
the correct parameter values were found within 9 iterations. When 5% normally distributed noise was added, the convergence criterion was not matched within 20 iterations; small fluctuations existed in the parameter estimates. However, after seven iterations, the variation in the residual error became less than 1% and the measurement data were fit very well (Fig. 2.7). Comparison between the parameter errors after 20 iterations and the estimated standard deviations learns that the errors were well in range with the expected variation due to the applied noise (Table 2.3). The relative standard deviation of the residual errors  $\hat{s}_{res}$  yielded 0.068, which was in agreement with the relative standard deviation of the applied noise. Simulations were repeated for several initial parameter sets; the final estimates were all in the expected range. Some



(a)



(b)



(c)

**Figure 2.7:** First principal strain (a), second principal strain (b) and indentation force (c) as a function of indentation depth for simulation B. Experimental data (cross) are fit very well by the model (solid line).

correlation existed between the parameters, although less than in simulation A (Table 2.4). The shear modulus  $G$  showed low correlation with the other parameters, while especially  $k_2$  and  $\sigma$  were highly correlated.

**Table 2.4:** Correlation between the different parameters for simulation B.

	$G$	$k_1$	$k_2$	$\sigma$
$G$	1.000	-0.182	0.163	-0.173
$k_1$	-0.182	1.000	-0.802	0.667
$k_2$	0.163	-0.802	1.000	-0.961
$\sigma$	-0.173	0.667	-0.961	1.000

## 2.4 Discussion

An indentation experiment was proposed for characterization of the local, anisotropic, nonlinear material properties of planar soft biological tissues. In the present study, large deformations (60% global indentation) were used to reveal the nonlinear behavior, while in previous indentation studies infinitesimal strain theory was applied. Material anisotropy was revealed by combining indentation force and deformation gradient information, both as a function of indentation depth. This way, *one single* spherical indentation test provided sufficient information to characterize the material, while in a comparable computational study by Bischoff (2004), several (cylindrical) indentation tests were necessary to reveal material anisotropy. As a typical example, the aortic heart valve leaflet was chosen, and a computational model was used to show the feasibility of the proposed experimental set-up. A recently proposed incompressible fiber-reinforced material model was adopted, assuming geometrical and material nonlinearity (Driessen et al., 2005a). Simulations were run for several angular fiber distributions. In contrast to traditional indentation tests, very large indentations (60% global indentation) were applied, resulting in maximal local principal stretches of almost 2. When a native valve fiber distribution was modeled, collagen locking phenomena occurred at 50% global indentation (Fig. 2.4), comparable to phenomena observed during pressurization (Driessen et al., 2005a), and in biaxial tensile testing (Billiar and Sacks, 2000b), both of the aortic valve leaflet. It was demonstrated that collagen locking was not completely caused by fiber reorientation. The main cause was a redistribution of the fiber stress over the different fiber directions. At lower indentations, the total fiber stress was dominated by the stress in the main fiber direction. At >50% global indentation, the maximal fiber stress shifted to directions more perpendicular to the main fiber direction (Fig. 2.5).

In addition to Bischoff (2004), parameter estimation was used to fit material parameters to artificially generated experimental data. The major advantage over real experimental data is that the parameter values to be estimated are known exactly, and therefore estimation can be analyzed under well defined conditions. Even after addition of 5% normally distributed relative noise,

the model fitted the experimental data very well (Fig. 2.6 and Fig. 2.7). The final parameter estimates were well within the range expected from the noise addition (Table 2.1 and Table 2.3). Although the estimation algorithm does not guarantee that an absolute minimal residual error is found, final parameter estimates for estimation runs using different initial parameter sets were all in the expected range. Analysis of the covariance matrix of the parameters learned that the parameter estimates in simulation A were correlated (Table 2.2). This indicates an overparameterization of the constitutive model. In simulation B, in plane deformations and indentation forces together were used to estimate matrix and fiber material parameters as well as the fiber distribution. Although four parameters were estimated instead of three, correlation between parameters was lower (Table 2.4). Still, correlation existed between especially  $k_2$  and  $\sigma$ . This might explain the fluctuations in the material parameter estimates. All parameter fluctuations were within the range predicted by the estimated standard deviation. To improve the orthogonality of the parameters, the number of measurement points could be increased, for instance by using deformation gradient data of more than one point at the interface between glass plate and tissue (Fig. 2.2). This could easily be implemented in the estimation algorithm, but was considered unnecessary for proof of principle. In real indentation experiments, best results are expected when the complete deformation gradient field in the vicinity of the indenter is used in the estimation runs.

Although the contribution of matrix material to the mechanical behavior is significant for relatively low deformations, matrix stresses were often assumed to be negligible (Billiar and Sacks, 2000a; Lanir, 1983), or the shear modulus was chosen such that its influence is negligible in a biaxial tensile test (Driessen et al., 2005b). Based on the correlation matrix for simulation B (Table 2.4), we expect that the matrix shear modulus  $G$  can be determined accurately using an indentation test. A possible explanation is that in indentation testing, the compression of the matrix material (in the direction of indentation), is larger than the in plane stretch of the collagen fibers. The relatively large compression of the matrix during indentation results in a significant contribution of the matrix to the bulk material response, which facilitates the accurate determination of the matrix material properties. The main fiber direction  $\mu$  was chosen along one of the material symmetry axes. In a real indentation experiment,  $\mu$  would coincide with the direction of least deformation. Therefore it could be obtained directly from the deformation gradient, and was not considered as a parameter in the estimation process. The total fiber volume fraction  $\phi_{tot}$  was assumed to be constant. However, considering the inhomogeneity of the aortic leaflet (Fig. 2.1), this is probably not correct. Therefore, in future, we should be able to measure the fiber volume fraction, locally, or the volume fraction should be taken into account as an extra parameter in the estimation process. As mentioned before, the aortic valve leaflet consists of three layers, the fibrosa, the spongiosa and the ventricularis. While ventricularis and fibrosa are both abundant in collagen and/or elastin fibers, the spongiosa forms a loose connective net between the other two layers. Therefore, it is possible that indentation of the complete aortic leaflet will mainly result in deformation of the spongiosa, the weaker layer. This layered structure was not taken into account in the computational model. This should be kept in mind when performing the indentation experiments. To elucidate the effect of the layered structure, the behavior of the

ventricularis and fibrosa could be investigated separately. Separation of the ventricularis and fibrosa was carried out before by Vesely and Noseworthy (1992), prior to uniaxial tensile testing. To determine the mechanical properties of the soft tissue locally, the indenter radius should be small compared to overall tissue dimensions. However, for continuum mechanics theory to be applicable, the indenter radius needs to be large relative to the dimensions of the tissue's microstructure. Therefore, the indenter radius was chosen equal to the average tissue thickness of 0.5 mm. Due to the presence of large collagen fiber bundles (Fig. 2.1), the continuum assumption might be questionable at some parts of the aortic leaflet. A  $1.5 \times 1.5 \times 0.5 \text{ mm}^3$  block of tissue was modeled in which mechanical properties were assumed to be uniform. It may be questioned whether the assumption of uniform material properties is valid. To what extent the measured mechanical properties at the center of indentation will be affected by this assumption is unknown. In our model, fiber kinematics were assumed to be affine, i.e. fiber deformation equals deformation of the surrounding matrix. Collagen fiber visualization techniques should be developed for real-time monitoring of the fiber distribution during an indentation experiment, see for example Billiar and Sacks (1997). This will enable the verification of the assumption of affine fiber kinematics. Other assumptions included frictionless contact between indenter and tissue, and between tissue and glass plate (Figure 2.2). These assumptions will be taken into account when designing the experimental set-up, for example by quantifying the effect of lubricant addition at the desired regions of frictionless contact.

In the current approach, the model fit is as good as the functional form that is chosen 'a priori'. Ideally, the functional form should follow directly from the experimental data (e.g. Humphrey et al. (1990)). The constitutive model in this study was based on work by Holzapfel et al. (2000). Although this model is very well capable of describing the (biaxial) mechanical behavior of porcine native aortic leaflets (Billiar and Sacks, 2000a; Driessen et al., 2005a), the authors would like to point out that the proposed approach is not limited to this particular model. Any type of structurally-based model may be applied. In the current study, an exponential stress-strain law was used to describe the nonlinear behavior of the collagen fibers. Alternatively, fiber recruitment functions may be used (Sacks, 2003; Lanir, 1983) to account for this nonlinearity. The matrix behavior was assumed to be linear Neo-Hookean. Other options include Mooney-Rivlin material models (Mooney, 1940), or the model proposed by Zulliger et al. (2004), which incorporates the contribution of elastin in the matrix behavior. Finally, the fiber distribution was assumed to be Gaussian, with one preferred direction. This may be altered by incorporating multiple preferred fiber directions (Driessen et al., 2005a), or by choosing some other fiber distribution, several have been proposed in a study by Zioupos and Barbenel (1994).

In the present study, indentation tests were all performed under quasi-static conditions. However, the proposed experimental set-up is not limited to that, and in future work, indentation tests may be used to determine viscoelastic properties of planar soft biological tissues as well. Despite the indicated limitations, the proposed set-up has a large potential for the local mechanical characterization of planar biological soft tissues. The combination of numerical and experimental tools provides a deeper insight into the structure-function relationships of the tissue. The feasibility of the proposed approach was demonstrated by a computational study, which serves

---

as an ideal preparation for future indentation experiments.





---

### **Experimental validation: small deformations and isotropy**

---

*An earlier study on a finite element model of the aortic valve leaflet demonstrated that combining force and deformation gradient data and using large deformations, one single indentation test provides sufficient information to characterize the local material behavior. In the current study, indentation tests are performed on PDMS rubbers, to validate the proposed combined numerical-experimental approach. Results are compared to small deformations JKR theory.*

The content of this chapter is based on:

Cox, M.A.J., Driessen, N.J.B., Bouten, C.V.C., and Baaijens, F.P.T. *Mechanical characterization of anisotropic planar biological soft tissues using large indentation: An experimental validation study*. In H. Rodrigues, M. Cerrolaza, M. Doblare, J. Ambrosio, and M. Viceconti, editors, Proceedings of ICCB 2005, pp. 339-350. Lisbon, Portugal, 2005.

### 3.1 Introduction

The typical highly nonlinear and anisotropic behavior of soft tissues (Clark, 1973; Lanir and Fung, 1974b; Humphrey, 2002), puts high demands on their mechanical characterization. Therefore, sophisticated experimental techniques need to be developed to determine these (local) mechanical properties. In this study, the focus will be on a method for the characterization of planar soft biological tissues, such as skin, mitral valve, or aortic heart valve leaflet material. Although a topic of extensive research for the last few decades, mechanical characterization of planar biological soft tissues remains far from trivial. The highly nonlinear behavior puts high demands on the resolution as well as the range of (e.g. force) measurement set-ups. The presence of prestresses and stretches in the *in vivo* situation, complicates the definition of a stress-free reference configuration. Furthermore, biological tissues are often inhomogeneous in nature, which necessitates a method for the *local* determination of mechanical properties. Traditionally, the main focus point of research has been on the determination of *global* mechanical properties, using uniaxial (Clark, 1973; Ghista and Rao, 1973) or biaxial (Lanir and Fung, 1974a,b; Vito, 1980; Billiar and Sacks, 1997, 2000b) tensile testing. However, uniaxial tensile tests do not provide sufficient information to fully map the anisotropic material behavior (Fung, 1973; Chew et al., 1986; May-Newman and Yin, 1995; Billiar and Sacks, 2000a), although one study by Lanir et al. (1996) suggested the combination of two separate perpendicular uniaxial tests, performed in a biaxial test set-up. Biaxial tensile experiments are difficult to perform, and boundary effects limit the test region to a small central portion of the tissue (Nielsen et al., 1991). In addition, as mentioned before, tensile testing in general only applies to the determination of global mechanical properties. The interested reader is referred to some extended reviews on the multiaxial mechanical testing of planar biological materials (Sacks, 2000; Sacks and Sun, 2003).

*Local* mechanical properties of biological soft tissues have been obtained mostly by indentation tests (Gow and Vaishnav, 1975; Hori and Mockros, 1976; Gow et al., 1983; Zheng and Mak, 1996; Lundkvist et al., 1997; Han et al., 2003; Ebenstein and Pruitt, 2004). However, mostly linear elastic material properties and infinitesimal deformations have been assumed. In that case Hertz-contact may be applicable, which yields an analytical solution for the force-depth relationship (Hertz, 1881). In 1971, Johnson et al. made an extension to this theory to account for the adhesive forces between two materials in close contact, which is nowadays known as the JKR theory (Johnson et al., 1971). In some special cases, analytical solutions even include nonlinear material properties (Green and Zerna, 1968; Humphrey et al., 1991), and/or finite layer thickness (Hayes et al., 1972; Matthewson, 1981). Costa and Yin showed that for finite indentations of nonlinear materials, the infinitesimal strain theory is no longer valid (Costa and Yin, 1999). In a recent computational study by Cox et al. (2006), it was shown that one single indentation test, combining force and deformation gradient data, provides enough information for local characterization of the aortic valve leaflet, including anisotropic properties. In the current study, experiments are carried out to validate the proposed combined numerical-experimental approach. Indentation tests are performed on PDMS (polydimethylsiloxane) rubbers. Parame-

ter estimation is used to fit a Neo-Hookean material model to the experimental results. Small deformations are applied to enable the validation of the model using JKR theory.

## 3.2 Materials and methods

### 3.2.1 Experimental set-up

A schematic view of the experimental set-up is given in Fig. 3.1. A semi-spherical lens of PDMS rubber was indented in a flat block of the same material. The rubber block was put on a counter plate, that was mounted on an inverted microscope to enable monitoring of deformations. PDMS was chosen as a model material because of its elastic properties, relatively low stiffness and easy handling. Furthermore, by varying the molecular weight between cross-linkers (Li et al., 2004), or by adjusting the amount of dangling chains (defects in the molecular structure) (Amouroux and Leger, 2003), samples could be obtained with a range of elastic moduli. Indentations were applied using a surface force apparatus (Fig. 3.2) developed by

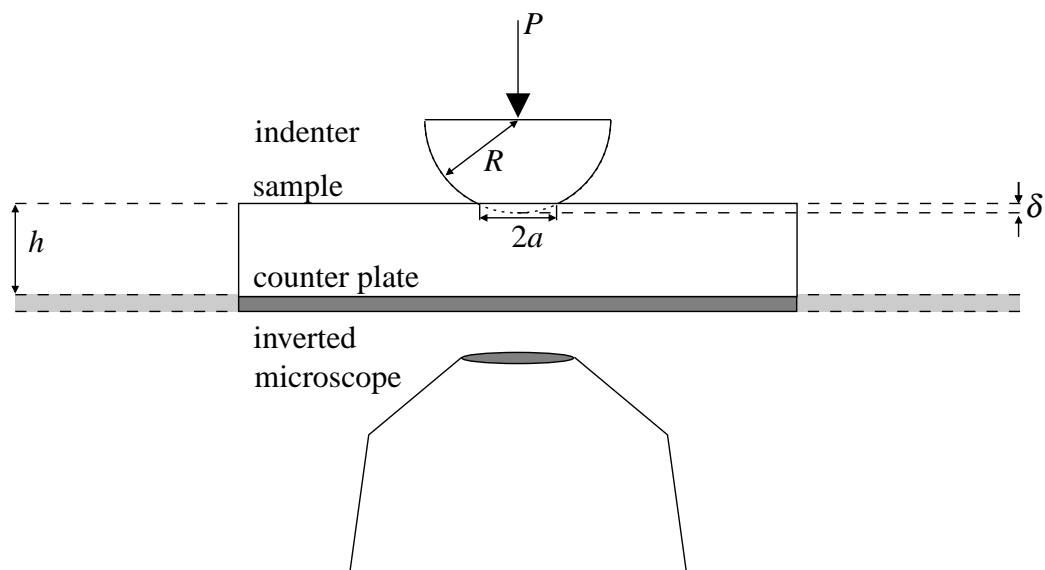


**Figure 3.1:** A schematic view of the simulated set-up. Spherical indentation tests are performed on top of an inverted microscope.

Vaenkatesan et al. (2006) to study the adhesion behavior of polymers. The instrument contains both a vertical and a horizontal leaf-spring. In our case, only the vertical leaf-spring was used, which has a stiffness of 1320 N/m. The motor that controls the leaf-spring can move with speeds ranging from 0.05 to 1500  $\mu\text{m/s}$  with a very low noise floor over the entire speed range. The indenter is attached to a sample holder on the leaf-spring. Deflection of the leaf-spring due to contact of the samples can be measured with a resolution of  $\sim 15$  nm. The force is measured using a capacitive sensor with a resolution of  $\sim 15$   $\mu\text{N}$ . For more details see Vaenkatesan et al. (2006).

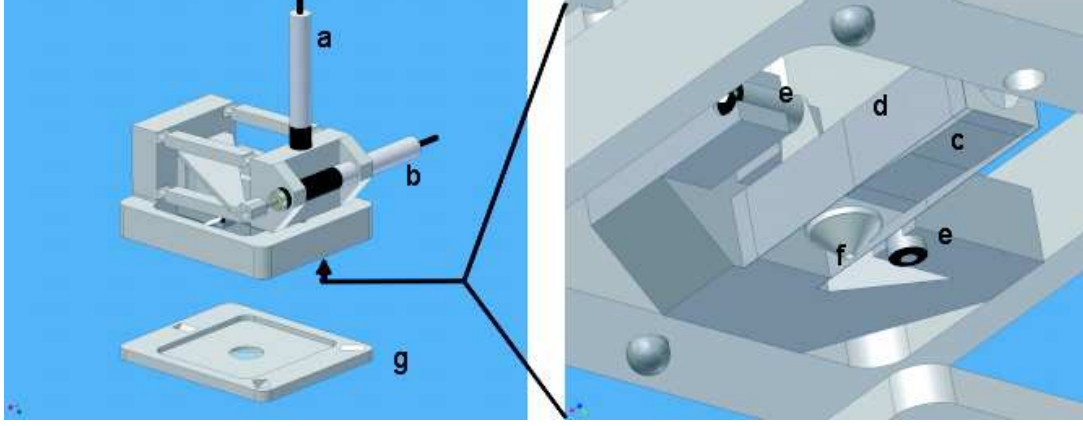


**Figure 3.2:** Drawing of the surface force apparatus. a,b) vertical and horizontal motors, c,d) vertical and horizontal leaf-springs, e) capacitive sensors, f) indenter and g) counter plate.

### 3.2.2 JKR theory

To define the mechanical properties of the test sample, the theory on contact between two smooth elastic bodies as first proposed by Hertz (1881) could be used. Assumptions include axial symmetry, small deformation theory and elasticity. Furthermore, the sample is considered as an infinite halfspace. For two spherical elastic bodies with radii of curvature  $R_1$  and  $R_2$ , and elastic moduli  $E_1$  and  $E_2$ , the system is defined by an equivalent radius of curvature  $R$  and an equivalent modulus  $K$ :

$$\frac{1}{R} = \frac{1}{R_1} + \frac{1}{R_2}, \quad (3.1)$$

$$\frac{1}{K} = \frac{3(1-\nu_1^2)}{4E_1} + \frac{3(1-\nu_2^2)}{4E_2}, \quad (3.2)$$

where  $\nu_1$  and  $\nu_2$  are the Poisson's ratios of the two elastic bodies. In our case, a spherical indenter ( $R_1$ ) was applied to a flat ribbon ( $R_2 = \infty$ ), and therefore, Eq. (3.1) reduces to  $R = R_1$ . The indenter and flat ribbon were made of incompressible PDMS rubber of similar properties, and thus  $E_1 = E_2 = E_{\text{PDMS}}$  and  $\nu_1 = \nu_2 = 0.5$ . Equation (3.2) then reduces to  $K = \frac{8}{9}E_{\text{PDMS}}$ . In case of Hertz-contact, the indentation depth  $\delta_h$  only depends on the radius of contact  $a$ , and the equivalent radius of curvature  $R$ ,

$$\delta_h = \frac{a^2}{R}. \quad (3.3)$$

For very soft materials, adhesive forces between the two bodies come to play a significant role at relatively low loads. Therefore, Johnson et al. (1971) proposed an extension to the Hertz-theory to account for these adhesive forces. According to JKR-theory, the indentation depth  $\delta$  also depends on the indentation force  $P$ . Assuming that the contact radius  $a$  is small compared to the sample thickness  $h$ , ( $\frac{a}{h} < 0.1$ ), the relationship between  $a$ ,  $P$  and  $\delta$  is defined according to Shull (2002):

$$\delta = \frac{a^2}{3R} + \frac{2P}{3aK}. \quad (3.4)$$

When the quantities  $a$ ,  $P$  and  $\delta$  are measured during an indentation test, Eq. (3.4) may be used to estimate the equivalent modulus  $K$ .

### 3.2.3 Finite element model

A three-dimensional finite element model was used to fit the indentation experiments. Under symmetry assumptions, a quarter tissue block was modeled (Fig. 3.3). Sample dimensions and indenter radius were adjusted for each experiment. Contact between the indenter and the test sample disk as well as between the sample and the counter plate was assumed to be frictionless. The indentation was applied in vertical ( $z$ ) direction.

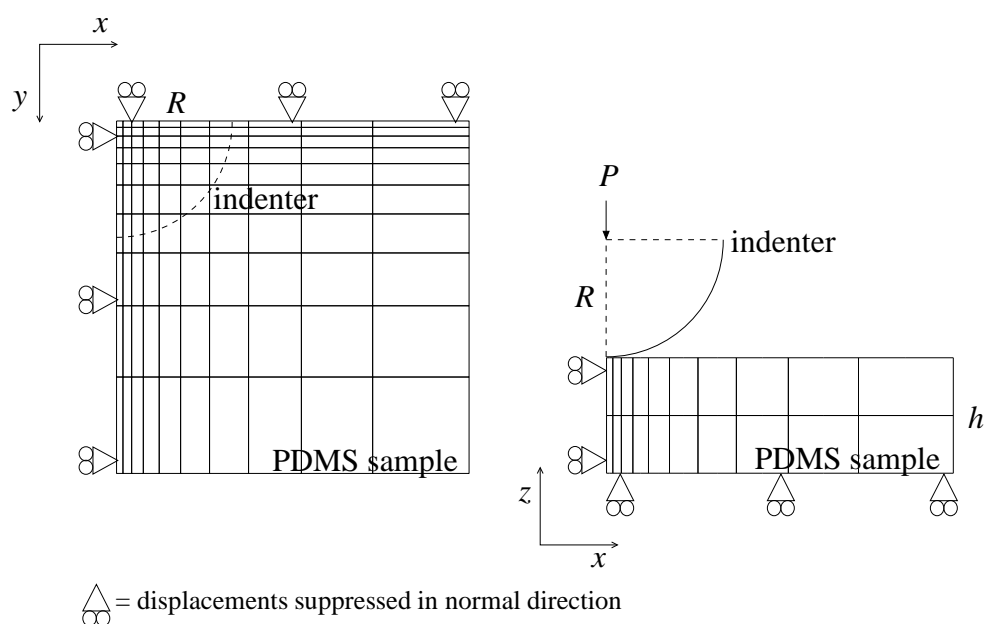


**Figure 3.3:** Top view (left) and front view (right) of the 3D model, showing indenter and boundary conditions.

In the absence of inertia and body forces, the balance of momentum was given by

$$\vec{\nabla} \cdot \boldsymbol{\sigma} = \vec{0}, \quad (3.5)$$

where  $\boldsymbol{\sigma}$  represents the Cauchy stress. Conservation of mass was preserved by the incompressibility condition

$$J - 1 = 0, \quad (3.6)$$

with  $J = V/V_0 = \det(\mathbf{F})$ .  $V$  and  $V_0$  denote the volume in current and reference configuration respectively and  $\mathbf{F}$  is the deformation gradient tensor. The Cauchy stress  $\boldsymbol{\sigma}$  consisted of the hydrostatic pressure  $p$  and the extra stress  $\boldsymbol{\tau}$ ,

$$\boldsymbol{\sigma} = -p\mathbf{I} + \boldsymbol{\tau}, \quad (3.7)$$

where  $\mathbf{I}$  represents the unity tensor. The material behavior was described with an incompressible Neo-Hookean model,

$$\tau = G(\mathbf{B} - \mathbf{I}), \quad (3.8)$$

where  $G$  is the shear modulus. The left Cauchy-Green deformation tensor  $\mathbf{B}$  was given by  $\mathbf{B} = \mathbf{F} \cdot \mathbf{F}^T$ .

The elastic modulus of the PDMS sample was estimated by fitting the model to an experimental force-indentation curve. In the indentation experiments, both indenter and sample were deformable bodies. In the computational model however, the indenter was modeled as a rigid body. This should be corrected for when fitting the model to the experimental results. Since we can assume that JKR theory is valid under given circumstances, we can use it to determine what the equivalent modulus  $K$  would be in case of a rigid indenter ( $E_1 = \infty$ ). From Eq. (3.2) follows that  $\frac{1}{K} = \frac{3(1-\nu_2^2)}{4E_2}$  and thus  $K = \frac{16}{9}E_2$ . This shows that the equivalent modulus of a system with a rigid indenter is two times higher. The best fit between model and experiment is obtained when the equivalent moduli are equal. Therefore the sample stiffness  $E_2$  that is found in the computational model is two times lower than the actual stiffness of the PDMS sample:  $E_{\text{PDMS}} = 2E_2$ . The elastic modulus  $E_2$  of the sample was derived from the shear modulus according to

$$E_2 = 2G(1 + \nu_2), \quad (3.9)$$

and thus, the modulus of the PDMS sample was given by  $E_{\text{PDMS}} = 2E_2 = 6G$ .

### 3.3 Results

Indentation tests were performed with three different samples of PDMS rubber. The sample thickness  $h$  was equal to 1 mm in all cases, and the radius of curvature  $R$  of the samples was approximately 2 mm, exact values can be found in Table 1. Differences in stiffness resulted from differences in molecular weight between cross-linkers. Deformation was applied in one loading and unloading cycle, with a speed of  $0.2\mu\text{m/s}$ , and up to a maximum of 2.5% of the sample thickness. Indentation depth  $\delta$  and force  $P$  were measured with the surface force apparatus. An inverted microscope was used in transmission mode to determine the radius of contact  $a$ . With these data, the equivalent modulus  $K$  was estimated according to Eq. (3.4). For consistency with the calculations for the finite element model, only the unloading curve was used in the estimation of  $K$ . The force-indentation curve was predicted very well by the JKR theory (Fig. 3.4). The resulting elastic moduli  $E_{\text{PDMS}}$  of the test samples are given in Table 3.1.

Loading and unloading curves for the PDMS samples were almost identical, as expected for a linear elastic material. Main differences were found at low indentation depths. While loading the sample, a sudden drop was observed in the indentation force near an indentation depth of zero. This is explained by adhesive forces that occur when two elastic bodies are in the proximity of touching each other. During unloading, adhesive forces make that the sample and indenter stay in contact, even for negative indentation depths (Fig. 3.4). In the finite element

**Table 3.1:** Material parameters for the three test samples. From left to right: indenter radius of curvature  $R$ , elastic moduli  $E_{\text{JKR}}$  and  $E_{\text{FEM}}$  according to JKR and model respectively, and the deviation between model and JKR theory.

sample	$R$ [mm]	$E_{\text{JKR}}$ [MPa]	$E_{\text{FEM}}$ [MPa]	deviation [%]
1	2.020	0.49	0.39	-20%
2	1.947	0.55	0.47	-15%
3	1.898	0.93	0.73	-22%

model, Neo-Hookean material behavior was assumed. Since the Neo-Hookean material model does not account for adhesive forces, a correction was made to the data prior to fitting of the computational model. The unloading force-indentation curve was used since the adhesive effects were less abrupt. It was shifted such that the minimum force was located at the origin and negative indentation depths were ignored. The shear modulus  $G$  was estimated by fitting the model to the experimental data. The shifted force-indentation curves and the model fit are shown in Fig. 3.4. Again, there was a very close match between model predictions and experimental results. The resulting elastic moduli are given in Table 3.1. Compared to JKR theory, the finite element model underestimated the elastic modulus by approximately 20%.



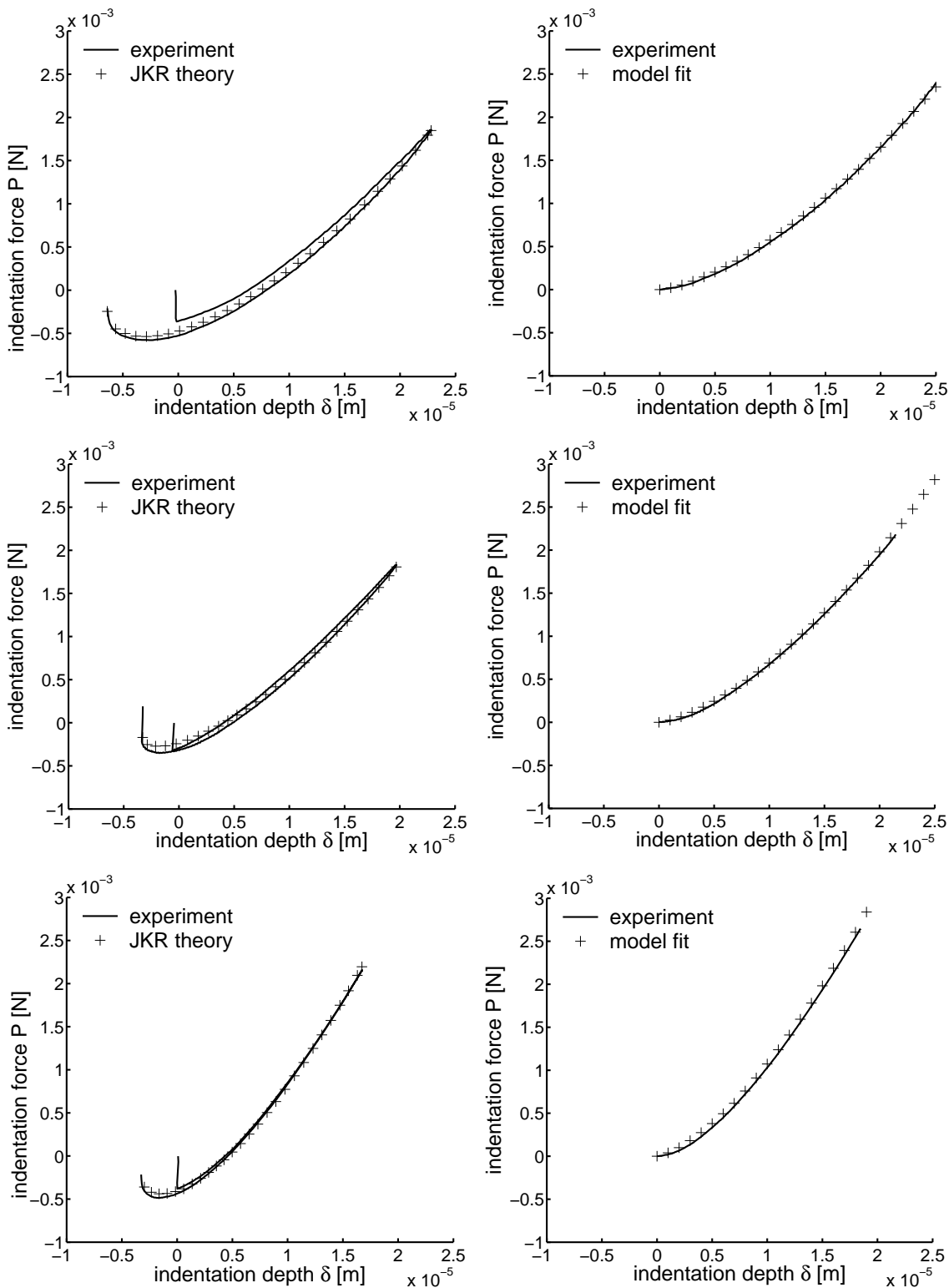


**Figure 3.4:** Left column: Force-indentation curves for three different PDMS samples subjected to one loading-unloading cycle (solid line). The unloading curve is fit by JKR theory (+). Right column: Shifted force-indentation curves (unloading part, solid line). The curve is fit by a Neo-Hookean model (+).

### 3.4 Discussion

In a previous publication (Cox et al., 2006), an indentation experiment was proposed for characterization of local, anisotropic and nonlinear mechanical properties of planar soft biological tissues, with a specific aim at the aortic valve leaflet. It was shown that one single spherical indentation test provides sufficient information for characterization of the mechanical behavior. Large deformations were applied (60% global indentation) and anisotropy was revealed by looking at the deformation gradient of the tissue during indentation. In the present study, the proposed combined numerical-experimental approach was validated. A surface force apparatus (Vaenkatesan et al., 2006) was used to indent a slab of PDMS rubber with a semi-spherical lens of the same material. PDMS rubber was chosen because of its linear elastic material properties. Samples of different stiffness were obtained by adjusting the molecular weight between cross-linkers (Li et al., 2004). Elastic moduli were estimated from the indentation experiments by JKR theory, and by the proposed finite element model using Neo-Hookean material behavior. Since JKR theory only holds for relatively small deformations, maximal indentation depths were up to 2.5% of the sample thickness. The elastic moduli that were found, were well in range with data reported in literature (Amouroux and Leger, 2003). Compared to JKR theory, the estimated elastic moduli of the finite element model were approximately 20% lower. This is well within the range that is found in literature when comparing currently used methods. The Neo-Hookean material model does not incorporate adhesive forces, which was taken into account by shifting the force-indentation curve prior to fitting. This may be an explanation for the underestimation of the stiffness. However, since the absolute value of the adhesive force is independent of the maximal indentation depth, the relative error caused by the adhesive forces will be much smaller when large deformations are applied. Another explanation for the difference may be that in the experiment, two deformable bodies were used, while the finite element model assumed the indenter to be rigid. This was corrected for in the determination of the equivalent modulus  $K$ . However, experiments should be repeated using a rigid indenter to verify these results. Furthermore, experiments should be conducted for large deformations. Results may be validated for example by comparing them to uniaxial or biaxial tensile tests. Contact between indenter and sample, and between sample and supporting base was assumed to be frictionless. By adding lubricants to the test set-up, the influence of these assumptions may be investigated. Since PDMS is completely isotropic, the feasibility of deformation gradients in the test sample for determination of material anisotropy has not yet been tested. Therefore, in future, indentation tests should be applied to fiber-reinforced model materials. As a next step, validation experiments may be carried out on native porcine leaflets. On these specimens, several assumptions can be tested. In (multi)axial testing, preconditioning by multiple loading-unloading cycles is often necessary to obtain reproducible mechanical behavior. This probably applies to large indentation testing as well. Experiments are needed to elucidate the effects of preconditioning. In addition, the mechanical response of biological soft tissues is viscoelastic of nature. It may be tested what indentation rate should be applied to minimize these viscoelastic effects. It should be noted that using the proposed set-up, it is possible to quantify the viscoelastic na-

ture of biological materials as well. This may be a topic of future research.

Summarizing, although more validation experiments need to be carried out in the near future, the proposed model correlates well with small deformation theory for known model materials. This provides further proof that the combined numerical-experimental approach, as described in Cox et al. (2006), serves as an excellent tool for the characterization of local mechanical properties of planar soft biological tissues.

---

# Experimental validation: large deformations and anisotropy

---

*In the current chapter full experimental validation is provided. First, indentation tests with varying indenter sizes are performed on linear elastic PDMS rubbers and compared to tensile tests on the same specimens. For the second step, tissue constructs are engineered using uniaxial or equibiaxial static constrained culture conditions to create test tissues with different anisotropy. Indentation tests are performed to quantify these anisotropic properties.*

The content of this chapter is based on:

Cox, M.A.J., Driessen, N.J.B., Boerboom, R.A., Bouten, C.V.C., and Baaijens, F.P.T. *Mechanical characterization of anisotropic planar biological soft tissues using finite indentation: experimental feasibility*. J. Biomech., 41(2):422-429, 2008.

## 4.1 Introduction

Tissue engineered heart valves (TEHV) offer a promising alternative to current replacement strategies, e.g., synthetic or bioprosthetic heart valves (Mol and Hoerstrup, 2004; Hoerstrup et al., 2000). TEHV have the ability to grow, repair and remodel *in vivo*, which is especially important for pediatric patients. In the TE approach, autologous cells are seeded on a biodegradable carrier. Chemical and mechanical stimuli are applied in a bioreactor system during culturing to induce tissue formation. Mechanical conditioning is an important tool for improvement of the properties of the construct during *in vitro* culturing (Mol et al., 2003). Although TEHV do show anisotropic material behavior after 4 weeks of culturing in a bioreactor (Mol et al., 2006), the exact mechanisms are unknown. Ideally, mechanical conditioning should be used as a tool to improve *and* control the evolution of the structural behavior of TEHV towards the typical inhomogeneous and anisotropic morphology of the native valve leaflets. The highly nonlinear, anisotropic and inhomogeneous mechanical properties of native heart valve leaflets are largely determined by a mesostructural collagen fiber network. The collagen network is a hammock-like structure, with parallel bundles starting from the commissures and diverging to a branching network of fibers in the belly of the leaflet (Sauren, 1981; Doehring et al., 2005). Sacks et al. (1998) demonstrated a regional variance in collagen fiber alignment for porcine aortic valves using small angle light scattering (SALS). Also model predictions by Driessen et al. (2008) indicate high alignment in the commissural (edge) region and a more disperse distribution in the belly (center) of the leaflet. Finally Mirnajafi et al. (2006) recently quantified the flexural properties of native porcine leaflets and they found that the effective stiffness of the commissural region is at most one-third of the effective stiffness of the belly region. Thus, a method for mechanical characterization of TEHV should be able to measure nonlinear, local and anisotropic mechanical properties. Mostly, mechanical testing of planar biological tissues is performed by (multi)axial tensile testing. However, uniaxial tensile tests do not provide sufficient information for a full characterization of the anisotropic properties of the leaflet (Billiar and Sacks, 2000a), while biaxial tensile experiments are difficult to perform, and boundary effects limit the test region to a small central portion of the tissue (Nielsen et al., 1991). For both methods, the determination of local mechanical properties is non-trivial. Local mechanical properties of biological soft tissues have been obtained mainly by indentation tests, (e.g., Gow and Vaishnav (1975); Hori and Mockros (1976); Gow et al. (1983); Zheng and Mak (1996)). A disadvantage of these tests is that most often linear elastic material properties and infinitesimal deformations are assumed. In that case Hertz-contact is applicable, which yields an analytical solution for the force-indentation depth relationship (Hertz, 1881). In some special cases, analytical solutions even include nonlinear material properties (Humphrey et al., 1991) and finite layer thickness (Hayes et al., 1972). Costa and Yin (1999) showed that for finite indentations of nonlinear materials, as is the case for soft biological tissues, the infinitesimal strain theory is no longer valid. Therefore combined numerical-experimental techniques have been adopted for mechanical characterization of biological tissues using an indentation test, (e.g., Lei and Szeri (2007); Erdemir et al. (2006); Delalleau et al. (2006)). In this approach, one or more material

parameters are estimated by fitting a numerical model to the experimental force-indentation data. To determine anisotropic material properties, direction-dependent information has to be extracted from the indentation test. This may for example be done by simultaneously indenting and stretching the material (Karduna et al., 1997). Another option is the approach by Bischoff (2004), who showed that using several tests with asymmetric indenters, anisotropic tissue behavior may be revealed. In addition to that, a recent study by Cox et al. (2006) showed that by combining force and deformation gradient data, one single indentation test provides sufficient information for local characterization of the aortic valve leaflet, including anisotropic properties. In a follow-up study experimental validation was carried out for small deformations (Cox et al., 2005).

The current study aims at demonstrating the feasibility of this approach for finite deformations and anisotropic material properties. A quantitative validation is performed by comparing indentation tests with varying indenter sizes on rubber materials to uniaxial tensile tests on the same materials. As demonstrated by Costa et al. (2003) and Thomopoulos et al. (2005) for uniaxial tissue strips, static loading (i.e., constraining without applying additional strains) during *in vitro* culture leads to collagen orientation along the constrained direction. Therefore, to demonstrate the feasibility for anisotropic materials, small rectangular and circular cardiovascular tissue constructs are cultured *in vitro* using uniaxial and equibiaxial static culture conditions, respectively. Parameter estimation is used on the indentation test results to characterize the mechanical behavior of the tissue. It is hypothesized that the uniaxial samples will exhibit anisotropic behavior, while the equibiaxial samples will behave in a more isotropic way. Although the method is developed for characterization of TE cardiovascular tissues, it is emphasized that it can be applied to planar soft biological tissues in general.

## 4.2 Materials and methods

### 4.2.1 Experiments

Indentations were applied using a surface force apparatus developed by Vaenkatesan et al. (2006). In the current study an indentation speed of 0.01 mm/s was used for all tests. Although both PDMS rubbers and biological tissues are viscoelastic in nature, no different force-indentation response was found for lower speeds (data not shown) for both types of samples. Therefore, quasistatic loading conditions were assumed. Spherical sapphire indenters were used, which were available in diameters of 1, 2 and 3 mm. For each test preconditioning was applied until results were reproducible. The whole setup was mounted on top of an inverted confocal laser scanning microscope (CLSM) to enable visualization of the deformations in the bottom plane of the sample during indentation. Digital Image Correlation (DIC) was used to quantify these deformations.

## PDMS rubbers

Indentation tests and uniaxial tensile tests were performed on flat PDMS (polydimethylsiloxane) samples (PP1-ZPFN, Gelest Inc, USA). PDMS was chosen as a model material because of its elastic properties, easy handling and relatively low stiffness, comparable to soft biological tissues. Samples ( $n=5$ ) were cured overnight in a rectangular teflon mold. A dumbbell-shaped cutting tool was used to obtain the final specimen geometry with a minimal width of 5.0 mm and a length of 35 mm. Two consecutive indentation tests were applied to the center of the samples, up to 30% of the sample thickness. To validate the indentation results, uniaxial tensile tests were performed on a tensile testing device (Zwick Z010, Zwick GmbH, Germany) with a 20N load cell (Kap-Z, AST GmbH, Germany) at a constant speed of 0.2 mm/s until break or slip, which in all cases occurred at  $>100\%$  strain. The first 50% of the strain curve was used for the mechanical characterization.

## Tissue engineered constructs

Cardiovascular tissues were engineered *in vitro* from human myofibroblast cells seeded on a PGA (polyglycolic acid, Cellon, Luxembourg) and fibrin scaffold. Uniaxial strips ( $24 \times 5 \times 1$  mm<sup>3</sup>) were created by attaching the ends of the scaffold to a supporting membrane using Silastic MDX4-4210 (Dow Corning, USA). Equibiaxial constructs were created by attaching circular scaffolds (diameter 13 mm, thickness 1 mm) at all sides to the supporting membrane. The tissue constructs were cultured for 20 days (5% CO<sub>2</sub>, 37°C). More details on the tissue culture may be found in Boerboom et al. (2007a). Prior to testing, the samples were stained overnight with a fluorescent CNA35-OG488 probe to enable visualization of the collagen fibers (Nash-Krahn et al., 2006; Boerboom et al., 2007b). Samples were detached from the supporting membrane and placed upside down onto the glass plate of the inverted CLSM to enable visualization of the top layer of the construct. Indentation was applied to the center of the samples using a 2 mm indenter. Two consecutive indentation tests were performed. Confocal images (magnification 10x, excitation 488nm, emission 500nm high-pass) were taken of the bottom plane of the sample during the indentation test.

### 4.2.2 Numerical model

A three-dimensional finite element model was used to fit the indentation experiments (Cox et al., 2006). Under symmetry assumptions, a quarter sample block was modeled. Sample dimensions and indenter radius were adjusted for each experiment to mimic the test geometry and boundary conditions. Contact between the indenter and the test sample was assumed to be frictionless. The indentation was applied in the vertical ( $z$ ) direction (Fig. 4.1).

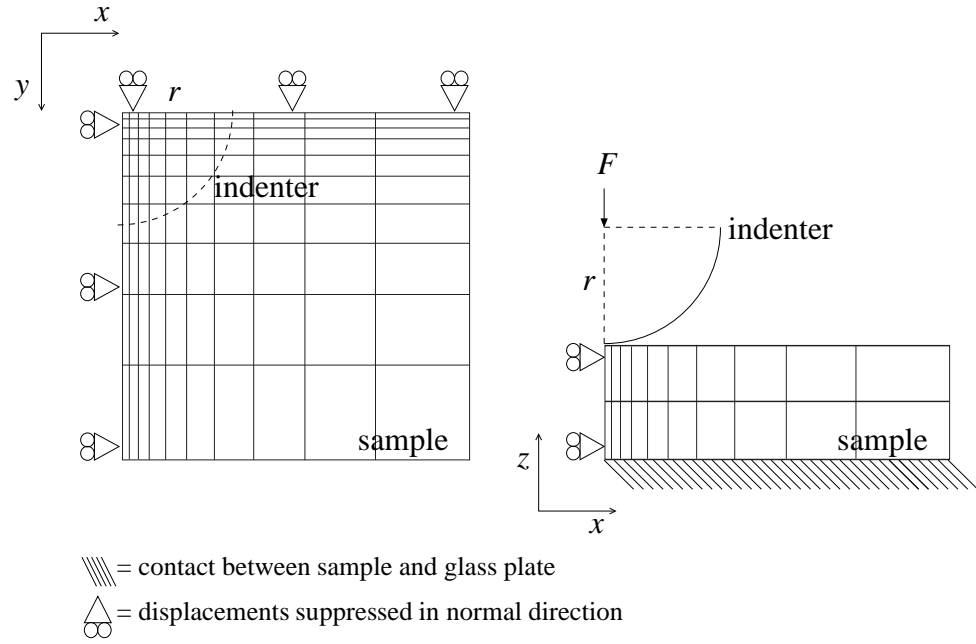


**Figure 4.1:** Top view (left) and front view (right) of the 3D model, showing indenter and boundary conditions. The indenter radius  $r$  and indentation force  $F$  are also indicated.

## PDMS rubbers

The material behavior of the PDMS rubbers was described with a linear incompressible Neo-Hookean model, in which case the extra stress  $\tau$  was given by

$$\tau = G(\mathbf{B} - \mathbf{I}), \quad (4.1)$$

where  $G$  is the shear modulus,  $\mathbf{B}$  the left Cauchy-Green deformation tensor and  $\mathbf{I}$  represents the unity tensor. All displacements were constrained at the bottom plane to mimic stick between the PDMS sample and the bottom plate.

## Tissue engineered constructs

The TE constructs were modeled as incompressible fiber-reinforced composite materials (Driessen et al., 2005b). The extra stress  $\tau$  was split into an isotropic matrix part and an anisotropic fiber part,

$$\tau = \tau_{\mathbf{m}} + \sum_{i=1}^{N_f} \phi_f^i \left[ \psi_f^i - \vec{e}_f^i \cdot \tau_{\mathbf{m}} \cdot \vec{e}_f^i \right] \vec{e}_f^i \vec{e}_f^i. \quad (4.2)$$

The isotropic matrix stress  $\tau_{\mathbf{m}}$  was modeled as an incompressible Neo-Hookean material with matrix shear modulus  $G_m$ . An in-plane fiber distribution was modeled as a summation over a discrete number of fibers  $N_f$ , with a volume fraction  $\phi_f$  in the direction  $\vec{e}_f$ . A  $\pi$ -periodic version of the normal distribution function was used for the fiber volume fractions (Gasser et al., 2006;



Driessen et al., 2008):

$$\phi_f^i(\gamma_i) = A \exp \frac{\cos[2(\gamma_i - \alpha)] + 1}{\beta}. \quad (4.3)$$

In Eq. (4.3),  $\gamma_i$  was defined as the fiber angle with the x-direction (Fig. 4.1) in undeformed configuration. The fiber dispersion parameter  $\beta$  determines the amount of anisotropy. When  $\beta$  approaches zero, the fiber distribution becomes uniaxial, while for large  $\beta$  a uniform distribution is obtained. The scaling factor  $A$  was used to ensure that the total fiber volume fraction equals  $\phi_{tot}$ . To allow the use of quarter symmetry, the main fiber direction  $\alpha$  was always chosen along the x-direction for the simulations, i.e.,  $\alpha = 0^\circ$ . Finally the constitutive equation for the fiber stress  $\psi_f$  was defined according to Holzapfel et al. (2000),

$$\psi_f = 2k_1 \lambda_f^2 (\lambda_f^2 - 1) \exp(k_2 (\lambda_f^2 - 1)^2). \quad (4.4)$$

In Eq. (4.3),  $k_1$  is a stress-like parameter and  $k_2$  a non-linearity parameter. The fiber stretch is denoted by  $\lambda_f$ . For the TE constructs, contact between the construct and the supporting glass plate was assumed to be frictionless.

### 4.2.3 Parameter estimation

For the coupling between experiments and simulations, a mixed numerical experimental approach was used (Meuwissen, 1998; Cox et al., 2006). A quadratic objective function  $\Omega$  was defined which was minimized in the parameter estimation algorithm:

$$\Omega(\underline{\theta}) = [\underline{m} - \underline{h}(\underline{u}, \underline{\theta})]^T \underline{V} [\underline{m} - \underline{h}(\underline{u}, \underline{\theta})]. \quad (4.5)$$

The column  $\underline{m}$  contained experimental data while  $\underline{h}(\underline{u}, \underline{\theta})$  contained the model predictions, that were a function of the material parameters  $\underline{\theta}$  and the prescribed boundary conditions  $\underline{u}$ . Finally,  $\underline{V}$  is a positive definite symmetric weighting matrix. More details on the implemented estimation algorithm can be found in Cox et al. (2006).

### PDMS rubbers

In case of the PDMS rubbers, the shear modulus  $G$  was the only material parameter. For the indentation test,  $\underline{m}$  contained the indentation forces  $F_{exp}$  measured as a function of indentation depth. The model predictions  $\underline{h}$  contained the modeled indentation force  $F_{mod}$ . For the tensile test,  $\underline{m}$  contained the Cauchy tensile stresses  $\sigma_{t_{exp}}$ , while  $\underline{h}$  was filled with the modeled Cauchy tensile stresses  $\sigma_{t_{mod}}$ . For a uniaxial tensile test on a linear incompressible Neo-Hookean material  $\sigma_{t_{mod}}$  is given by

$$\sigma_{t_{mod}} = G(\lambda_t^2 - 1/\lambda_t), \quad (4.6)$$

where  $\lambda_t$  denotes the tensile stretch.

## Tissue engineered constructs

For the TE constructs five material parameters may be defined, namely the matrix shear modulus  $G_m$ , the fiber distribution parameters  $\alpha$  and  $\beta$ , and the fiber mechanical parameters  $k_1$  and  $k_2$ . The total fiber volume fraction  $\phi_{tot}$  was chosen to be constant and equal to 0.5 (Driessen et al., 2007). To determine displacement fields from the confocal images during indentation, Digital Image Correlation (DIC) was performed using the commercially available imaging software package ARAMIS (GOM mbH, Germany). Local deformation gradients and strain fields were obtained from the 2D displacement fields using the algorithm by Geers et al. (1996). The assumption was made that the material behavior is stiffest in the main fiber direction. Therefore, the main fiber orientation  $\alpha$  was determined *directly* from the experimental results as the direction of least deformation. For in plane deformations, this equals the second principal strain direction. The experimental results were averaged over all four quadrants to obtain quarter symmetry. The four remaining parameters  $G_m$ ,  $\beta$ ,  $k_1$  and  $k_2$  were determined by the parameter estimation algorithm. The measurement column  $\underline{m}$  consisted of three quantities: the measured indentation force  $F_{exp}$ , the anisotropy index  $AI$  and the Green-Lagrange strain perpendicular to the main fiber direction,  $\varepsilon_y$ . The  $AI$  was defined as  $AI = \frac{\lambda_y}{\lambda_x} - 1$ , where  $\lambda_y$  and  $\lambda_x$  are the stretch perpendicular and parallel to the main fiber direction, respectively. For isotropic behavior  $AI$  equals zero, while  $AI$  increases for more anisotropic samples. Since the  $AI$  is a relative measure, the absolute measure  $\varepsilon_y$  was used in the estimation process as well.

## 4.3 Results

### 4.3.1 PDMS rubbers

The computational model fitted the indentation tests very well (Fig. 4.2a). The resulting shear moduli were  $175 \pm 9$  kPa,  $181 \pm 14$  kPa and  $183 \pm 12$  kPa for the 1 mm, 2 mm and 3 mm diameter indenter, respectively, resulting in an overall mean of  $179 \pm 12$  kPa. Independent student T-tests revealed no significant differences between two consecutive indentation tests ( $p > 0.5$ ) and one way ANOVA revealed no significant differences between the different indenter radii ( $p > 0.5$  for all cases), (Table 4.1). The tensile tests were also well characterized by the model (Fig. 4.2b). From the tensile tests, a shear modulus of  $174 \pm 14$  kPa was found. An independent student T-test revealed no significant differences between the indentation and tensile tests ( $p > 0.9$ ), (Table 4.1).

### 4.3.2 TE constructs

Strain fields resulting from the DIC are illustrated for both samples in Fig. 4.3. Arrows indicate the first and second principal strain directions and are scaled with their magnitude. For the uniaxial sample (sample A), a clear preferred direction of deformation was observed, while the

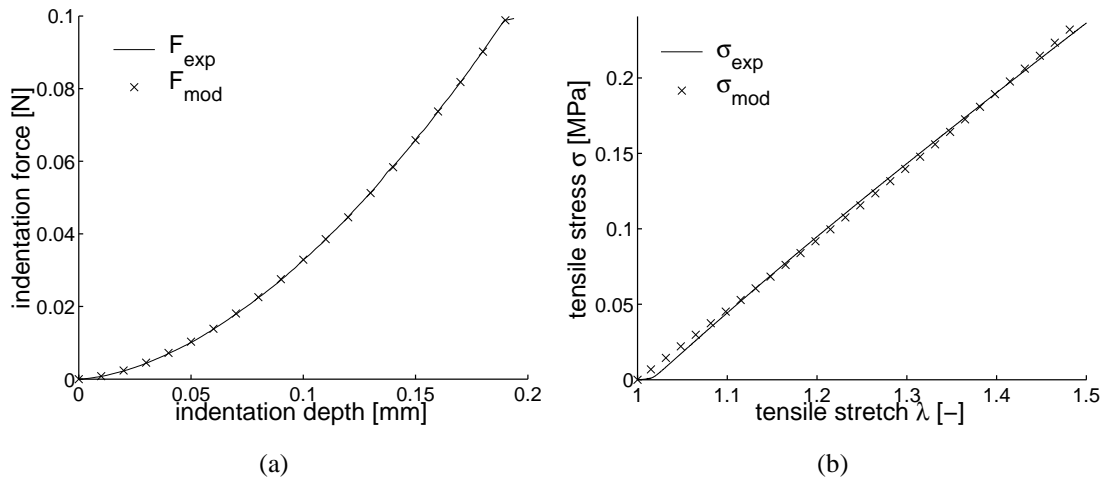


**Figure 4.2:** Representative fit between experiment (solid line) and model (cross) for the indentation tests (left) and the uniaxial tensile test (right) on PDMS samples.

indentation test diameter	$G$ (mean $\pm$ std) [kPa]	
	test 1	test 2
1mm (n=5)	174 $\pm$ 11	175 $\pm$ 9
2mm (n=5)	180 $\pm$ 15	181 $\pm$ 16
3mm (n=5)	182 $\pm$ 15	185 $\pm$ 9
mean	179 $\pm$ 12	
tensile test (n=5)	174 $\pm$ 14	

**Table 4.1:** Shear moduli of PDMS rubbers determined from indentation tests and tensile tests. Independent student T-tests revealed no significant differences between two consecutive indentation tests ( $p > 0.5$ ). One way ANOVA revealed no significant differences between the different indenter radii ( $p > 0.5$  for all cases). Finally, an independent student T-test revealed no significant differences between the indentation and tensile tests ( $p > 0.9$ ).

equibiaxial sample (sample B) demonstrated a more uniform deformation pattern. Figure 4.4 illustrates the fit between the experimental and numerical results for sample A and B. To illustrate the results for the  $AI$  and  $\epsilon_y$ , these were averaged for each measured indentation depth. As expected, the  $AI$  was highest for sample A. For sample B, a fixed value was chosen for the shear modulus  $G_m = 1.0$  kPa. Not fixing  $G_m$  led to very low values for  $G_m$ , which caused instabilities in the estimation algorithm. All estimated material parameters are summarized in Table 4.2. In Fig. 4.5a, the estimated fiber distributions are visualized for both samples. To illustrate the effect of the estimated fiber parameters  $k_1$  and  $k_2$ , the fiber stress is plotted as a function of fiber stretch (Fig. 4.5b).

To investigate the correlation between the parameters, an estimated correlation matrix was used, as described by Cox et al. (2006). The diagonal terms of this matrix are equal to one; off-diagonal terms close to  $[-1, 1]$  indicate high correlation between the corresponding param-

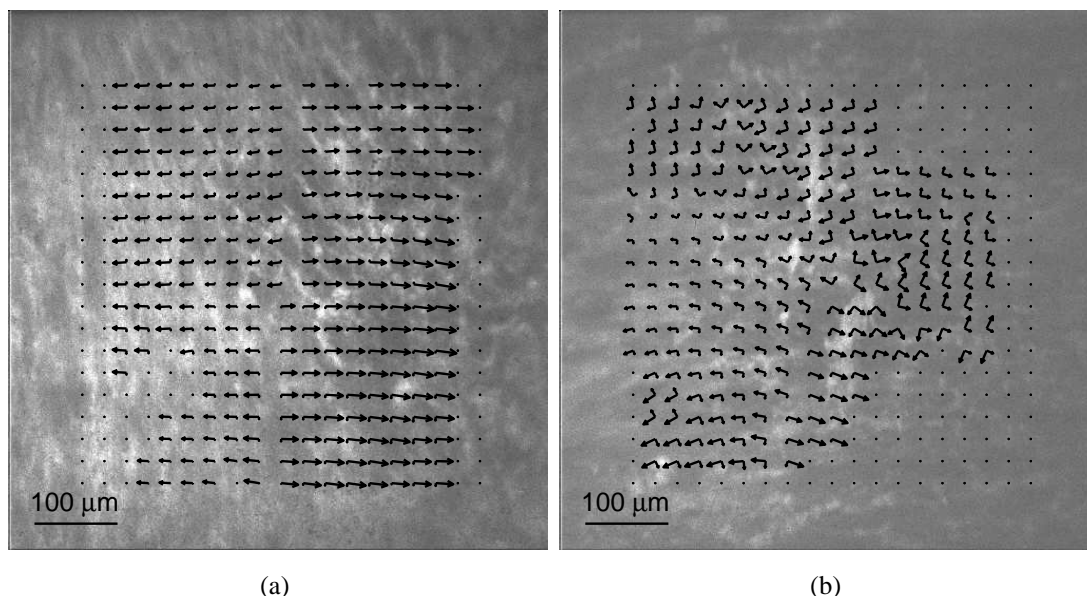


**Figure 4.3:** Confocal images at 25% indentation of sample A (left) and sample B (right). The arrows indicate first and second principal strain directions, arrow length is proportional to the strain magnitude. Black dots indicate points that were lost in the image correlation process.

Parameter	Uniaxial			Equibiaxial		
	Initial	Final		Initial	Final	
		Test 1	Test 2		Test 1	Test 2
$G$ [kPa]	1.0	3.3	3.4	1.0	1.0	1.0
$k_1$ [kPa]	10	6.2	13	20	74	96
$k_2$ [-]	10	86	74	5.0	0.99	0.79
$\beta$ [-]	1.5	0.070	0.11	3.0	3.0	3.3
$\alpha$ [°]	-	0	-2	-	-19	-21

**Table 4.2:** Initial and final parameter estimates for the TE constructs.

eters. Estimated correlation matrices for sample A and B are given in Table 4.3 and 4.4. High correlation was found between parameters  $k_1$ ,  $k_2$  and  $\beta$ .

	$G$	$k_1$	$k_2$	$\beta$
$G$	1.00	0.23	-0.10	0.06
$k_1$	0.23	1.00	-0.95	0.91
$k_2$	-0.10	-0.95	1.00	-0.99
$\beta$	0.06	0.91	-0.99	1.00

**Table 4.3:** Correlation between the estimated parameters for the uniaxially strained sample A.

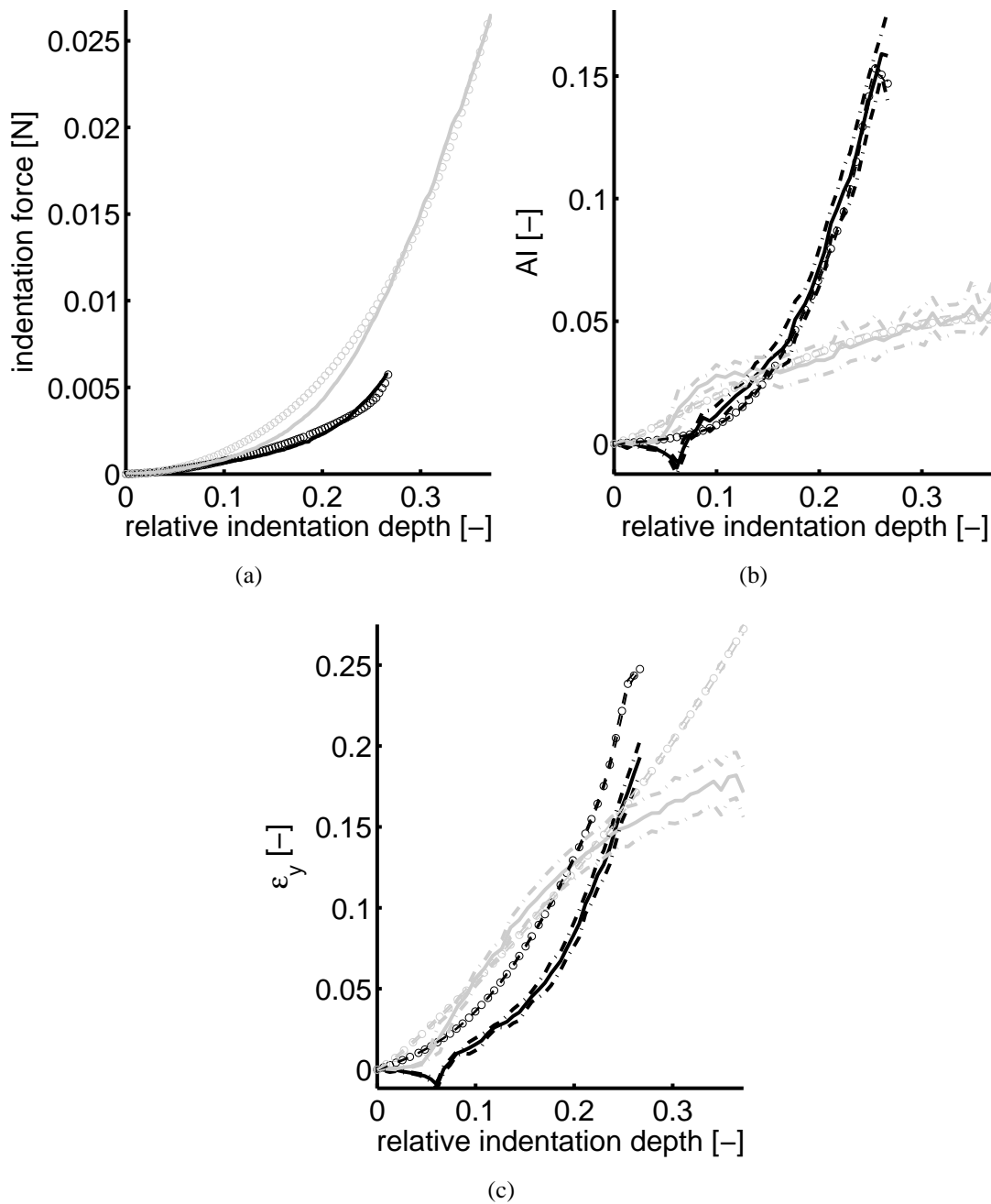


**Figure 4.4:** Experimental results (solid line) and model fit (o) for sample A (black) and sample B (gray) as a function of relative indentation depth. Left: Indentation force [N], middle: Anisotropy Index ( $AI$ ) [-] and right: strain perpendicular to main fiber direction ( $\epsilon_y$ ) [-]. For the  $AI$  and  $\epsilon_y$  the average value is plotted for each indentation depth. The spread is indicated by mean  $\pm$  standard deviation for the experimental results (dash-dotted lines) and the model fit (dashed lines).

## 4.4 Discussion

A new combined numerical-experimental method for mechanical characterization of planar soft biological tissues using finite indentations (Cox et al., 2006) was experimentally validated us-

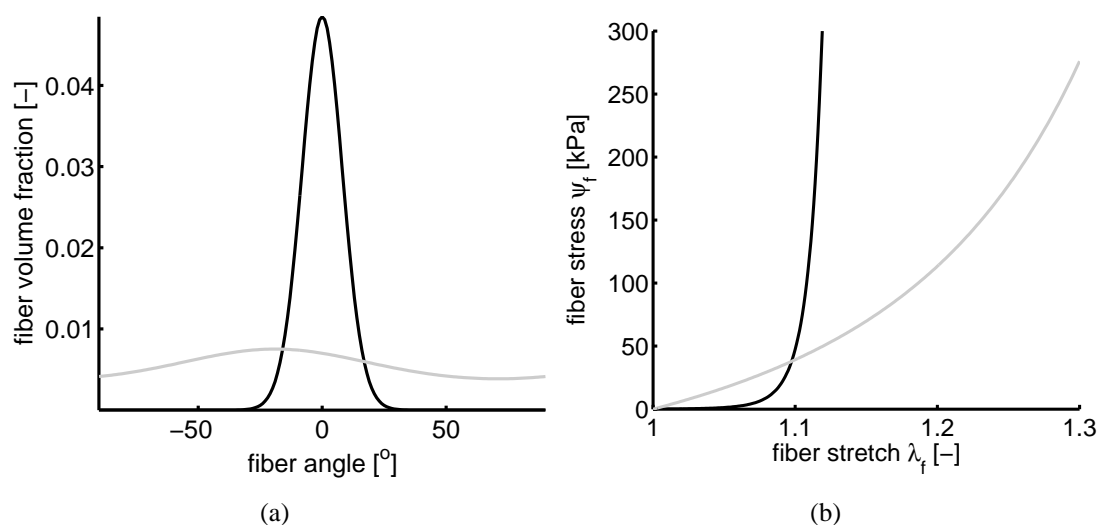


**Figure 4.5:** Estimated fiber distribution (left) and fiber stress-stretch behavior (right) for sample A (black,  $\alpha_A = 0^\circ$ ,  $\beta_A = 0.07$ ;  $k_{1A} = 6.2$  kPa,  $k_{2A} = 87$ ) and sample B (gray,  $\alpha_B = -19^\circ$ ,  $\beta_B = 3.0$ ;  $k_{1B} = 74$  kPa,  $k_{2B} = 0.99$ ).

	$k_1$	$k_2$	$\beta$
$k_1$	1.00	-0.87	0.70
$k_2$	-0.86	1.00	-0.81
$\beta$	0.70	-0.81	1.00

**Table 4.4:** Correlation between the estimated parameters for the equibiaxially strained sample B.

ing PDMS rubbers and tissue engineered constructs. For the PDMS rubbers, identical estimated shear moduli were found for indentation tests using three different indenter diameters and uniaxial tensile tests (Table 4.1). The model fitted both indentation and tensile tests very well (Fig. 4.2).

To demonstrate the feasibility of the approach for anisotropic materials, cardiovascular tissue constructs were cultured in vitro using either uniaxial (sample A) or equibiaxial (sample B) static constrained conditions. It was hypothesized that the collagen fibers in the uniaxial samples would orient along the strain direction, leading to anisotropic behavior, while the equibiaxial samples would behave in a more isotropic way. Deformation patterns during an indentation test showed a clear difference between the two protocols (Fig. 4.3) and the inverse characterization confirmed a narrow fiber distribution ( $\beta_A = 0.08$ ) oriented along the strain direction ( $\alpha_A = 0^\circ$ ) for sample A and a more isotropic distribution ( $\beta_B = 3.3$ ,  $\alpha_B = -18^\circ$ ) for sample B (Fig. 4.5a). Interestingly, the apparent fiber mechanics of the two samples were very different as well (Fig. 4.5b). Sample A was characterized by a low initial stiffness, followed by a highly nonlinear increase at a fiber stretch of 1.1. The fiber mechanics of sample B was more linear, whereas the initial stiffness was much higher. It needs to be emphasized that the number of samples that was used is limited. Therefore no conclusions may be drawn on the actual mechanical

properties of the TE constructs. The only conclusion that can be drawn is that the mechanical behavior of samples with different amounts of anisotropy was captured well with the proposed approach. A study including more samples is necessary for a quantitative comparison of the different culture conditions.

Because of the highly adhesive properties of PDMS, contact between the rubber samples and the underlying glass plate was modeled by fixing all in-plane movement at the bottom of the sample. Results confirm that this was a good assumption. Contact between the indenter and the rubber sample, however, was assumed to be frictionless. Since no significant differences were found between the indentation and tensile tests, the error introduced by this assumption seems minimal. Since the TE constructs were wet during testing, no friction was assumed between sample and bottom plate, and between sample and indenter. The presence of experimental friction would lead to an overestimation of the in plane strains by the numerical model. Although Fig. 4.4 shows that the mechanical behavior of the tissue constructs was well characterized by the model,  $\epsilon_y$  was indeed overestimated, which may indicate that the experimental friction was not equal to zero. Furthermore, the spread in  $AI$  and  $\epsilon_y$  for each indentation depth was higher in the experiments (Fig. 4.4). Analysis of the experimental data revealed no correlation between the strain values and the distance to the center of indentation. Therefore, it is suggested that this spread originates from local inhomogeneities in e.g., tissue structure or friction. In future work, experimental friction should be minimized, for example by adding a hydrophobic coating to the indenter and to the baseplate. Another option would be to include friction in the model (Belytschko et al., 2000). However, this is not a trivial task and would mean introduction of one or more extra parameters in the mechanical characterization, which is not desirable at this moment.

Repeated indentation tests showed good reproducibility for the TE constructs. Except for  $k_1$  in the uniaxial sample, final parameter estimates of the second indentation test were within 20% of the first. Different initial parameter sets did not always result in exactly the same final parameters for the uniaxial sample, although the difference in residual error was less than 2%. Apparently, the larger spread in the experimental data resulted in a similar fit for a range of parameter combinations. This may also explain the high correlation between the parameters  $k_1$ ,  $k_2$  and  $\beta$  (Table 4.3 and 4.4). However, in the computational study by Cox et al. (2006), high correlation was also found when the model was fit to artificially generated experimental data, even though the correct parameters were found by the model. Therefore, the high correlation is likely to be partially inherent to the constitutive model.

An important model assumption is uniform mechanical behavior throughout the thickness of the construct. Histology and 2-photon microscopy of comparable TE constructs (Boerboom et al., 2008) revealed that both collagen content and collagen organization are higher in the top layer of the construct. The effect of this on the indentation force and in plane strains remains unclear. Computational modeling incorporating depth-variations may provide more insight, but is beyond the scope of the current study. It is remarked that in (multiaxial) tensile tests generally a uniform thickness is assumed as well. However, tensile tests are performed in the tissue plane, while indentation tests are applied perpendicular to it. Therefore, the implications of

this assumption are probably different for both types of tests. To investigate these implications, indentation tests should be validated against one or more uniaxial tensile tests on the same sample. A suitable model material could be pericardium, since it is readily available, and the anisotropic in plane mechanical behavior has been well described (e.g., Zioupos and Barbenel (1994); Sacks and Chuong (1998); Trowbridge (1989)).

To conclude, the numerical-experimental approach by Cox et al. (2006) was successfully validated for different indenter diameters and large deformations of PDMS rubbers. Furthermore the feasibility of the approach for anisotropic materials was demonstrated using engineered cardiovascular tissues. It was shown that static constraining during *in vitro* culture may be used to tune the anisotropic in plane mechanical behavior of TE constructs. In future work we will quantify this relationship. This method will provide more insight into the (development of) mechanical properties of tissue engineered heart valves. Furthermore, the effect of multiaxial, dynamic straining protocols during tissue culture will be investigated (Boerboom et al., 2007a). These results will be used to optimize straining protocols, ultimately leading to a tissue engineered heart valve that is able to withstand the high pressures and strains that occur in the *in vivo* environment. Although the specific aim of the research is heart valve tissue engineering, it is emphasized that the approach proposed in this study may be applied to planar soft biological tissues in general.





---

# Application: mechanical characterization of Bio-Artificial Muscle

---

*The mechanical properties of soft biological tissues in general and early stage engineered tissues in particular limit the feasibility of conventional tensile tests for their mechanical characterization. In this chapter the feasibility of our approach is demonstrated with indentation tests applied to Bio-Artificial Muscle (BAM) tissue. BAMs are cultured in vitro with or without cells to quantify the effect of the cells on the passive transverse mechanical properties.*

The content of this chapter is based on:

Cox, M.A.J., Gawlitta, D., Driessen, N.J.B., Oomens, C.W.J., and Baaijens, F.P.T. *The non-linear mechanical properties of soft engineered biological tissues determined by finite spherical indentation*, Comp. Meth. Biomech. & Biomed. Engng., 11(5), 585-592, (2008)

## 5.1 Introduction

The prevalence of pressure ulcers, i.e. damaged skin and/or underlying tissue following sustained mechanical loading, remains unacceptably high (Vanderwee et al., 2007). Pressure ulcers may be divided into two categories: superficial wounds, which originate in the skin layers and may progress to deeper tissues, or deep tissue injury (DTI (Donnelly, 2005)) which originates in the deep layers, most often in the skeletal muscle tissue, underneath an intact skin. Once deep tissue injury extends to the skin, a stage III or IV open pressure ulcer has developed (Ankrom et al., 2005). The etiology of pressure ulcers is not yet completely understood. Main hypotheses trying to explain their etiology include ischemia, reperfusion and/or cellular deformation as causal factors. Most probably, the onset of damage occurs due to a combination of these factors. To be able to discriminate between these different phenomena, a range of experimental model systems have been employed, varying from whole rat models (Stekelenburg et al., 2007) to single cell studies (Peeters et al., 2005). Furthermore, computational models become increasingly important (Stekelenburg et al., 2007; Ceelen et al., 2008; Linder-Ganz and Gefen, 2004; Gefen et al., 2005; Breuls et al., 2003a). In the current study, an in vitro muscle model is considered. Bio-Artificial Muscle (BAM) tissue is engineered from muscle derived cells seeded on a gel mixture (Vandenburgh et al., 1996; Bouten et al., 2001; Breuls et al., 2003b; Gawlitta et al., 2007). BAMs have been used to study the combined effects of sustained deformation on the *onset* of tissue damage (Bouten et al., 2001; Breuls et al., 2003b; Gawlitta et al., 2007). Recently, Gawlitta et al. (2007) showed in a compression experiment that the initial damage is caused by compression rather than by oxygen deprivation. Computational models of such an experiment will elucidate the correlation between local stresses and strains and local damage initiation. Knowledge of the mechanical properties of BAMs is vital for accurately predicting the local stress and strain characteristics during a compression experiment. However, the mechanical properties and low structural integrity of BAMs inhibit the use of standard tensile tests for their mechanical characterization. Indentation tests may provide an alternative, (e.g. Gow and Vaishnav (1975); Hori and Mockros (1976); Gow et al. (1983); Zheng and Mak (1996)), although these are often limited to small deformation theory. As shown by Costa and Yin (1999), the infinitesimal deformation theory is no longer valid for finite indentations of non-linear materials, which is typical for soft biological tissues. Therefore, combined numerical-experimental approaches have been employed as well (e.g., Erdemir et al. (2006); Delalleau et al. (2006); Cox et al. (2006); Lei and Szeri (2007)). In these approaches a numerical model is iteratively fitted to experimental results using a parameter estimation algorithm. In the current study, a spherical indentation test is proposed in which finite deformations are applied. The BAMs are modeled as incompressible non-linear Neo-Hookean materials. To demonstrate the feasibility of the proposed approach, the passive mechanical properties of BAMs seeded with cells are compared to BAMs without cells. The resulting material parameters are used to simulate compression experiments on BAMs by Breuls et al. (2003b). Stress and strain distributions are compared qualitatively to the spatial damage variation as observed experimentally. It is emphasized that the proposed method is not limited to the characterization of BAMs, it is ex-

pected to be feasible for the characterization of the non-linear, isotropic mechanical behavior of soft planar biological tissues in general.

## 5.2 Materials and methods

### 5.2.1 Bio-Artificial Muscle

C2C12 murine skeletal fibroblasts (ECACC, Salisbury, UK) were cultured in growth medium in an incubator at 37°C and 5% CO<sub>2</sub>. Growth medium consisted of high glucose DMEM with L-glutamine (Gibco, Breda, The Netherlands), 15% fetal bovine serum (FBS), 2% hepes, 1% non-essential amino acids and gentamicin (all from Biochrom AG, Berlin, Germany). At passage 14 they were harvested and seeded into a mixture of collagen I gel and Matrigel (both BD Biosciences, Alphen a.d. Rijn, The Netherlands). The cell/gel mixture was molded in a Petri dish between two anchoring points, resulting in a rectangular tissue construct ( $\sim 22\text{mm} \times 5\text{mm}$ ). After molding, growth medium was added to the BAMs. After 24 hours the medium was replaced by differentiation medium, thus inducing fusion of the cells into myotubes. Differentiation medium contained 0.4% Ultrosor G (BioSeptra, Cergy-Saint-Christophe, France) instead of FBS. Total culture time was 8 days. For the BAMs without cells the same protocol was used, except that no cells were added to the collagen I/Matrigel mixture. In total 20 BAMs with cells and 12 BAMs without cells were cultured. For a more detailed description of the culture protocol the reader is referred to Gawlitta et al. (2007).

### 5.2.2 Indentation tests

Indentations were applied using a surface force apparatus developed by Vaenkatesan et al. (2006). Indentation force and depth were measured with a resolution of  $\sim 15 \mu\text{N}$  and  $\sim 15 \text{nm}$ , respectively. In the current study a sapphire indenter with a diameter of 2 mm was used at a speed of 0.01 mm/s for all tests. Although biological tissues are generally viscoelastic in nature, no different force-indentation response was found for lower speeds (data not shown). Therefore, quasistatic loading conditions were assumed. Indentation was applied at the center of the sample, up to 80% of the initial specimen thickness.

### 5.2.3 FE model

A three-dimensional finite element model was used to fit the indentation experiments (Cox et al., 2006). Under symmetry assumptions, a quarter sample block was modeled. Sample dimensions and indenter radius were adjusted for each experiment to mimic the test geometry and boundary conditions. Contact between the indenter and the test sample, and between the sample and the supporting glass plate was assumed to be frictionless. The indentation was

applied in the vertical ( $z$ ) direction (Fig. 5.1).

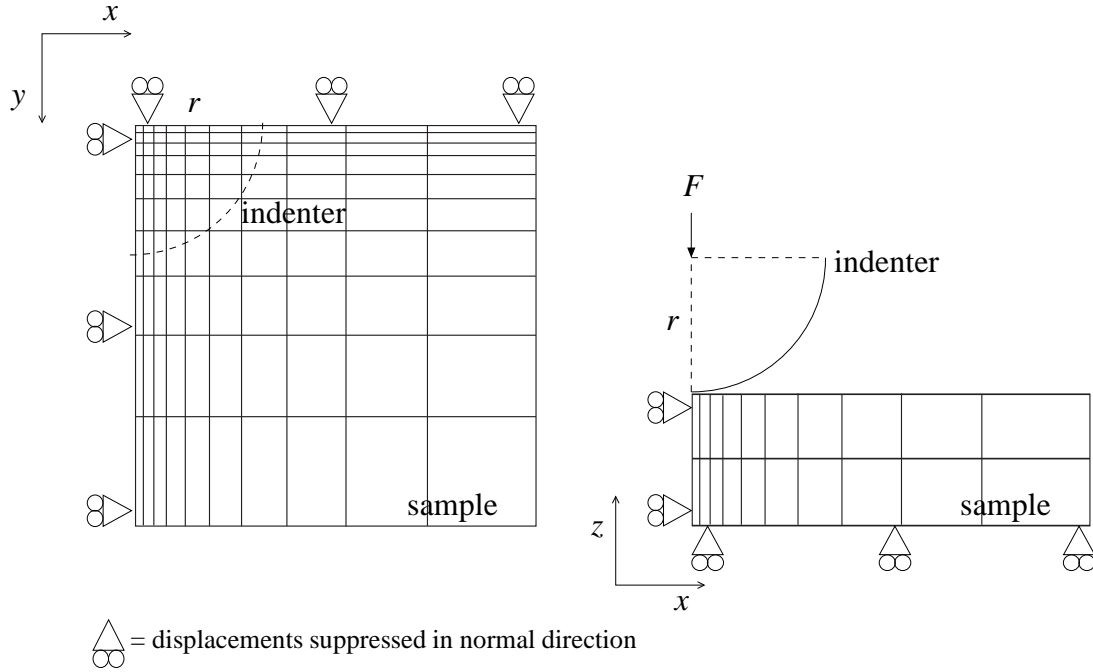


**Figure 5.1:** Top view (left) and front view (right) of the 3D model, showing indenter and boundary conditions. The indenter radius  $r$  and indentation force  $F$  are also indicated.

In the absence of inertia and body forces, the balance of momentum was given by

$$\vec{\nabla} \cdot \boldsymbol{\sigma} = \vec{0}, \quad (5.1)$$

where  $\boldsymbol{\sigma}$  represents the Cauchy stress. Conservation of mass was preserved by the incompressibility condition

$$J - 1 = 0, \quad (5.2)$$

with  $J = V/V_0 = \det(\mathbf{F})$ .  $V$  and  $V_0$  denote the volume in the current and the reference configuration respectively, and  $\mathbf{F}$  is the deformation gradient tensor. The Cauchy stress  $\boldsymbol{\sigma}$  consists of the hydrostatic pressure  $p$  and the extra stress  $\boldsymbol{\tau}$ ,

$$\boldsymbol{\sigma} = -p\mathbf{I} + \boldsymbol{\tau}, \quad (5.3)$$

where  $\mathbf{I}$  represents the unity tensor. The material behavior was described with an incompressible non-linear Neo-Hookean model,

$$\boldsymbol{\tau} = G(\mathbf{B} - \mathbf{I}), \quad (5.4)$$

where the left Cauchy-Green deformation tensor  $\mathbf{B}$  is given by  $\mathbf{B} = \mathbf{F} \cdot \mathbf{F}^T$ . The shear modulus  $G$  was defined according to Driessen et al. (2005c):

$$G = G_0 \left( \frac{\text{tr}(\mathbf{B})}{3} \right)^n, \quad (5.5)$$

where  $G_0$  is the initial shear modulus in reference configuration ( $\mathbf{F} = \mathbf{I}$ ) and  $n$  a non-linearity parameter. Note that for  $n = 0$ , Eq. (5.5) simplifies to  $G = G_0$  which represents standard Neo-Hookean material behavior.

## 5.2.4 Parameter estimation

For the coupling between experiments and simulations, a mixed numerical experimental approach was used (Meuwissen, 1998; Cox et al., 2006). A quadratic objective function  $\Omega$  was minimized in the parameter estimation algorithm:

$$\Omega(\boldsymbol{\theta}) = [\underline{m} - \underline{h}(\underline{u}, \boldsymbol{\theta})]^T \underline{V} [\underline{m} - \underline{h}(\underline{u}, \boldsymbol{\theta})]. \quad (5.6)$$

The column  $\underline{m}$  contains experimental data while  $\underline{h}(\underline{u}, \boldsymbol{\theta})$  contains the model predictions that are a function of the material parameters  $\boldsymbol{\theta}$  and the prescribed boundary conditions  $\underline{u}$ . Finally,  $\underline{V}$  is a positive definite symmetric weighting matrix. More details on the implemented estimation algorithm can be found in Cox et al. (2006). In our case,  $\underline{m}$  contained the experimental indentation force  $F_{\text{exp}}$  as a function of indentation depth, while  $\underline{h}$  contained the modeled indentation force  $F_{\text{mod}}$ . The material parameters to be estimated were  $G_0$  and  $n$ .

## 5.2.5 Compression test simulation

The estimated material parameters for the BAMs with cells were used to simulate compression experiments by Breuls et al. (2003b). In their experiments, BAMs were compressed 50% for 8h using a circular indenter (diameter 5mm). The spatial distribution of dead cells was determined at several time points. In the current study, a quasistatic simulation of these experiments was performed using the average dimensions and material parameters of the BAMs after 8 days of culturing, as determined in the current study. A rectangular mesh of the center of the BAMs was used assuming quarter symmetry. Mesh refinement was applied near the indenter edges. The indenter was modeled as a cylinder (diameter 5 mm) with slightly rounded edges (radius of curvature 0.25 mm) to allow the 50% compression. Frictionless contact was assumed between the indenter and the BAM tissue, and between the BAM tissue and the supporting glass plate.

## 5.3 Results

Figure 5.2 shows an example of a BAM seeded with cells (left) and a BAM without cells (right), both after 7 days of in vitro culturing. For the BAMs with cells, a clear decrease in width due to cell compaction was observed, while the BAMs without cells retained their rectangular shape. The correlation between the model and the experiment was quantified with the mean relative

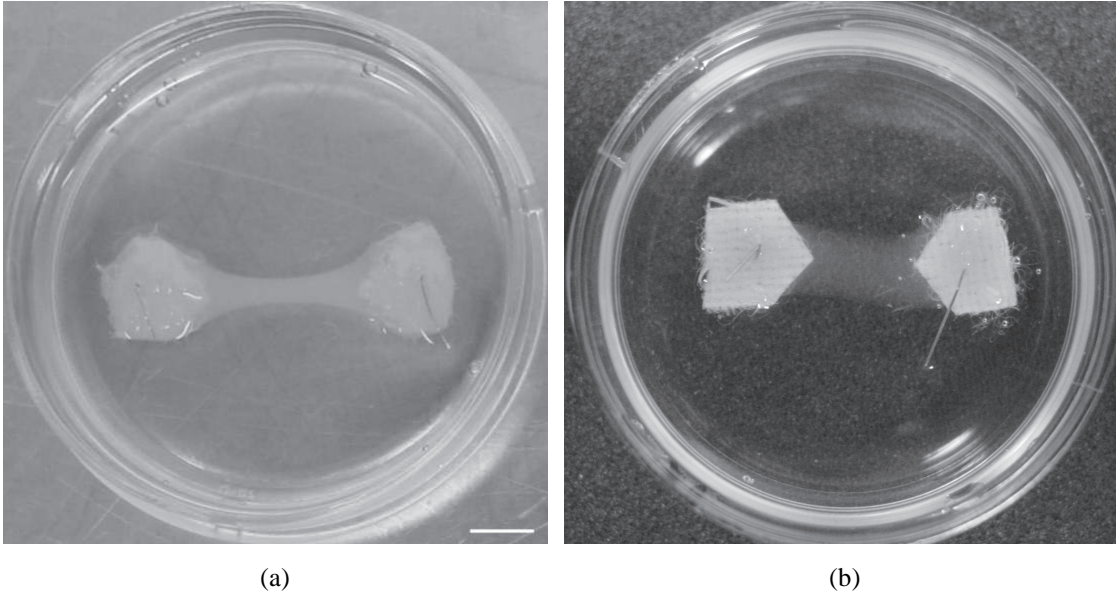


**Figure 5.2:** BAM seeded with cells (left) and without cells (right) after 8 days of culturing.

error (MRE):

$$\text{MRE} = \frac{1}{N} \sum_{i=1}^N \frac{|F_{\text{exp}}(i) - F_{\text{mod}}(i)|}{\bar{F}_{\text{exp}}} \cdot 100\%, \quad (5.7)$$

where  $N$  is the number of experimental data points, and  $\bar{F}_{\text{exp}}$  the mean experimental force. The experimental force indentation curves were fitted well by the numerical model. Figure 5.3 shows the best (top) and worst (bottom) fits for the samples with cells (left) and without cells (right). The overall MRE with cells was 4.0% and without cells 14%. For the BAMs with cells a shear modulus  $G_{0c} = 0.38 \pm 0.12 \text{ kPa}$  and a non-linearity parameter  $n_c = 2.6 \pm 0.8$  were found (mean  $\pm$  standard deviation). For the BAMs without cells,  $G_{0nc} = 0.087 \pm 0.033 \text{ kPa}$  and  $n_{nc} = 0.60 \pm 0.75$  were obtained. Figure 5.4 shows boxplots of the estimated material parameters. As can be seen, the non-linearity parameter  $n_{nc}$  of the BAMs without cells is biased towards zero. In several cases  $n = 0$  was found as final estimate, which is the lower limit of  $n$  in the estimation algorithm. Although  $n < 0$  would result in a better fit, this limit was chosen since  $n < 0$  would represent strain-softening behavior, which is not realistic for biological materials (Fung, 1973). An independent student T-test revealed that the shear modulus was significantly higher for BAMs seeded with cells ( $p < 0.01$ ). Because of the skewed distribution of  $n_{nc}$ , a non-parametric (Wilcoxon rank-sum) test was used to compare the results for the non-linearity parameter. The non-linearity parameter with cells was found to be significantly higher than without cells ( $p < 0.01$ ). Thus, the BAMs with cells were both stiffer and more non-linear than the BAMs without cells.

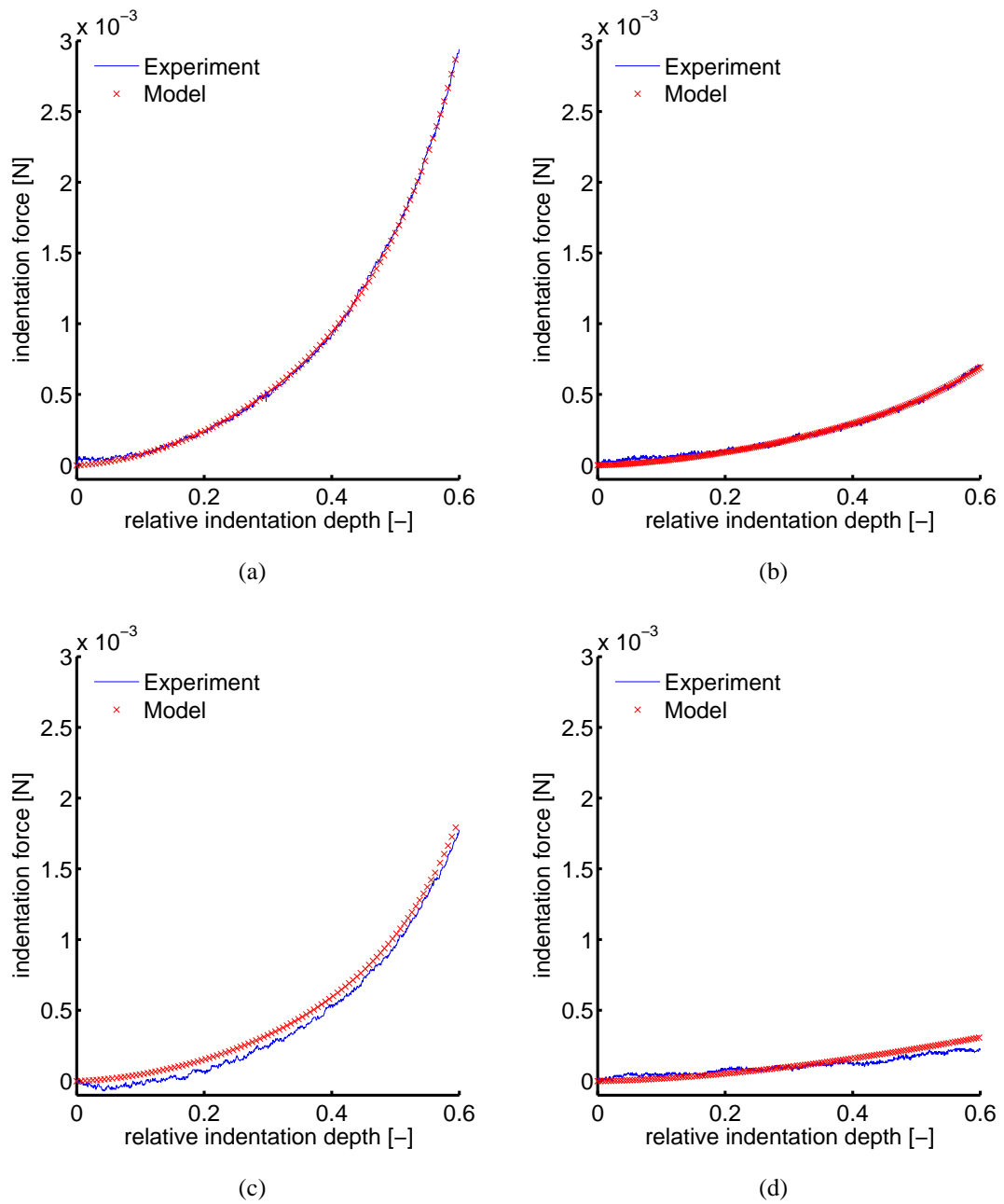


**Figure 5.3:** Best fit (a,b) and worst fit (c,d) between experiment (solid line) and model (cross) for the BAMs seeded with cells (a,c) and without cells (b,d). The MREs for these fits were a) 1.9% b) 5.7% c) 16% and d) 29%.

### 5.3.1 Compression test simulation

The maximal shear stresses and strains at 50% indentation are shown in Fig. 5.5. The indenter contours were clearly visible from the stress and strain patterns. In Fig. 5.6 the stresses and strains are plotted along the long axis of the sample, through the center of indentation to illustrate the spatial variation in more detail. Both stress and strain values decreased slightly from



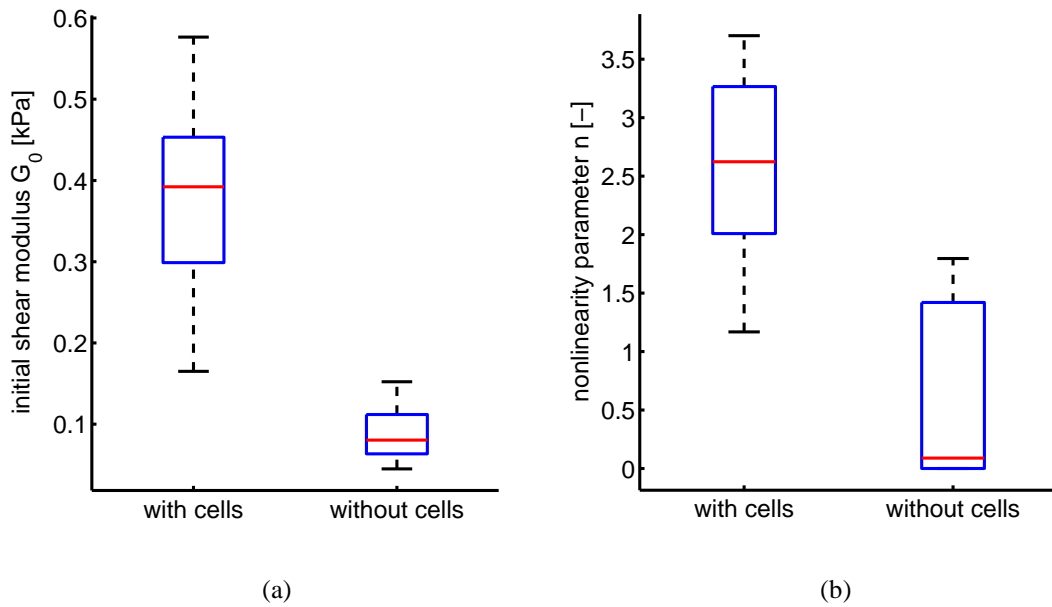


**Figure 5.4:** Boxplots of the estimated parameters shear modulus  $G_0$  (a) and non-linearity parameter  $n$  (b).

the center to a local minimum close to the edge of the indenter. At the edge, a small peak was observed followed by a strong decrease. Due to the non-linear material behavior, these observations were more pronounced for the maximal shear stress. In the compression experiments

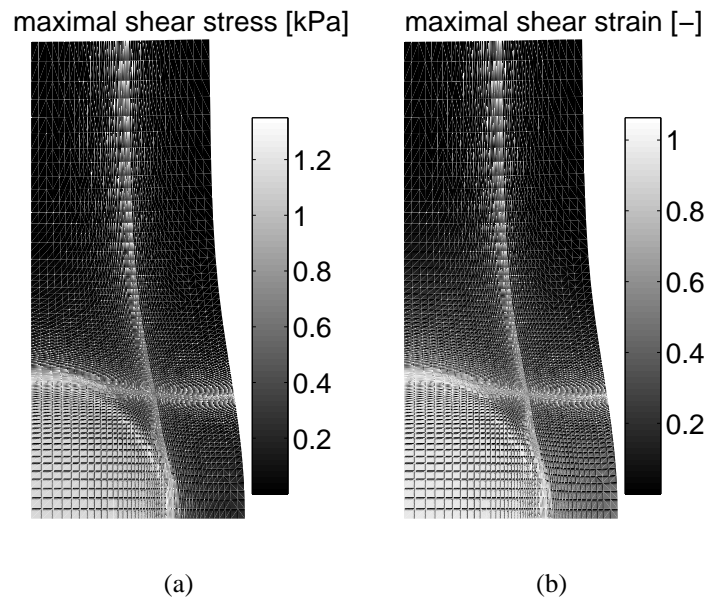


**Figure 5.5:** Simulated maximum shear stress and strain distributions at 50% relative indentation of a BAM with cells.

by Breuls et al. (2003b), a uniform damage distribution was found under the indenter. Further-

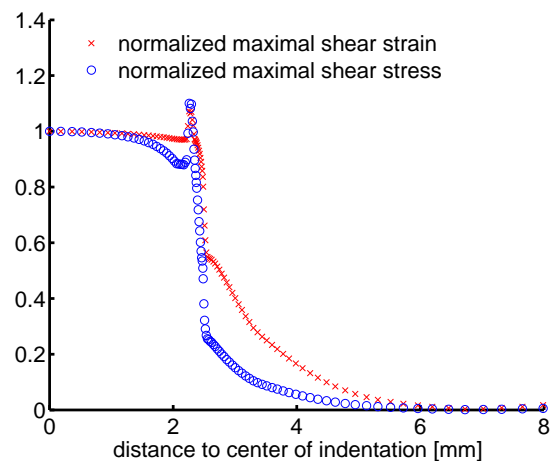
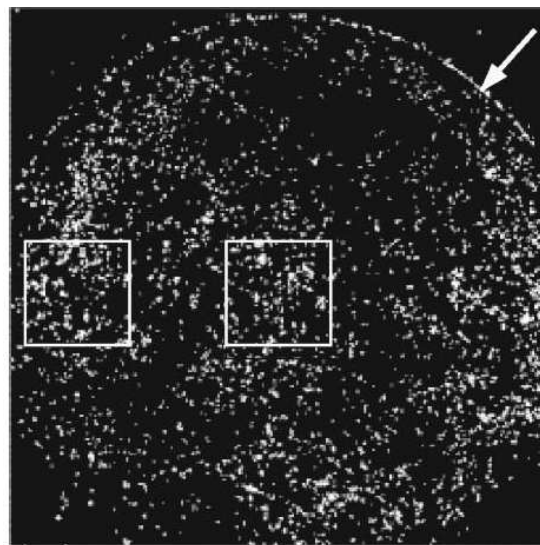


**Figure 5.6:** Simulated maximum shear stress and strain along the long axis of the BAM, starting from the center of indentation.

more, a clear demarcation line was found at the indenter edge (Fig. 5.7). Both observations may



(a)

**Figure 5.7:** The distribution of dead cells in a BAM after 4hrs of 50% compression. Nuclei of dead cells are indicated by the white dots. The edges of the indenter are clearly visible, as indicated by the arrow. Adapted from (Breuls et al., 2003b).

be explained qualitatively by the simulation results. Also, stresses and strains were uniform and high under the indenter, while the demarcation line coincides with the peak stresses and strains at the indenter edge. However, the peak stresses and strains were not much higher than the average values found under the indenter. Therefore, the demarcation line may correlate better with the high stress and strain gradients than with the absolute values at the indenter edge.

## 5.4 Discussion

A combined numerical-experimental approach was used to characterize Bio-Artificial Muscle (BAM) tissue from a finite spherical indentation test. Indentation tests were performed on BAMs seeded with and without cells. Despite their mechanical properties and low structural integrity, the BAMs were well characterized by the computational model (Fig. 5.3). The material behavior was described by two parameters: the initial shear modulus  $G_0$  and the non-linearity parameter  $n$ . Both parameters were significantly higher for the BAMs with cells, thus indicating that the presence of cells during culturing results in stiffer and more non-linear material behavior. The cells had a visible macroscopic effect as well, BAMs seeded with cells showed a decrease in width (compaction) while BAMs without cells largely retained their initial rectangular shape. The mature BAMs consist of a gel mixture and myoblast cells, which are fused into myotubes. It has been shown that the myotubes align between the two anchoring points (Gawlitta et al., 2007). Furthermore, free tissue compaction is allowed but is restricted between the anchoring points. These effects will induce tissue alignment, most probably resulting in anisotropic material properties, which was not taken into account in the model. To enable characterization of the anisotropic mechanical properties, direction-dependent information has to be extracted during the indentation test. Cox et al. (2006) showed in a computational study that the current approach may be used to determine the anisotropic mechanical properties as well, provided that confocal imaging is used to track deformation gradients in the bottom plane of the sample during the indentation test.

Frictionless contact was modeled between the indenter and the tissue, and between the tissue and the supporting glass plate. This assumption seems reasonable, since tests were performed under wet circumstances. Still, it is important to minimize friction during testing. This may be realized for example by adding a hydrophobic coating to the indenter and the glassplate.

Indentations were applied up to 80% of the tissue thickness, resulting in very high local tissue deformations. Although no sustained loading was applied, this may have resulted in tissue damage in some cases. This may also explain that BAMs without cells appeared to demonstrate strain-softening behavior, which was not incorporated into the model. Still, reasonable fits were obtained for all samples, although a large spread was found for the non-linearity parameter of the BAMs without cells.

The parameters found in the current study may provide input to computational models of muscle tissue damage development. To illustrate this, compression experiments on BAMs by Breuls et al. (2003b) were simulated using the averaged parameters of the BAMs with cells. Stress and strain distributions showed good qualitative agreement with the spatial distribution of dead cells found by Breuls et al. (2003b). The current model is a first step towards better understanding of the processes involved in the onset of deformation-induced damage. The model may be improved by incorporating damage laws (Ceelen et al., 2008; Breuls et al., 2003a; Linder-Ganz and Gefen, 2004) or by embracing mechanically induced collagen remodeling laws (Driessen et al., 2003, 2008; Baek et al., 2006). Another option would be to include tissue compaction to predict residual stresses and strains resulting from this phenomenon (Barocas and Tranquillo,

1997). Thus, valuable information will be obtained on the different aspects that play a role in the evolution of deformation-induced tissue damage.



---

# Tissue engineered heart valves develop native-like structural properties *in vitro*

---

*In this chapter, the local structural mechanical properties of human tissue engineered heart valves are characterized with the indentation test approach described in the previous chapters. Heart valves are engineered for four weeks in a bioreactor, where they are subjected to different mechanical loading conditioning protocols. The goal of this study is to determine to what extent tissue engineered heart valves develop native-like structural properties in vitro, and how this can be regulated using mechanical conditioning protocols.*

The content of this chapter is based on:

Cox, M.A.J., Kortsmits, J., Driessen, N.J.B., Bouten, C.V.C., and Baaijens, F.P.T. *Tissue engineered heart valves develop native-like structural properties*. Tissue Engineering Part A, 2009. Under review.

## 6.1 Introduction

Annually 6.000 children are born in Europe with a heart valve defect, often resulting in valve replacement (Hoffman and Kaplan, 2002; Dolk, 2005). Currently existing heart valve replacements lack the ability to grow, repair and remodel and therefore no sufficient lifetime solution exists for these children. In case of aortic valve failure, the Ross procedure, where the aortic valve is replaced with the patient's pulmonary valve, has been the procedure of choice for the last decades (Ross, 1967; Oswald, 1999). Although this leads to an autologous solution for the aortic site, a replacement valve is still needed at the pulmonary position. In addition, long term studies indicate that the pulmonary valve eventually can not adapt sufficiently to the aortic environment (Carr-White et al., 2001; Klieverik et al., 2007; Takkenberg et al., 2009). Heart valve tissue engineering seeks to provide an optimal solution by creating a living, autologous heart valve that has the capacity to grow, repair and remodel (Schoen and Levy, 1999; Rabkin and Schoen, 2002; Haverich, 2004; Mol and Hoerstrup, 2004; Vara et al., 2005). For a tissue engineered heart valve to be functional, it should be able to withstand the high physiological pressures and flows that occur in vivo. Nature's solution for this challenge can be found in the complex collagen fiber architecture of the native aortic valve leaflet (Fig. 6.1 a).

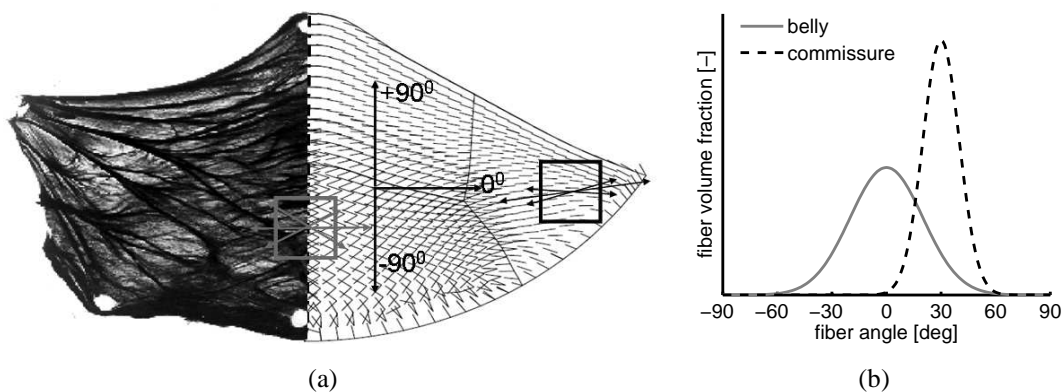


**Figure 6.1:** a) Native valve leaflet fiber distribution (left) and prediction based on remodeling algorithms (right), adapted from Sauren (1981); Driessen et al. (2008), and b) schematic representation of native fiber distributions in belly (solid) and commissures (dashed).

Thick parallel collagen fiber bundles run from the commissures towards a more branched, hammock-like network in the belly region (Sauren, 1981; Doehring et al., 2005). In Fig. 6.1 b, the collagen fiber architecture of the leaflet is schematically represented by a moderately aligned circumferentially orientated fiber distribution curve ( $0^\circ$ ) in the belly, and a highly aligned fiber distribution in the commissures, with main orientation towards the belly ( $\sim 30^\circ$ ). Note that this is a qualitative representation of the native fiber distribution as, to the best of our knowledge, quantitative data on local fiber distribution are scarce. Due to this collagen fiber network the native valve mechanical properties are highly inhomogenous, anisotropic and nonlinear. Besides the fiber distribution, the mechanical properties of the individual collagen fibers are important for the mechanics of the valve. Driessen et al. (2008) successfully predicted the native fiber

distribution with a collagen remodeling algorithm based on the strain distributions during the diastolic loading phase (closed configuration) of the cardiac cycle. An important assumption in their model is homogeneity in the collagen fiber mechanics, i.e. one single fiber in the belly will have the same intrinsic mechanical properties as one single fiber in the commissures.

Mol et al. (2005a) demonstrated with their Diastolic Pulse Duplicator (DPD) that by mimicking the diastolic phase *in vitro* in a bioreactor, indeed strong tissue engineered heart valves were obtained. Following this approach, they recently cultured human heart valves that showed sufficient mechanical strength to withstand *in vivo* aortic demands (Mol et al., 2006). Uniaxial tensile tests in two orthogonal directions demonstrated that the leaflets were stiffer in circumferential than in radial direction (Driessen et al., 2007), and thus showed mechanical anisotropy, similar to native valve leaflets. It was also demonstrated using tissue engineered strips that large strains are beneficial for developing strong tissue (Mol et al., 2003).

Although all these results indicate that global mechanical conditioning can be used to regulate/steer the global mechanical properties towards native tissue, it is unclear whether the local structural organization of the leaflet is developing towards the local fiber structure typical for native valve leaflets. The current study aims to provide experimental proof for some of the model assumptions and hypotheses of Driessen et al. (2008) by coupling global conditioning protocols to local tissue mechanics and tissue structure. It is hypothesized that 1) tissue engineered heart valves will develop a native-like fiber distribution if subjected to diastolic loading protocols *in vitro* in a bioreactor, 2) increased loading during culture will lead to increased collagen fiber alignment and 3) intrinsic collagen fiber mechanics will be similar in the belly and in the commissures.

Since it is not straightforward to assess local tissue structure in a (multiaxial) tensile test, indentation tests combined with confocal imaging are applied to the belly and commissural region of tissue engineered valve leaflets. Cox et al. (2006) demonstrated that one single indentation test provides sufficient information to characterize the local fiber distribution and fiber mechanics. The heart valves are engineered in the bioreactor developed by Kortsmits et al. (2009). This bioreactor has the important advantage over the DPD that the volumetric deformation of the valve leaflets can be accurately measured and feed-back controlled. Using numerical simulations, it was demonstrated that the relation between volumetric deformation and tissue strains is consistent for a range of tissue mechanical properties. Therefore, this bioreactor allows accurate and consistent application of a range of different loading protocols. The current study will lead to increased insight into the relationship between global mechanics and local tissue structure. As a result, improved remodeling algorithms can be designed which will result in improved heart valve tissue engineering protocols.



## 6.2 Materials and methods

### 6.2.1 Tissue engineered heart valves

#### Cell and tissue culture

Ten tissue-engineered heart valves (TEHV) were cultured for four weeks, using different conditioning protocols in three successive, but independent experiments. In all three experiments, culture conditions were identical except for the applied mechanical conditioning protocols. Two valves were cultured in the first experiment, while in the second and third experiment four valves were produced. Cells harvested from the human vena saphena magna were expanded using regular cell culture methods, using DMEM Advanced (Gibco, USA), supplemented with 10% Fetal Bovine Serum (FBS; PAN Biotech, Germany), 1% GlutaMax (Gibco, USA), and 0.1% gentamycin (PAN Biotech, Germany) as a culture medium (Schnell et al., 2001). After expansion, cells were seeded onto an anatomically shaped trileaflet scaffold using fibrin as a cell carrier (Mol et al., 2005b). Cell densities ranged from 2.5 to 4.5 million (passage 7) per  $\text{cm}^3$  scaffold. The scaffold was cut out of non-woven polyglycolic acid meshes (PGA; thickness 1.0 mm; specific gravity 70  $\text{mg}/\text{cm}^3$ ; Concordia Manufacturing Inc, USA) and coated with a thin layer of poly-4-hydroxybutyrate (P4HB; molecular weight:  $1 \times 10^6$  Dalton; TEPHA Inc., Cambridge, MA). The medium used for seeding and subsequent tissue culture contained 0.3% gentamycin and additional L-ascorbic acid 2-phosphate (0.25  $\text{mg}/\text{ml}$ ; Sigma, USA) (Mol et al., 2003).

#### Mechanical conditioning protocols

After seeding, the constructs were placed in the strain bioreactor system developed by Kortsmit et al. (2009) and subjected to culture medium circulation at low speed for 7 to 10 days to allow initial tissue development. Thereafter, dynamic pressure differences (at 1 Hz) were applied to the heart valve leaflets for the remaining culture period. Applied pressure differences were measured as well as the volumetric deformation during pressurization of the leaflets. Induced deformation increased gradually during culture. Although there were small differences in speed of increase, protocols were roughly divided in three loading regimes A, B and C based on the maximal applied volumetric deformation, which increased from A to C (Fig. 6.2). In each of the experiments two different loading protocols were applied: protocol B and C in experiment 1, and protocol A and B in experiment 2 and 3. The experiments were therefore summarized as 1B, 1C, 2A, 2B, 3A and 3B.

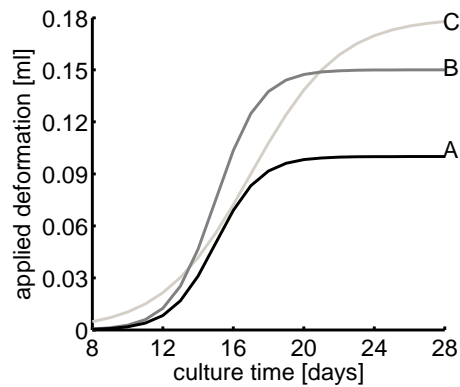


**Figure 6.2:** Schematic overview of applied loading protocols. For zero applied deformation a small perfusion flow was still present.

## 6.2.2 Determination of local fiber distribution and fiber mechanics

### Method

To determine the local fiber mechanics an inverse numerical-experimental method was used (Cox et al., 2008), which is schematically shown in Fig. 6.3. An indentation device (Vaenkatesan et al., 2006) was mounted on top of an inverted microscope, with the tissue laid flat on the base plate. The indentation test was performed using a small spherical indenter and indentation force, and confocal images of the tissue at the base plate were recorded during the indentation test. After that, Digital Image Correlation (DIC) was used to quantify in-plane deformations from these images. In addition, a dedicated finite element (FE) analysis of the indentation test was performed. Parameter estimation was used to couple the FE results to the experimental data. The resulting material parameters represent the local fiber distribution and fiber mechanics.

The relatively small size of the indenter, in comparison with the global tissue dimensions, makes it possible to assess local tissue properties using this method. Moreover, the inverse numerical-experimental technique allows quantification of the local tissue anisotropy. Since fibers are stiffer than the surrounding tissue, deformation perpendicular to the main fiber direction is largest. It should be emphasized that in our approach the local fiber architecture is estimated from, and therefore directly coupled to the local mechanical behavior.

### Indentation tests and Digital Image Correlation

Indentations were applied to the belly and commissural region of each leaflet of each valve. A spherical sapphire indenter (diameter 2 mm) was used for all tests at a constant indentation speed of 0.01 mm/s to simulate quasistatic loading conditions. After one preconditioning cycle, two more indentation tests were performed in combination with confocal imaging. Samples were stained with a fluorescent collagen probe (Nash-Krahn et al., 2006) to enable visualization

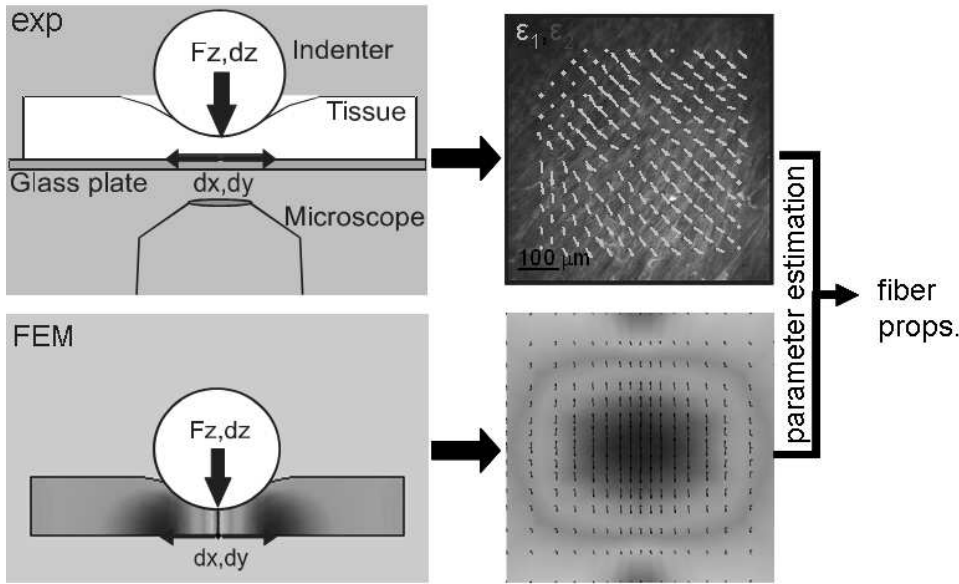


**Figure 6.3:** General overview of method. Spherical indentations are combined with confocal imaging and Digital Image Correlation (DIC) to measure deformations during the indentation test. A Finite Element (FE) analysis is inversely coupled to these results using parameter estimation. As a result, the local structural mechanical behavior is characterized.

of the tissue deformations. Afterwards, DIC was performed on the confocal images using the commercially available imaging software package ARAMIS (GOM mbH, Germany), resulting in 2D displacement fields. Finally, deformation gradients and strain fields were obtained from the displacements using the algorithm developed by Geers et al. (1996).

### Computational model

For the inverse FE analysis, the numerical model proposed by Driessen et al. (2008) was implemented into the commercially available package SEPRAN (Segal, 1984). A small block of tissue surrounding the indentation site was modeled. Quarter symmetry was assumed and material behavior was considered homogeneous for this block (Fig. 6.4). Contact between the indenter and the tissue as well as contact between the tissue and the supporting glass plate were assumed to be frictionless. Thickness was adjusted for each simulation to match the experimental thickness. Neglecting inertia and body forces and assuming tissue incompressibility the balance of momentum and conservation of mass were given by

$$\vec{\nabla} \cdot \sigma = \vec{0}, \quad (6.1)$$

$$J - 1 = 0, \quad (6.2)$$

where  $\sigma$  represents the Cauchy stress and  $J = V/V_0 = \det(\mathbf{F})$ . Here  $V$  and  $V_0$  denote the volume in current and reference configuration respectively and  $\mathbf{F}$  is the deformation gradient tensor. The

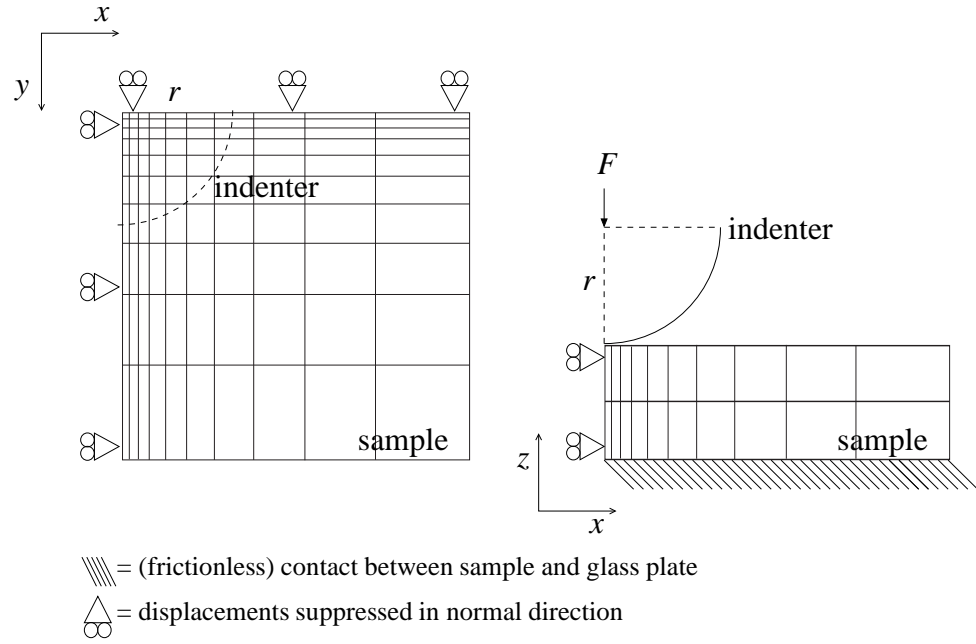


**Figure 6.4:** Top view (left) and front view (right) of the 3D model, showing indenter and boundary conditions. The indenter radius  $r$  and indentation force  $F$  are also indicated.

Cauchy stress  $\sigma$  consisted of the hydrostatic pressure  $p$  and the extra stress  $\tau$ ,

$$\sigma = -p\mathbf{I} + \tau, \quad (6.3)$$

where  $\mathbf{I}$  represents the unity tensor. The local collagen fiber architecture was incorporated in the computational model by splitting the extra stress  $\tau$  into an isotropic matrix part  $\tau_m$  (cells, GAGs, etc) and an anisotropic fiber part  $\tau_f$ . Incompressible Neo-Hookean material behavior was assumed for the matrix part, defined by matrix shear modulus  $G_m$ . The extra stress  $\tau$  was written as

$$\tau = \tau_m + \tau_f = G_m (\mathbf{F} \cdot \mathbf{F}^T - \mathbf{I}) + \sum_{i=1}^{N_f} \phi_f^i \left[ \psi_f^i - \vec{e}_f^i \cdot \hat{\mathbf{t}} \cdot \vec{e}_f^i \right] \vec{e}_f^i \vec{e}_f^i, \quad (6.4)$$

A discrete number of fibers  $N_f$  was modeled in directions  $\vec{e}_f$  and with a volume fraction  $\phi_f$  each. To further minimize the number of parameters, the fibers were modeled by a periodic normal distribution (Gasser et al., 2006; Driessen et al., 2008):

$$\phi_f^i(\gamma_i) = A \exp \frac{\cos[2(\gamma_i - \alpha)] + 1}{\beta}. \quad (6.5)$$

In Eq. (6.5)  $\gamma_i$  was defined as the fiber angle with the x-direction (Fig. 6.4) in undeformed configuration. Fibers were assumed to run only in the tissue plane (no z-component). This way, only two material parameters were introduced, namely the main fiber direction  $\alpha$ , and the dispersity parameter  $\beta$ . When  $\beta$  approaches zero, the fiber distribution becomes uniaxial, while for large  $\beta$  a uniform distribution is obtained. The scaling factor  $A$  was used to ensure the total fiber volume fraction equaled  $\phi_{tot}$ . In all simulations the total fiber volume fraction was

set to 0.5 (Driessen et al., 2007). Two additional material parameters were used to define the constitutive behavior of the collagen fibers by describing the fiber stress  $\psi_f$  as a function of the fiber stretch  $\lambda_f$  (Holzapfel et al., 2000):

$$\psi_f = 2k_1 \lambda_f^2 (\lambda_f^2 - 1) \exp(k_2 (\lambda_f^2 - 1)^2). \quad (6.6)$$

In Eq. (6.6),  $k_1$  is a stiffness-like parameter and  $k_2$  a non-linearity parameter. The fiber stretch was denoted by  $\lambda_f = \frac{l}{l_0}$ , with  $l$  and  $l_0$  the current and reference length, respectively.

### Parameter estimation

To determine material properties of the TEHV, the computational model was fitted iteratively to each individual experiment using a mixed numerical experimental approach (Meuwissen, 1998; Cox et al., 2006). Five material parameters were defined: the matrix shear modulus  $G_m$ , the fiber distribution parameters  $\alpha$  and  $\beta$ , and the fiber mechanical parameters  $k_1$  and  $k_2$ . The matrix shear modulus was fixed at 1.0 kPa, which was in all cases small compared to  $k_1$ , and, therefore, of little influence on the simulation outcome. The four remaining parameters were estimated by minimizing the difference between experimental data  $\underline{m}$  and model predictions  $\underline{h}(\underline{u}, \underline{\theta})$  using a Gauss-Newton minimization algorithm (Cox et al., 2006). The experimental data column  $\underline{m}$  contained the recorded indentation force  $F$  and the anisotropic index  $AI$ . The anisotropic index was defined as the ratio between first and second principle stretch minus one,  $AI = \frac{\lambda_1}{\lambda_2} - 1$ .  $AI$  equals zero for isotropic materials and increases with increasing anisotropy. For each experimental data point  $m_i$  the model prediction  $h_i$  was calculated as a function of the material parameters  $\underline{\theta}$  and applied boundary conditions  $\underline{u}$ . Since  $k_2 < 0$  represents strain-softening behavior, which is atypical for biological tissues, a lower limit of  $k_2 = 0$  was maintained. Convergence was reached when the sum of the relative changes in parameters was less than 1%. The correlation between the model ( $_{mod}$ ) and the experiment ( $_{exp}$ ) was quantified with separate mean relative errors for the indentation force ( $MRE_F$ ) and the anisotropic index ( $MRE_{AI}$ ):

$$MRE_F = \frac{1}{n} \sum_{i=1,n} \frac{|F_{exp}(i) - F_{mod}(i)|}{\overline{F}_{exp}(i)} \cdot 100\% \quad (6.7)$$

$$MRE_{AI} = \frac{1}{n} \sum_{i=1,n} \frac{|AI_{exp}(i) - AI_{mod}(i)|}{\overline{AI}_{exp}(i)} \cdot 100\% \quad (6.8)$$

where  $n$  is the number of experimental data points, and  $\overline{F}$  and  $\overline{AI}$  represent mean experimental force and anisotropic index, respectively. Estimations with an  $MRE_F$  or  $MRE_{AI}$  higher than 35% were discarded as a poor fit.

### Fiber distribution and fiber mechanics

The parameter estimation algorithm resulted in a set of fiber parameters for each indentation test. While the parameters  $\alpha$  and  $\beta$  represent the fiber distribution, parameters  $k_1$  and  $k_2$  represent the local fiber mechanics. Average fiber distributions (e.g. for all valves in protocol

B) were obtained by averaging the corresponding individual fiber distributions. After that, averaged fiber parameters  $\bar{\alpha}$  and  $\bar{\beta}$  were determined by fitting Eq. (6.5) to the averaged fiber distribution using least squares optimization.

Similarly, averaged fiber mechanics were obtained by averaging the corresponding individual fiber tensile curves. After that, averaged fiber tensile properties  $\bar{k}_1$  and  $\bar{k}_2$  were obtained by fitting Eq. (6.6) to the averaged fiber tensile curves.

## 6.3 Results

### 6.3.1 Indentation test and Digital Image Correlation

For a total of ten TEHV indentation tests were applied to all three leaflets in the belly and commissural region. Two consecutive tests from each indentation site were used in the analysis, yielding a total of 120 experimental datasets. DIC was performed successfully in 112 cases. Sample results from a belly and commissural region clearly show that tissue indeed deforms mainly perpendicular to the expected main fiber direction (Fig. 6.5).

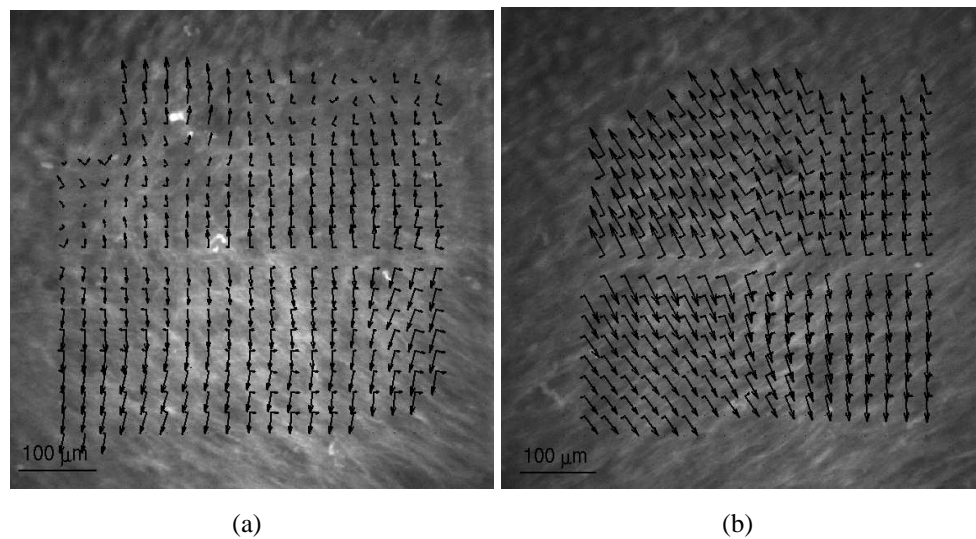


**Figure 6.5:** Confocal images and DIC from a belly region (left) and a right commissural region (right). Circumferential direction is from left to right. Arrows indicate directions of first and second principal stretches, and are scaled by strain magnitude.

### 6.3.2 Parameter estimation

For 84 samples the parameter estimation algorithm converged to a stable solution *and* mean relative errors were smaller than 35%. A typical fit between experiment and simulation is demonstrated in Fig. 6.6. Parameter estimation was successful for at least two leaflets of each

valve for each location.

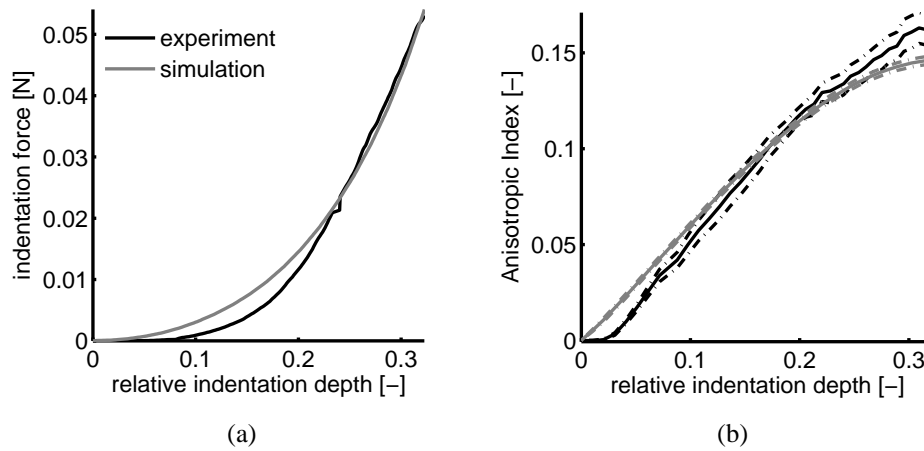


**Figure 6.6:** Fit between experimental (black) and numerical results (gray). Left: indentation force, right: Anisotropic Index, both as a function of indentation depth. For the Anisotropic Index the range at each indentation depth is indicated with a dashed line.

### 6.3.3 Estimated fiber distribution and fiber mechanics

An overview of all averaged material parameters is given in Table 6.1. Additionally, the number of parameter sets that were available within each group and the mean relative errors are shown. For 9 out of 10 valves, the main fiber direction in the belly region was close to circumferential ( $0^\circ$ ) or oriented more towards the commissures (0 to  $30^\circ$ ). Only 1 valve in experiment 1B demonstrated a different orientation ( $-37^\circ$ ), although alignment was not pronounced. For the commissures the alignment ranged between approximately  $0^\circ$  and  $40^\circ$  in 9 out of 10 valves as well. Again, the only deviation was found for 1 valve in experiment 1B. Figure 6.7 (left) shows the fiber distribution averaged for all belly and commissures, respectively. The error bars represent the standard error of the mean (SEM) obtained when averaging the individual fiber distributions. A clear circumferential alignment was found ( $9^\circ$ ) in the belly. The commissural fiber distribution was shifted slightly to the right ( $15^\circ$ ). Furthermore, alignment was higher in the commissural region ( $\beta = 1.7$ ) than in the belly ( $\beta = 2.6$ ). The fiber tensile behavior was moderately nonlinear;  $k_1$  was in the order of magnitude of 100 kPa and  $\beta$  was between 0 and 4 for all experiments. The averaged fiber tensile behavior (Fig. 6.7, right) indicates that the fiber mechanical behavior was similar in the belly ( $k_1 = 2.0 \cdot 10^2$  kPa,  $k_2 = 1.6$ ) and commissural ( $k_1 = 2.1 \cdot 10^2$  kPa,  $k_2 = 1.6$ ) region.

The relationship between loading protocol and collagen fiber distribution and mechanics is illustrated in Fig. 6.8, top row. Results indicate that estimated fiber distributions as well as fiber mechanics were similar for protocol A and B. Only for protocol C higher fiber alignment was observed in belly and commissures, and stiffer fiber mechanics in the belly. It needs to be re-

**Table 6.1:** Material parameters and mean relative errors (MRE) per experimental group. Number of valves (#valves) and parameter sets (#exp) per group are indicated as well.

Exp	$\Delta V_{max}$ [ml]	#valves	location	#exp	$G_m$ [kPa]	$k_1$ [kPa]	$k_2$ [-]	$\alpha$ [°]	$\beta$ [-]	$MRE_F$ [%]	$MRE_{AI}$ [%]
1B	0.15	1	belly	2	1	1.5E+02	1.6	-37	2.6E+00	27	34
			commissure	5	1	1.5E+02	3.0	-26	1.4E+00	10	15
1C	0.18	1	belly	3	1	5.2E+02	3.6	10	5.2E-01	16	15
			commissure	5	1	1.9E+02	3.4	40	1.2E+00	7	14
2A	0.10	2	belly	9	1	2.6E+02	1.1	-2	2.4E+00	13	20
			commissure	11	1	2.8E+02	1.8	24	1.0E+00	9	16
2B	0.15	2	belly	7	1	3.0E+02	1.4	-1	1.9E+00	16	17
			commissure	9	1	4.2E+02	1.1	1	1.3E+00	12	25
3A	0.10	2	belly	9	1	7.8E+01	0.4	29	2.4E+00	10	19
			commissure	7	1	9.9E+01	0.7	-3	3.2E+00	8	18
3B	0.15	2	belly	9	1	1.1E+02	0.2	32	5.6E+00	13	21
			commissure	8	1	4.3E+01	1.0	16	9.7E-01	16	24
All A	0.10	4	belly	18	1	1.7E+02	0.9	14	2.9E+00	12	19
			commissure	18	1	2.1E+02	1.6	20	1.5E+00	9	17
All B	0.15	5	belly	18	1	1.9E+02	1.1	3	3.7E+00	17	22
			commissure	22	1	2.2E+02	1.3	4	1.6E+00	13	23
All C	0.18	1	belly	3	1	5.2E+02	3.6	10	5.2E-01	16	15
			commissure	5	1	2.0E+02	3.4	40	1.2E+00	7	14
All		10	belly	39	1	2.0E+02	1.6	9	2.6E+00	14	20
			commissure	45	1	2.1E+02	1.6	15	1.7E+00	11	19



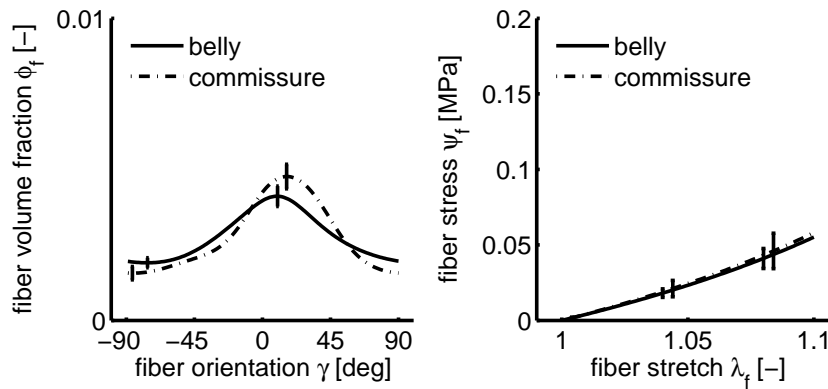


**Figure 6.7:** Averaged fiber distribution (left) and fiber mechanics behavior (right) in the belly (solid) and commissures (dashed). Error bars indicate standard error of the mean.

marked that only one valve was subjected to protocol C. To investigate the effect of experimental variability, averaged fiber distributions and fiber mechanics for protocol B were compared between the different experiments (Fig. 6.8, bottom row). Results indicate that experimental variation was significant for both the estimated fiber distributions and the fiber mechanics.

## 6.4 Discussion

Although several numerical as well as experimental studies indicate that global mechanical conditioning can be used to regulate/steer the global mechanical properties towards native tissue, it is unclear whether the local structural organization of the leaflet is developing towards the local fiber structure typical for native valve leaflets. Therefore, the current study aimed at providing experimental proof for some of the model assumptions and hypotheses of Driessen et al. (2008) by coupling global conditioning protocols to local tissue mechanics and tissue structure. To this end, ten heart valves were engineered in three consecutive independent experiments using three different loading protocols, divided over these experiments. Collagen fiber distribution and structural fiber mechanics were estimated in an inverse numerical-experimental approach, which included indentation testing of the commissural and belly region of each leaflet of each valve. It was hypothesized that 1) tissue engineered heart valves will develop a native-like fiber distribution if subjected to diastolic loading protocols *in vitro* in a bioreactor, 2) increased loading during culture will lead to increased collagen fiber alignment and 3) intrinsic collagen fiber mechanics will be similar in the belly and in the commissures.

Based on hypothesis 1 a circumferential fiber orientation ( $0^\circ$ ) was expected in the belly region while fibers in the commissures should orient towards the belly (between 0 and  $45^\circ$ ). Furthermore fiber alignment in the commissures was expected to be higher. Our results indicated an average orientation of  $9^\circ$  in the belly, which is indeed close to circumferential. For the commissures the main fiber angle was  $15^\circ$ , which is indeed larger than in the belly. Also, alignment

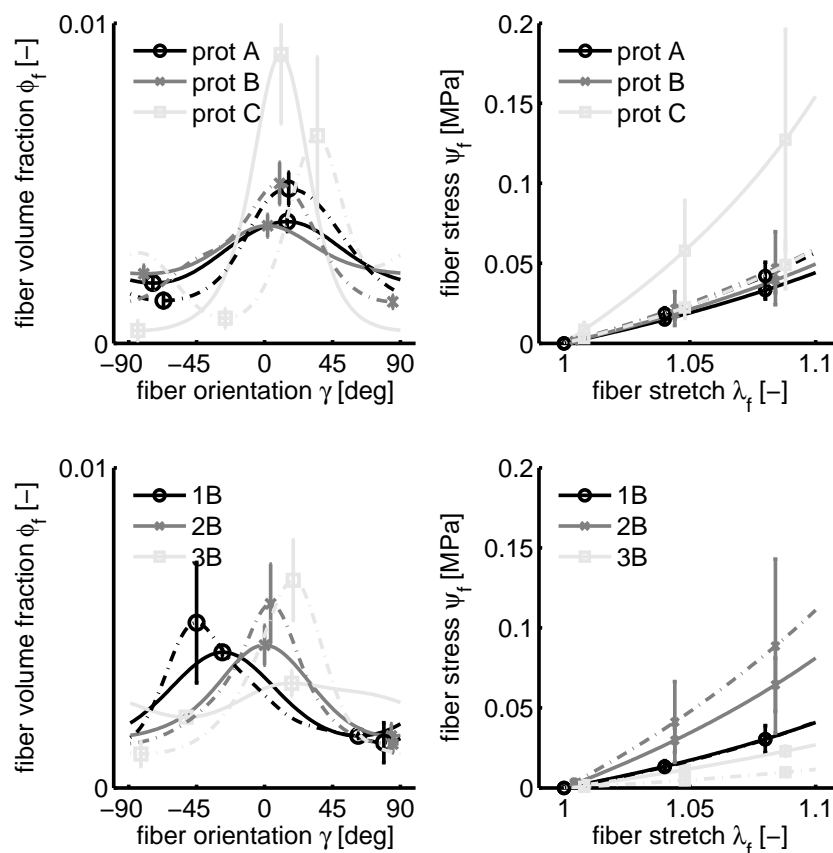


**Figure 6.8:** Averaged fiber distributions (left) and fiber tensile behavior (right) in the belly (solid) and commissure (dashed) for different loading protocols (top row) and different experiments in loading protocol B (bottom).

was higher in the commissures ( $\beta = 1.6$ ) than in the belly ( $\beta = 2.7$ ). These results confirm our first hypothesis, although it should be noted that differences are more pronounced in the native adult heart valve. To assess our second hypothesis the results per loading protocol were compared (Fig. 6.8, top row). For loading protocols A and B, very similar fiber distributions were obtained. For loading protocol C, in which applied load was highest, alignment was much more pronounced in the belly and commissural region. However, since only one valve was tested in group C it is questionable whether these differences are significant. Therefore we can not yet conclude whether the estimated fiber distribution is sensitive to loading protocol or not. Additional experiments are necessary to test our second hypothesis. The third hypothesis was tested by evaluating the local fiber mechanics, which were derived from parameters  $k_1$  and  $k_2$ . The averaged fiber mechanics for belly ( $k_1 = 2.0 \cdot 10^2$  kPa,  $k_2 = 1.6$ ) and commissure ( $k_1 = 2.1 \cdot 10^2$  kPa,  $k_2 = 1.6$ ) were similar, thus indicating that collagen fiber mechanics are indeed independent of location. Fiber mechanics were also insensitive to loading protocol (Fig. 6.8, top row), except for the belly in protocol C. As in this particular group the amount of available data was

limited, significance of these differences is questionable and therefore additional experiments are desired. Generally, the results indicate that fiber type is at least mechanically similar for different locations and for the majority of tested protocols.

When results for loading protocol B were compared between experiments, obvious differences were observed for the apparent fiber distribution as well as the fiber mechanics. This indicates that inter-experiment variability has a larger impact than the difference in loading protocols. These results were confirmed by tensile tests performed on the tissue engineered heart valves (data not shown), also indicating larger stiffness differences between experiments than between protocols. Differences may for example be caused by inter-specimen variability, phenotype changes during culture or heterogeneity in the harvested cell population. This variability is inherent to the tissue engineering process, and controlling this remains one of the largest challenges towards clinical applications.

In the current study, a total of 120 indentation tests were performed, of which 84 successfully resulted in a set of material parameters. An explanation for this difference is that the used characterization method includes several steps that all need to be successful to yield convergence. Imaging should provide sufficient contrast for DIC, which should provide sufficient detail for calculating deformation gradients, which provides the input for the parameter estimation process. One of the potential sources of uncertainty is local friction. While the FE model assumes frictionless contact between tissue and bottom plate, stick-slip behavior may occur in the experiments, for example because of local tissue inhomogeneity or heating of the sample. As a result, deformation may be inhomogeneous or small. In both cases a mismatch will exist between model and experiment, thus compromising a good fit. Therefore efforts should be made to minimize friction, e.g., by coating the bottom plate with a lubricant, or by minimizing tissue exposure to the confocal laser.

Another consequence of the chosen method is that comparative statistics are difficult to perform. The various steps in assessing the fiber parameters are still followed by an averaging step to yield parameters per experimental group. As it is virtually impossible to assign confidence intervals for each of these steps, we restricted ourselves to a qualitative comparison of the obtained results. Despite given limitations our method provides significant advantages over uniaxial tensile tests, which are the current standard for mechanical characterization of TE. Uniaxial tensile tests most often provide one-dimensional information, like ultimate tensile strength or tissue stiffness in the loading direction. Tissue stiffness is mostly determined as the slope in the end part of the stress-strain curve, and thus at high deformations, (e.g., Clark (1973); Vesely and Noseworthy (1992); Sodian et al. (2000); Neidert et al. (2002); Kadner et al. (2004); Stradins et al. (2004); Mol et al. (2006); Balguid et al. (2007)). Although these results provide important information on the maximal load-bearing capacity of the valve, little information is provided on the small deformation behavior. In our indentation test, the in plane loading conditions are essentially equibiaxial, which is comparable to the pressurization of the leaflets during diastole. Simulations performed by Kortsmits et al. (2009) indicate that the maximal volumetric deformation in loading protocols B and C, 0.15 ml and 0.18 ml, respectively, correspond with diastolic loading of the pulmonary valve, while volumetric deformation in the

aortic leaflet during diastole was estimated at 0.40 ml. Biaxial tensile tests on native porcine valves (Billiar and Sacks, 2000a; Driessen et al., 2005b) resulted in a  $k_1$  of less than 1 kPa, and a  $\beta$  of almost 10, which is 2 orders of magnitude lower and 5 times higher respectively than in our experiments ( $k_1 = 2.0 \cdot 10^2$  kPa,  $k_2 = 1.6$ ). Although these results were obtained over a larger strain regime and from biaxial rather than indentation tests, this indicates that the small strain behavior of our TEHV is significantly stiffer than native, even though end stiffness may be comparable (Mol et al., 2006; Balguid et al., 2009). As uniaxial tensile tests are mainly used to evaluate the end stiffness, it is important that our method provides an accurate measure of the fiber architecture and mechanics for relatively small fiber deformations.

Our main finding is that TEHV develop a collagen fiber architecture with native-like characteristics when subjected to diastolic loads in a bioreactor. Furthermore it was found that the estimated fiber mechanics were relatively insensitive to the applied loading protocol, at least within the range tested. Inter-experiment variability had a larger impact. In future experiments differences in maximal applied load between protocols will be increased to investigate the relation between loading magnitude and collagen fiber architecture over a broader range. However, results from our study clearly indicate that a deeper understanding of the experimental variation inherent to tissue engineering is desired before mechanical loading protocols can be used as a tool for controlling *and* fine tuning the mechanical properties of *in vitro* tissue engineered heart valves for clinical applications.



---

**Local structural mechanics of  
aortic, pulmonary and tissue-engineered  
heart valves**

---

*Local structural mechanics of native ovine aortic and pulmonary heart valves and human tissue engineered heart valves are compared in this chapter. Information on the native heart valves will provide experimental validation for remodeling hypotheses based on earlier computational and experimental studies. In addition, native material parameters will provide a benchmark for the tissue engineered heart valves.*

## 7.1 Introduction

One of the major challenges in heart valve tissue engineering is to create tissues that are strong enough to withstand the *in vivo* hemodynamical demands. One obvious strategy towards this goal is to mimic nature's solution. The mechanical strength of native aortic valve leaflets is known to be largely determined by a highly organized network of collagen fibers. Stresses are transferred to the aortic root through thick parallel fiber bundles running from the commissural edges towards a circumferentially oriented branched network of collagen fibers in the central belly region (Fig. 7.1).

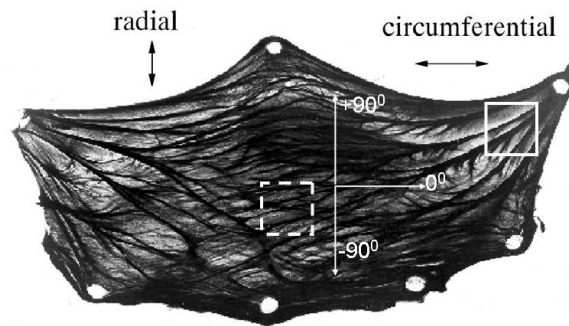


**Figure 7.1:** Histology image of a porcine aortic valve leaflet, clearly showing a highly organized collagen fiber network. Belly (dashed rectangle) and commissural region (solid rectangle) are indicated as well. Circumferential and radial orientation were defined at  $0^\circ$  and  $\pm 90^\circ$ , respectively. Adapted from Sauren (1981).

Both valve mechanics and fiber structure have been subject of extensive study. Clark (1973) found that human aortic valve leaflets are stiffer in circumferential than in radial direction by performing uniaxial tensile tests in both directions, which is explained by the circumferential collagen fiber orientation in the belly. The leaflets' tensile behavior is characterized by an initial expansion at low stress, followed by a sharp transition region after which stiffening occurs. The initial expansion is caused by the fact that collagen fibers are crimped in the unloaded configuration of the valve, which is hypothesized to relate to a radially oriented network of elastin fibers (Scott and Vesely, 1996) which keeps the collagen fiber network under compression. Upon pressurization, the load is carried by this elastin network until the collagen fibers are stretched and take over. Indeed, Adamczyk et al. (2000) found that when the contribution of elastin to the aortic valve mechanics is disrupted, valves distend and become stiffer and less extensible mainly in radial direction.

The most complete characterization of both valve mechanics and collagen fiber architecture was performed by Billiar and Sacks (2000b), who used porcine aortic valves for their research. Local collagen fiber direction and dispersity were measured with small angle light scattering (SALS), a non-invasive method developed by the same group (Billiar and Sacks, 1997). Furthermore, a range of biaxial test regimes was applied for a full characterization of the in-plane mechanical behavior (Billiar and Sacks, 2000b). Local strain fields were also measured during

equibiaxial tension, and mapped to the local fiber orientation found by SALS. They observed that local maximal strains were perpendicular to the local collagen orientation, thus indicating that collagen fibers are stiffer than the surrounding tissue and influence local mechanical behavior accordingly. This structure-function relationship was quantified by Billiar and Sacks (2000a), by fitting a structural constitutive model to their experimental results (Billiar and Sacks, 2000b). Fiber tensile behavior was assumed to be exponential and fiber distribution was assumed to be Gaussian. Using local fiber orientations from SALS measurements, only three structural parameters were sufficient to model the full biaxial mechanical behavior of the aortic valve. It needs to be remarked that to perform biaxial tests, specimen size needs to be relatively large and boundary effects limit the test region to a small central portion of the tissue (Nielsen et al., 1991). Therefore, the results of Billiar and Sacks (2000a) mainly represent the belly region of the leaflet. Driessen et al. (2008) used the parameters obtained by Billiar and Sacks (2000a) in a fiber remodeling algorithm to predict the native collagen fiber distribution based on the local strains that occur during diastolic loading. Assuming that intrinsic fiber mechanical properties were homogenous throughout the entire valve, a good qualitative match was found with the native fiber structure. A nearly uniaxial fiber distribution was found in the commissures, while in the belly region a more biaxial fiber distribution was found, with the main orientation in the circumferential direction. These findings feed the hypothesis that tissue remodeling and development is mediated by mechanical conditioning. As deformation and pressurization of the aortic valve is maximal during the diastolic phase, it is not surprising that diastolic loading appears to be key in tissue development.

In line with this hypothesis, Mol et al. (2005a) developed a diastolic pulse duplicator (DPD) for tissue engineering of heart valves. The DPD is a bioreactor that mimics the diastolic loading phase of the cardiac cycle *in vitro*. Recently, human heart valves were tissue engineered in the DPD that were mechanically strong enough to withstand the high systemic pressures that occur at the aortic position (Mol et al., 2006), thus confirming the results of Driessen et al. (2008). Nonetheless, experimental evidence is still lacking that diastolic loading indeed stimulates tissue development towards the *structural* mechanics of native heart valves. Mechanical characterization of native aortic valves was only performed for the belly region. Although one study investigated the flexural rigidity in the commissural region of the aortic valve (Mirnajafi et al., 2006), this was not coupled to local fiber structure. Local structural mechanical characterization of the native valve is necessary to validate the assumption that intrinsic mechanical properties of the collagen fibers are similar throughout the leaflet.

Recently, Cox et al. (2009) used spherical indentation combined with confocal imaging to quantify the local structural mechanics of human tissue engineered heart valves (TEHV). Intrinsic fiber mechanical properties in the belly and commissural regions of the TEHV were indeed similar. Also a clear circumferential fiber orientation was found in the belly region. For the commissures, fiber orientation was rotated compared to the belly, and alignment was higher, although differences were small. These findings provide important experimental validation for our hypotheses. In the current study, the same method is applied to native ovine heart valves, both aortic and pulmonary. Ovine valves are used, as sheep are the model of choice



for preclinical testing of heart valve prostheses, and therefore also for tissue engineered heart valves. The pulmonary valve is also of interest, as the first clinical application is expected to be a pulmonary valve substitute. Few researchers have reported on the structural mechanics of pulmonary valves, and findings were inconclusive. David et al. (1994) found comparable elastic moduli for porcine pulmonary and aortic valves using uniaxial tensile testing in radial and circumferential direction, although pulmonary valve leaflets were thinner. Christie and Barratt-Boyes (1995) on the other hand concluded from equibiaxial tension tests that porcine pulmonary valves were more extensible in the radial direction compared to aortic valves. Finally Stradins et al. (2004) concluded from uniaxial tensile tests on human pulmonary and aortic valves that overall mechanical differences were minimal. It should be emphasized that with the proposed method, the fiber structure is estimated from and therefore directly coupled to the local mechanical behavior, as opposed to a separate fiber distribution measurement, e.g., by using small angle light scattering (Billiar and Sacks, 1997). Results will be compared to human tissue engineered heart valves, and will provide a benchmark for further optimization of tissue engineering protocols as well as the evolution of structural and mechanical properties of TEHV after implantation.

## **7.2 Materials and methods**

### **7.2.1 Native and tissue engineered heart valves**

Three mature native ovine hearts were obtained immediately after termination as secondary-use material from non valve-related animal studies and transported at room temperature in a saline solution. The pulmonary and aortic valve leaflets were excised within 2 hours following termination and stored at 4°C in a saline solution until experimental testing, which was performed within 24 hours. Mechanical test results will be compared to result for human tissue engineered heart valves (n=10), which were cultured for four weeks in an improved version of the DPD (Kortsmit et al., 2009), where they were subjected to gradually increasing volumetric deformations. For a detailed description of the applied culture and conditioning protocols one is referred to Chapter 6.

### **7.2.2 Local structural mechanics**

#### **Method overview**

To determine the local structural mechanics, indentation tests were combined with confocal imaging in an inverse numerical-experimental approach (Cox et al., 2008). An indentation device (Vaenkatesan et al., 2006) was mounted on top of an inverted confocal laser scanning microscope (CLSM), with the leaflet laid flat on a base plate (Fig. 7.2). The indentation test was performed with a small spherical indenter, and confocal imaging was used to record tissue

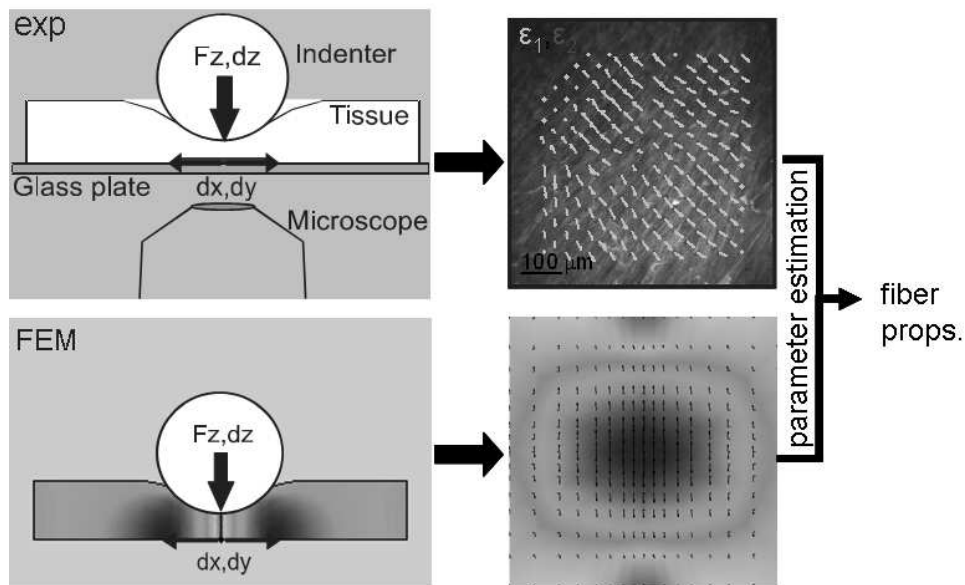


**Figure 7.2:** General overview of method. Spherical indentations are combined with confocal imaging and Digital Image Correlation (DIC) to measure deformations during the indentation test. A Finite Element (FE) analysis is inversely coupled to these results using parameter estimation. As a result, the local structural mechanical behavior is characterized.

deformations near the base plate. Subsequently, Digital Image Correlation (DIC) was applied to the recorded images to extract principal strain fields. In addition, a finite element (FE) analysis was performed of the indentation experiment and fitted to the experimental results using parameter estimation. The resulting material parameters represent the local fiber structure and intrinsic fiber mechanical properties.

As the indenter was small relative to global tissue dimensions, local mechanical properties could be determined. Furthermore, confocal imaging allowed determination of local fiber orientation, as deformation perpendicular to the main fiber orientation was largest (Billiar and Sacks, 2000b).

### Indentation tests and Digital Image Correlation

Indentations were applied to the belly and commissural region of each leaflet of each valve, with the ventricularis layer facing up. Sample thickness was measured prior to each indentation test at the initial point of contact between tissue and indenter. Indentation was applied up to 60% of the tissue thickness. After one preconditioning cycle, two consecutive indentation tests were performed to each test region. In the current study a spherical sapphire indenter (diameter 2 mm) was used for all tests. Indentation was performed at a constant indentation speed of 0.01 mm/s. All leaflets were stained overnight with a vital fluorescent collagen probe to allow confocal imaging during the indentation test without altering mechanical properties (Nash-Krahn

et al., 2006). DIC was performed on the confocal images using the commercially available imaging software package ARAMIS (GOM mbH, Germany), resulting in 2D displacement fields. Local deformation gradients and strain fields were obtained from the displacement fields using the algorithm developed by Geers et al. (1996).

### Numerical model

For the inverse FE analysis, the numerical model proposed by Driessen et al. (2008) was implemented into the commercially available package SEPRAN (Segal, 1984). A small block of tissue surrounding the indentation site was modeled, assuming quarter symmetry (Fig. 7.3). To

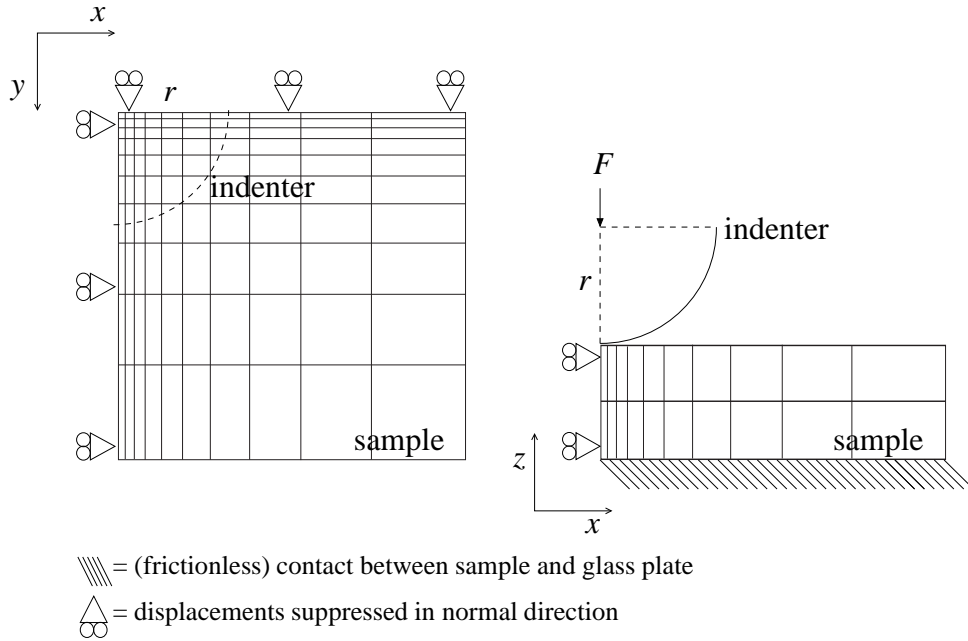


**Figure 7.3:** Top view (left) and front view (right) of the 3D model, showing indenter and boundary conditions. The indenter radius  $r$  and indentation force  $F$  are also indicated.

limit the amount of parameters, homogeneous material behavior was assumed for this block. Contact between the indenter and the tissue as well as contact between the tissue and the supporting glass plate were assumed to be frictionless. In each simulation the experimentally derived thickness was used. Neglecting inertia and body forces and assuming tissue incompressibility the balance of momentum and conservation of mass were given by

$$\vec{\nabla} \cdot \boldsymbol{\sigma} = \vec{0}, \quad (7.1)$$

$$J - 1 = 0, \quad (7.2)$$

where  $\boldsymbol{\sigma}$  represents the Cauchy stress and  $J = V/V_0 = \det(\mathbf{F})$ . Here  $V$  and  $V_0$  denote the volume in current and reference configuration, respectively and  $\mathbf{F}$  is the deformation gradient tensor. The Cauchy stress  $\boldsymbol{\sigma}$  contained the hydrostatic pressure  $p$  and the extra stress  $\boldsymbol{\tau}$ ,

$$\boldsymbol{\sigma} = -p\mathbf{I} + \boldsymbol{\tau}, \quad (7.3)$$

where  $\mathbf{I}$  represents the unity tensor. The local collagen fiber architecture was incorporated by splitting the extra stress  $\boldsymbol{\tau}$  into an isotropic matrix part  $\boldsymbol{\tau}_m$  (cells, GAGs, etc) and an anisotropic collagen fiber part  $\boldsymbol{\tau}_f$ . Incompressible Neo-Hookean material behavior was assumed for the matrix part, defined by matrix shear modulus  $G_m$ . The extra stress  $\boldsymbol{\tau}$  was given by:

$$\boldsymbol{\tau} = \boldsymbol{\tau}_m + \boldsymbol{\tau}_f = G_m (\mathbf{F} \cdot \mathbf{F}^T - \mathbf{I}) + \sum_{i=1}^{N_f} \phi_f^i \left[ \psi_f^i - \vec{e}_f^i \cdot \hat{\boldsymbol{\tau}} \cdot \vec{e}_f^i \right] \vec{e}_f^i \vec{e}_f^i, \quad (7.4)$$

A discrete number of fibers  $N_f$  were modeled in directions  $\vec{e}_f$  and with a volume fraction  $\psi_f$  each. To further minimize the number of parameters the fibers were represented by a periodic normal distribution (Gasser et al., 2006; Driessen et al., 2008):

$$\phi_f^i(\gamma_i) = A \exp \frac{\cos[2(\gamma_i - \alpha)] + 1}{\beta}. \quad (7.5)$$

In Eq. (7.5),  $\gamma_i$  was defined as the fiber angle with the x-direction (Fig. 7.3) in undeformed configuration. Fibers were assumed to run only in the tissue plane (no z-component). This way only two material parameters were introduced, namely the main fiber direction  $\alpha$ , and the dispersity parameter  $\beta$ . When  $\beta$  approaches zero, the fiber distribution becomes uniaxial, while for large  $\beta$  a uniform distribution is obtained. The scaling factor  $A$  was used to ensure the total fiber volume fraction equaled  $\phi_{tot}$ . In all simulations the total fiber volume fraction was set to 0.5 (Driessen et al., 2007) Two additional material parameters were used to define the constitutive behavior of the collagen fibers by describing the fiber stress  $\psi_f$  as a function of the fiber stretch  $\lambda_f$  (Holzapfel et al., 2000),

$$\psi_f = 2k_1 \lambda_f^2 (\lambda_f^2 - 1) \exp(k_2 (\lambda_f^2 - 1)^2). \quad (7.6)$$

In Eq. (7.6),  $k_1$  is a stress-like parameter and  $k_2$  a non-linearity parameter. The fiber stretch is denoted by  $\lambda_f = \frac{l}{l_0}$ , where  $l$  and  $l_0$  are the current and reference length, respectively.

### Parameter estimation

A mixed numerical-experimental approach was used to fit the FE model iteratively to the indentation test results (Meuwissen, 1998; Cox et al., 2006). Five material parameters were defined, namely the matrix shear modulus  $G_m$ , the fiber distribution parameters  $\alpha$  and  $\beta$ , and the fiber mechanical parameters  $k_1$  and  $k_2$ . In some simulations the matrix shear modulus  $G_m$  was fixed at 1.0 kPa to avoid convergence problems for very low  $G_m$  values. Remaining material parameters were estimated by minimizing the difference between experimental data  $\underline{m}$  and model predictions  $\underline{h}(\underline{u}, \underline{\theta})$  using a Gauss-Newton minimization algorithm (Cox et al., 2006). The experimental data column  $\underline{m}$  contained the recorded indentation force  $F$  and the anisotropic index  $AI$ , which was defined as the ratio between first and second principle stretch minus one.  $AI$  equals zero for isotropic materials and increases with increasing anisotropy. For each experimental data point  $m_i$  the model prediction  $h_i$  was calculated as a function of the material parameters  $\underline{\theta}$  and applied boundary conditions  $\underline{u}$ . Since  $k_2 < 0$  represents strain-softening behavior,

which is atypical for biological tissues, a lower limit of  $k_2 = 0$  was maintained. Convergence was reached when the sum of the relative changes in parameters was less than 1%. The correlation between the model ( $_{mod}$ ) and the experiment ( $_{exp}$ ) was quantified with separate mean relative errors for the indentation force ( $MRE_F$ ) and the anisotropic index ( $MRE_{AI}$ ):

$$MRE_F = \frac{1}{n} \sum_{i=1,n} \frac{|F_{exp}(i) - F_{mod}(i)|}{\overline{F}_{exp}(i)} \cdot 100\% \quad (7.7)$$

$$MRE_{AI} = \frac{1}{n} \sum_{i=1,n} \frac{|AI_{exp}(i) - AI_{mod}(i)|}{\overline{AI}_{exp}(i)} \cdot 100\% \quad (7.8)$$

where  $n$  is the number of experimental data points, and  $\overline{F}_{exp}$  and  $\overline{AI}_{exp}$  represent mean experimental force and anisotropic index, respectively. Estimations with an  $MRE_F$  or  $MRE_{AI}$  higher than 35% were discarded as a poor fit.

### Structural fiber mechanics

The parameter estimation algorithm resulted in a set of fiber parameters for each indentation test. While the parameters  $\alpha$  and  $\beta$  represent the fiber distribution, parameters  $k_1$  and  $k_2$  represent the local fiber mechanics. Average fiber distributions (e.g. for all aortic valves) were obtained by averaging the corresponding individual fiber distributions. After that, averaged fiber parameters  $\overline{\alpha}$  and  $\overline{\beta}$  were determined by fitting Eq. (7.5) to the averaged fiber distribution using least squares optimization.

Similarly, averaged fiber mechanics were obtained by averaging the corresponding individual fiber tensile curves. After that, averaged fiber tensile properties  $\overline{k_1}$  and  $\overline{k_2}$  were obtained by fitting Eq. (7.6) to the averaged fiber tensile curves.

## 7.3 Results

### 7.3.1 Indentation test and Digital Image Correlation

Two consecutive indentation tests were applied to the belly and commissural region of each leaflet of each valve. Thus, a total of 72 indentation tests were performed on the aortic and pulmonary valves. Confocal imaging of the collagen fibers during indentation allowed real-time visualization of the tissue and fiber deformation behavior. On a microscopic scale it was observed that collagen fibers were crimped when the tissue was not loaded, and stretched when indentation was applied. On a mesoscopic scale, the valve appeared to be corrugated in the unloaded state, and during indentation the tissue unfolded (Fig. 7.4).

Confocal imaging and Digital Image Correlation was successful for 60 out of 72 cases. For one aortic valve, DIC was unsuccessful in the commissures of all three leaflets.

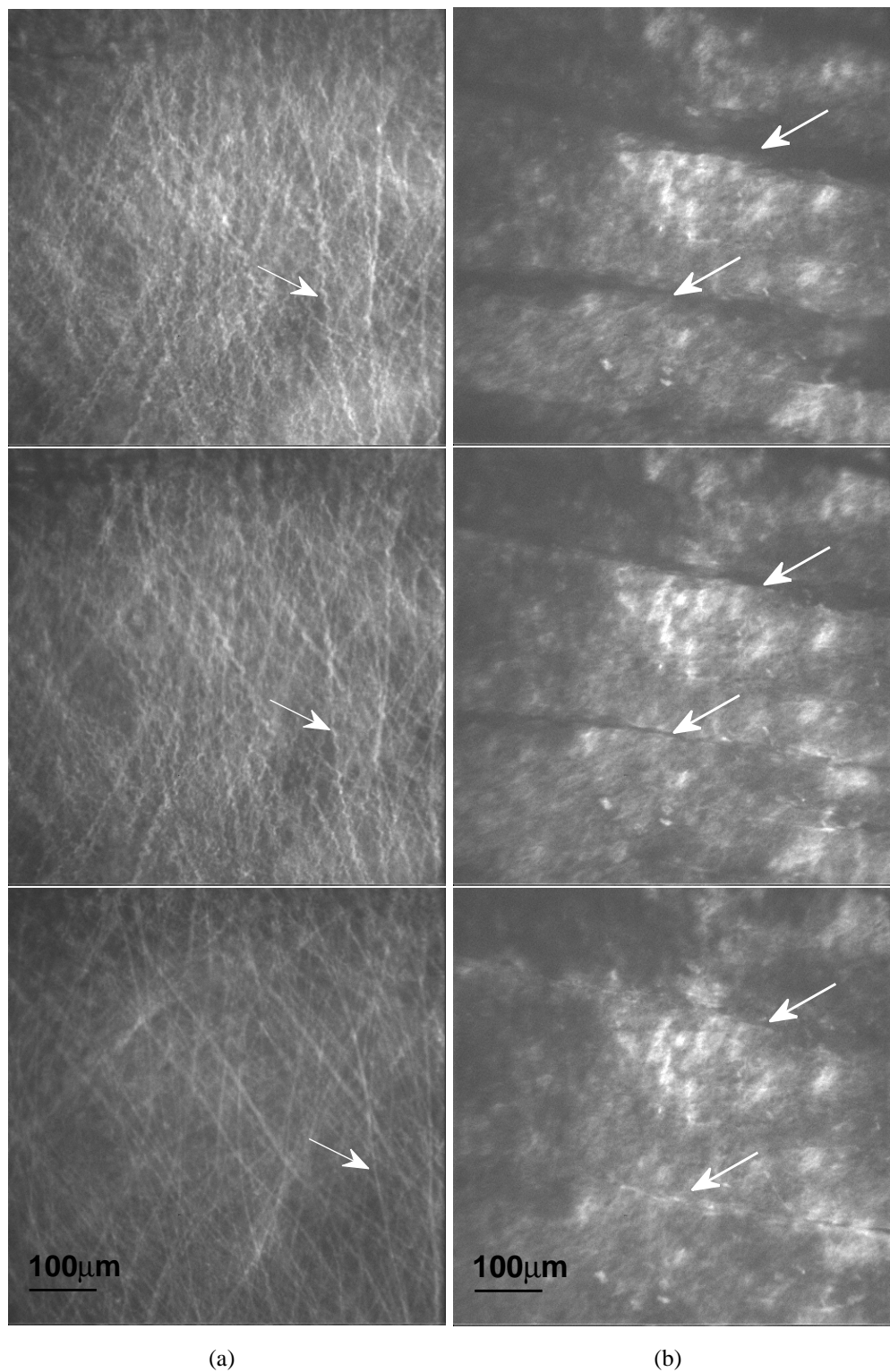


**Figure 7.4:** Confocal imaging during indentation shows collagen fiber uncrimping (microscopic scale) (a) as well as unfolding of the tissue (mesoscopic scale) (b). All images were taken at 10x magnification and are at same length scales.

### 7.3.2 Parameter estimation

Upon successful convergence in the parameter estimation algorithm, parameter sets with  $MRE_F$  or  $MRE_{AI}$  higher than 35% were excluded from further analysis, resulting in 19 parameter sets for the aortic valve, and 21 parameter sets for the pulmonary valve. For the main fiber orientation  $\alpha$ , the circumferential direction was defined at  $0^\circ$  and the radial direction at  $\pm 90^\circ$  (Fig. 7.1). Commissural fiber orientations were all calculated back to the right commissures. In Table 7.1 all averaged parameters and mean relative errors are given per experimental group. Number of valves and parameter sets per group are given as well.

**Table 7.1:** Material parameters and mean relative errors (MRE) per experimental group. Number of valves (#valves) and parameter sets (#exp) per group are indicated as well as the average leaflet thickness ( $\pm$ s.d.).

Valve	#valves	location	#exp	$G_m$ [kPa]	$k_1$ [kPa]	$k_2$ [-]	$\alpha$ [ $^\circ$ ]	$\beta$ [-]	$MRE_F$ [%]	$MRE_{AI}$ [%]	thickness [mm]
Aortic	3	belly	13	1.3	1.0E+01	0.5	4	0.8	8	20	0.48 $\pm$ 0.08
		commissure	6	1.0	2.0E+01	0.9	14	0.9	9	19	0.37 $\pm$ 0.11
Pulmonary	3	belly	11	1.0	1.0E+01	2.2	-2	0.6	9	19	0.36 $\pm$ 0.09
		commissure	10	1.1	1.8E+01	1.2	32	0.9	8	22	0.28 $\pm$ 0.07
TEHV	10	belly	39	1.0	2.0E+02	1.6	9	2.6	14	20	0.67 $\pm$ 0.22
		commissure	45	1.0	2.1E+02	1.6	15	1.7	11	19	0.70 $\pm$ 0.20

### 7.3.3 Structural fiber mechanics

As shown in Fig. 7.5, for both the aortic and pulmonary valves a clear circumferential fiber orientation was found in the belly region ( $\alpha = 4^\circ$  and  $\alpha = -2^\circ$ , respectively). In the commissural region main fiber orientation was shifted to the right, which appeared to be more pronounced for the pulmonary valve ( $\alpha = 32^\circ$ ) than for the aortic valve ( $\alpha = 14^\circ$ ). Interestingly, fiber alignment appeared to be equal or slightly higher in the belly regions of both the aortic ( $\beta = 0.8$ ) and pulmonary ( $\beta = 0.6$ ) valve than in the commissures, where  $\beta$  equaled 0.9 in both the aortic and the pulmonary valve. No or little differences were observed between aortic and pulmonary fiber alignment. For the fiber tensile mechanics again no large differences were found between the pulmonary and aortic valves. In all cases, the native valves were only moderately nonlinear for the tested strain range. Fiber initial stiffness in the commissural region appeared to be highest in the commissures for both valves, although differences were small. Leaflet thickness appeared to be highest in the belly, and also higher for the aortic valves than for the pulmonary valves. The estimated matrix shear modulus  $G_m$  was in the order of 1 kPa.

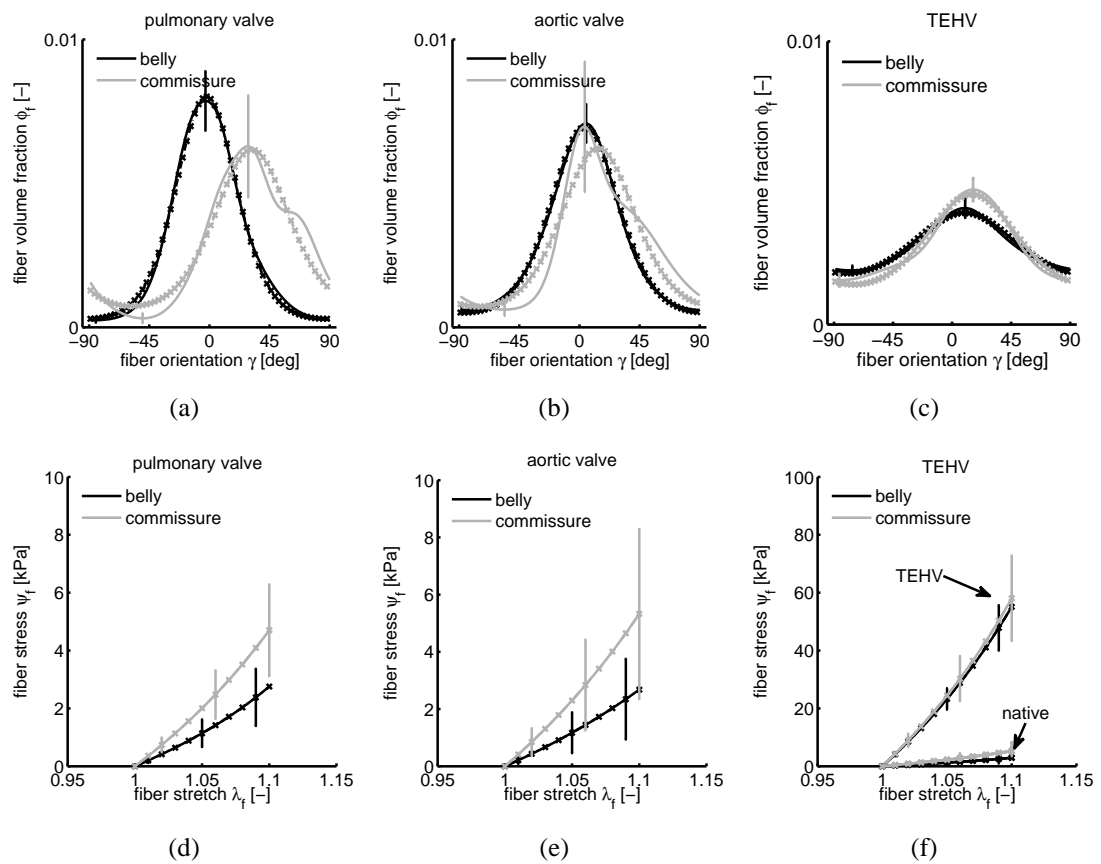


**Figure 7.5:** Estimated fiber distribution (a-c) and fiber mechanics (d-f) for ovine pulmonary (a,d) and aortic valves (b,e) and human TEHV (c,f). Errorbars indicate standard error of the mean (SEM) after averaging per experimental group. Crosses indicate fit with averaged material parameters (Table. 7.1).

### Native vs. tissue engineered

Native material parameters were compared to results for human tissue engineered heart valves (Chapter. 6). Results indicate that native and tissue engineered valves had similar main fiber orientations, although alignment was higher for native valves (Table 7.1, Fig. 7.5). Interestingly, in the tested strain regime the stiffness of the tissue engineered heart valves ( $k_1 \sim 200$  kPa) was, however, over an order of magnitude higher than native valve stiffness ( $k_1 \sim 10$  kPa). Furthermore, TEHV were thicker compared to native valves; even a factor two compared to pulmonary valves.

## 7.4 Discussion

Recent studies by Driessen et al. (2008) indicate a strong coupling between global mechanical conditions and local structural mechanics of heart valves. To validate the remodeling algorithms that were used to find this relationship, local structural mechanical characterization of



native as well as tissue engineered heart valves was performed in the current study. Indentation tests were combined with confocal imaging for mechanical characterization of native ovine pulmonary and aortic heart valve leaflets. During the indentation tests, two different deformation mechanisms were observed. At the microscopic scale, collagen fibers were initially crimped and straightened during indentation (Fig. 7.4a). At the mesoscopic scale, corrugations in the valve tissue unfolded upon loading (Fig. 7.4b).

For both the pulmonary and aortic valves, the numerical-experimental approach was successful in slightly over 50% of the performed experiments, which is lower than for TEHV ( $\sim 70\%$ , Chapter. 6). This is partly due to the inhomogeneity and corrugation of the native leaflets, which limit the possibilities for confocal imaging. Furthermore, in some cases, fiber bundles were rolling away during indentation, thus resulting in translation rather than deformation. Even though this study is the first to report on the local structural mechanics of native heart valve leaflets, the success ratio indicates that optimization is desirable. To this end a new, flattened indenter will be designed to increase deformation homogeneity in future experiments.

Mechanical characterization was performed in the belly and commissure regions of three native ovine pulmonary and aortic valves. Interestingly, no clear differences in *intrinsic* mechanical properties were found between the pulmonary and aortic valves. For both valves, a clear circumferential fiber orientation was found in the belly region, as expected. In the commissures, the main fiber orientation was shifted, which appeared to be less pronounced in the aortic valves ( $\alpha = 14^\circ$ ) than in the pulmonary valves ( $\alpha = 32^\circ$ ). However, it should be mentioned that only three out of nine aortic commissures were tested successfully, of which two were oriented at  $35^\circ$  and one at  $1^\circ$ . Therefore, it is likely that the main orientations in pulmonary and aortic valves do not significantly differ. Fiber alignment appeared to be slightly higher in the belly than in the commissural region, although differences were small. However, based on experimental findings (Sauren, 1981) as well as computational predictions (Driessen et al., 2008), maximal fiber alignment in the commissures was expected. As the ovine leaflets appeared to have a slightly different morphology than human or porcine leaflets, this difference might be species-related. Especially for the ovine aortic leaflets large circumferential fiber bundles were observed macroscopically, which appeared to run over the whole length of the leaflet, instead of towards the commissural edges. Another potential explanation may be that the relatively broad fiber distribution in the commissures is actually a summation of several narrow distributions with different orientations. As is clear from Fig. 7.1, main fiber orientation in the commissures varies significantly depending on the exact location. As no valve is exactly alike, it is not straightforward to test the exact same location in each leaflet. Furthermore, priority was given to obtaining a good location for confocal imaging.

Previous studies either found no differences between pulmonary and aortic valves (David et al., 1994; Stradins et al., 2004) or suggested that pulmonary valves were more extensible in radial direction (Christie and Barratt-Boyes, 1995). To compare our findings with these results, the leaflet thickness was measured to discriminate between the intrinsic and global tissue mechanics. Pulmonary valve leaflets appeared to be thinner than the aortic valve leaflets. This may indeed explain the inconclusive results from literature as Christie and Barratt-Boyes (1995) did

not correct for thickness differences in their calculations. Although *intrinsic* mechanics are similar, the pulmonary valve as a construct will still be more extensible than the aortic valve. Compared to the experimental results of Billiar and Sacks (2000b,a) with porcine aortic valves ( $k_1 \sim 1$  kPa,  $k_2 \sim 10$ ), our results indicated a higher initial stiffness ( $k_1 \sim 10$  kPa), and lower non-linearity ( $k_2 \sim 1$ ). Although this may be partly species-related, the strain regime in our experimental set-up was also narrower than in their biaxial tests. In a sense, our indentation represents a local equibiaxial loading state. As tissue will deform mainly perpendicular to the preferred fiber direction, fibers are not maximally stretched. Despite that local strains occasionally exceeded values of 100%, maximal strain in fiber direction was typically 20% to 25%. Therefore, our results can not predict the typical collagen locking phenomena that explain the highly nonlinear material behavior found by Billiar and Sacks (2000b). It needs to be remarked though that *in vivo* loading in essence is equibiaxial as well. Simulations of diastolic loading of the heart valve using the parameters of Billiar and Sacks (2000a) indicated *in vivo* strains of approximately 60% and 30% in radial and circumferential direction, respectively (Driessen et al., 2005b). Moreover, Adamczyk and Vesely (2002) found for glutaraldehyde-treated bio-prosthetic porcine valves that deformations during diastolic loading did not even exceed 5%. Therefore, it is our belief that our approach does provide relevant information for the valve behavior in the *in vivo* strain regime. However, to test the ultimate strength of biological tissues uniaxial, but preferably biaxial, tensile tests should be performed.

Mechanical properties of the native ovine valves were compared to those of human tissue engineered heart valves. The TEHV were found to have the same type of anisotropy, although less pronounced than in the native valves. This is an important result, as it indicates that *in vitro* mimicking the *in vivo* mechanical environment in a Diastolic Pulse Duplicator does stimulate local structural tissue development towards native tissue structure. Nonetheless, tissue engineered valve stiffness was an order of magnitude higher for the *in vivo* strain range. A possible explanation is that for the native valves, collagen fiber uncrimping as well as tissue unfolding were observed during the indentation tests (Fig. 7.4), which was not the case for the tissue engineered valves. However, animal studies with TEHV and TE blood vessels, indicate that tissue remodeling continues *in vivo* after implantation, and flexibility of the leaflets is increased quickly (Hoerstrup et al., 2000, 2002). In literature it is hypothesized that collagen crimping is caused by a radially oriented network of elastin, which keeps the collagen fiber network under compression in the absence of external loads (Scott and Vesely, 1996). As TEHV generally contain little or no elastin, this may explain why collagen fibers are not crimped in the TEHV. The TEHV leaflets were also found to be thicker than native valve leaflets, even a factor two compared to pulmonary leaflets. It is therefore suggested to aim for a reduction in thickness to increase flexibility of the TEHV.

One of the shortcomings of our approach for the TEHV was that on occasions, the FE model overestimated the experimentally measured strains, which was attributed to experimental friction (Chapter 6)(Cox et al., 2009). For the native valves, deformations were generally larger, and strain overestimation was hardly observed. These results may indicate that friction was actually lower for the native leaflets, e.g. because of a smoother surface, or smaller contact area

due to local corrugations.

In conclusion, this study was, to the best of our knowledge, the first to describe the *local* structural mechanics in the belly *and* commissural region of native ovine aortic and pulmonary heart valves. *Intrinsic* structural mechanical properties were found to be highly similar for the pulmonary and aortic valve. Pulmonary valve leaflets were, however, thinner than aortic valve leaflets, and therefore more extensible as a construct. As in the current study native ovine valves were compared to human tissue engineered valves, it is suggested to perform additional indentation tests on native porcine and human heart valves as well as tissue engineered ovine valves to exclude species-related effects.

When human tissue engineered valves were compared to native ovine valves, the tissue engineered valves were found to be much stiffer in the *in vivo* strain regime. It is expected that the observed differences are related to crimping of collagen fibers in the native tissue. Moreover, tissue engineered valve leaflets were thicker than their native counterparts. As our results clearly indicate that tissue thickness is an important parameter for mechanical behavior of heart valves in the *in vivo* strain regime, it is suggested to aim for tissue engineered heart valves with a lower leaflet thickness, obviously without compromising the ultimate tensile strength of the valves as a construct.

## Acknowledgements

The author would like to thank dr. Imo Hofer from the laboratory for Experimental Cardiology at University Medical Centrum Utrecht for providing the native ovine heart valves.

---

## General discussion

---

*In this chapter the main findings and conclusions of this thesis are summarized. Subsequently, the scope and limitations of the newly developed mechanical characterization method are discussed and compared to currently existing methods. The chapter is concluded with some recommendations and future perspectives.*

## 8.1 Summary and conclusions

During our whole life our body continues to grow, repair and remodel to adapt to changes in our environment. Training strengthens our muscles, and increases lung volume and maximal cardiac output. On the other hand, chronically overeating will cause our stomachs to stretch. This principle of internal adaptations to ensure stability despite changes in the outside environment is called homeostasis. An inability to maintain homeostasis may cause homeostatic imbalance, which may lead to disease or death.

As changes in tissue structure are mainly made at the microscopic level, there must be a mechanism that connects global conditions and local tissue remodeling. For the aortic valve, many studies were performed to relate local tissue structure to global mechanical properties. Importantly, Driessen et al. (2008) provided computational evidence for the reverse route: remodeling algorithms were used to qualitatively predict the native collagen fiber architecture as a result of local tissue strain during the diastolic loading phase of the cardiac cycle. Following this principle, tissue engineers were already successful in creating strong tissues *in vitro*, by using global mechanical conditioning protocols that mimic the *in vivo* mechanical environment during diastole. Human heart valves were engineered, which showed *in vitro* the ability to withstand the high systemic pressures that occur at the aortic valve position.

The aim of this thesis was to provide experimental validation and quantification for this apparent relationship. It was hypothesized that by mimicking diastolic loads *in vitro* in a bioreactor, tissue engineered heart valves can be stimulated to develop towards native valve local structural properties. To test this hypothesis, a mechanical characterization method needed to be developed that 1) allowed for local characterization of the tissue mechanics, 2) was able to capture the full in-plane mechanical behavior of biological tissues and 3) incorporated fiber structure and mechanics directly into the experimental set-up *and* in the resulting material model.

It was chosen to use a spherical indentation test, combined with confocal imaging. As the indenter size is small compared to global tissue dimensions, this method qualifies as a local measurement. Furthermore, confocal imaging allows visualization of the collagen fibers. Since fibers are stiffer than the surrounding tissue, deformation perpendicular to the main fiber direction is largest. Therefore, local tissue anisotropy can be quantified as well. Moreover, the estimated fiber structure is *directly coupled* to the local tissue mechanics.

In Chapter 2 to 4, extensive computational and experimental validation of the newly developed method was provided and it was demonstrated that one single indentation test provides sufficient information for characterization of the local tissue structural mechanics. Although this method was especially developed for application to native and tissue engineered heart valve leaflets, the method applies in general for planar soft biological tissues. In Chapter 5 the versatility of the methodology was demonstrated. Indentation tests on Bioartificial Muscle tissues (BAMs) revealed that these tissues became stiffer and more nonlinear when cells were added during tissue culture. In this specific case, tensile tests would not have been feasible due to the low mechanical integrity of the BAMs.

In the last two chapters, indentation tests were applied for the local structural mechanical char-

acterization of human tissue engineered heart valves (Chapter 6) and native ovine aortic and pulmonary heart valves (Chapter 7), respectively. In Chapter 6, human tissue engineered heart valves were cultured for four weeks in a bioreactor. During culture, the heart valves were subjected to gradually increasing pulsatile loads, thus mimicking diastolic conditions. For the tissue engineered heart valves, it was found that the local tissue structure was indeed developing towards native values, thus confirming the hypothesis of Driessen et al. (2008). Interestingly, no clear differences were found within the range of the different loading protocols that were applied, or at least, differences were smaller than the observed inter-experimental variability within the same protocol. For the native ovine valves (Chapter 7) *intrinsic* structural mechanical properties of the aortic and pulmonary valves were highly similar. Nonetheless, pulmonary valve leaflets appeared to be thinner than aortic valve leaflets, which makes the pulmonary valves more extensible compared to aortic valves.

Compared to native, tissue engineered valves expressed a similar collagen fiber orientation, although anisotropy was more pronounced in the native valves. Importantly, tissue engineered heart valves appeared to be an order of magnitude stiffer than the native valves in the *in vivo* strain regime. It is suggested that this is due to the fact that the collagen fibers in native valves are crimped in the unloaded state, while in the tissue engineered valves they are not. The current hypothesis is that collagen fiber crimping is caused by a radially oriented network of elastin fibers. As elastin is indeed scarce in tissue engineered valves, this provides a good explanation for the observed differences. It should be noted that animal studies provided strong indications that tissue engineered heart valves continue to remodel *in vivo*, leading to increased leaflet flexibility, indicating that such an elastin network will develop over time.

Returning to our objectives, it can be concluded that quantification of the relationship between global mechanical conditioning and development of local tissue structure was not realized yet. Within the range of tested protocols the effect of different mechanical conditioning protocols appeared to be smaller than the experimental variation. Nonetheless, it was found that tissue engineered heart valves develop native-like structural properties when subjected to diastolic loading *in vitro* in a bioreactor. Despite this good news, still some important differences were found between native and tissue engineered valves for the stiffness in the *in vivo* strain regime, which were explained by a difference in collagen fiber crimping.

## 8.2 Scope and limitations of the developed method

In this thesis a novel method was developed for the local, structural characterization of planar soft biological tissues. The currently most common techniques for mechanical characterization of soft biological tissues are uniaxial and biaxial tensile testing. Uniaxial tensile tests are easy to perform, and testing equipment is a commodity in most biomechanical laboratories. Although uniaxial tensile test do not provide sufficient information for a full characterization of the in-plane mechanical properties, tests are easy to perform, and results are easy to interpret and provide a means for direct comparison between different specimens. Biaxial tensile

tests are more difficult and time-consuming to perform, and correct interpretation of the results necessitates incorporation of an appropriate constitutive model to be fitted to the results. In addition, biaxial test equipment is significantly more expensive than uniaxial tensile machines. On the other hand, biaxial testing is accepted to be the method that provides the most complete mechanical characterization of biological tissues. A disadvantage of both uniaxial and biaxial testing is that it is difficult to define the unloaded configuration as soft biological tissues exhibit highly nonlinear tensile behavior. E.g., clamping the tissue will already induce a prestress. To improve this, Billiar and Sacks (2000b) suggested to submerge the test specimens in isotonic saline during the test, and add floats to make the sample neutrally buoyant. Markers were added to the tissue to record deformation and unloaded configuration was then defined as the free floating configuration. Although this way clamping prestretch may be quantified, prestretch will still be present.

Alternatively to (multi)axial tensile testing, researchers have proposed the use of inflation tests (Adamczyk et al., 2000), pipette aspiration (Aoki et al., 1997; Ohashi et al., 2005), three point bending tests (Mirnajafi et al., 2005, 2006) and indentation tests (Gow and Vaishnav, 1975; Hori and Mockros, 1976; Gow et al., 1983; Zheng and Mak, 1996; Lundkvist et al., 1997; Han et al., 2003; Ebenstein and Pruitt, 2004). Especially pipette aspiration and indentation, and to a lesser amount extent three point bending, are suitable for characterization of local tissue mechanics. However, most literature on these tests is limited to linear elastic and/or isotropic material behavior and therefore not suitable for our purposes.

The proposed new approach, combining indentation tests with confocal imaging, does allow for the local characterization of nonlinear and anisotropic properties. Nonetheless, there are also some limitations. Compared to biaxial tests, the range of strain regimes that can be applied is limited. In biaxial tests, loading regimes can vary from equibiaxial to uniaxial in either of two orthogonal directions, while in the indentation set-up the tissue is essentially subjected to equibiaxial tension. As tissue will deform mainly perpendicular to the preferred fiber direction, fibers are not maximally stretched. As a result, the apparent mechanical properties determined with our approach are only valid within a limited strain regime. Nonetheless, *in vivo* strains are within the range of our applied strain regimes and since *in vivo* loading conditions are roughly equibiaxial as well, our results do predict the *in vivo* mechanical behavior.

An important assumption in our and most other approaches is uniform mechanical behavior through the thickness of the tissue. However, aortic valves, as well as many other biological tissues, clearly have a layered structure. Thus, obtained material parameters represent the effective behavior as the sum of the contributions of the individual layers. Potentially, this has different influences in tensile tests, where the layers are tested in parallel, compared to indentation tests, where the layers are tested in series. An important advantage of the indentation test approach over tensile tests is that no clamping is needed; the tissue is naturally stress-free. Moreover, force resolution is sufficiently precise to allow for unambiguous definition of the initial point of contact between indenter and tissue.

A disadvantage of the chosen set-up is that friction between the tissue and base plate may reduce the observed experimental strains. As friction effects are difficult to quantify, reduction of

friction through modification of the base plate surface is the most feasible option for minimizing associated difficulties.

With regards to the inverse FE analysis, it should be remarked that a pseudo-inverse approach was used. In a true inverse approach, the functional form of the constitutive model follows directly from the experimental data (Humphrey et al., 1990). By choosing a structural constitutive model *a priori*, quality of fit is limited by the assumptions inherent to the chosen model. E.g., in our approach it was chosen to represent the fiber mechanics by an effective exponential fiber law (Billiar and Sacks, 2000a), while it is known from literature and our own experimental observations that a fiber recruitment law would be closer to reality (Lanir, 1983).

Overall, the proposed methodology offers a good alternative for biaxial testing, especially when local information is demanded. However, due to limitations in applicable strain regime, the method will not provide information on collagen-locking mechanisms or ultimate tensile strength.

### 8.3 Recommendations

For the human tissue engineered heart valves tested in Chapter 6 no effect was found of magnitude of mechanical conditioning on the developed architecture. As the range of tested conditioning protocols was small, it is suggested to repeat these experiments for a wider range of loading conditions. Ideally, this should lead to quantification of the effect of mechanical conditioning on local structural mechanics, and thus to optimized tissue engineering protocols. In Chapter 7, native ovine valves were tested and compared to human tissue engineered valves. Completion of these datasets with indentation tests on native human valves and tissue engineered ovine valves will allow for a better comparison between TE and native valves, and will provide additional information on species-related differences in TE, which is important towards clinical applications.

One of the most important findings of the current thesis is that in the *in vivo* strain regime, the tissue engineered valves' *intrinsic* stiffness appears to be an order of magnitude higher than that of native valves, possibly due to the absence of collagen fiber crimping in the tissue engineered heart valves. Currently, mechanical testing of tissue engineered heart valves is most often limited to uniaxial tensile tests, resulting in one-dimensional material parameters, e.g., radial and circumferential moduli and ultimate tensile stress. As these parameters are determined in the high strain regime, little information is obtained on the behavior for *in vivo* strains. Our results clearly underline the importance of measuring the low deformation behavior as well. Therefore it is proposed to incorporate routine testing of low strain behavior in the mechanical characterization of tissue engineered heart valves. The time-consuming and complex inverse analysis needed for our indentation approach makes it less suitable for routine testing purposes. To circumvent the inverse analysis part, one may consider parametrization of the solution space by performing forward simulations for a range of parameter values. By fitting this parametric surface to experimental results approximate parameter values may be obtained, which would



suffice for routine testing purposes. Alternatively, the use of three point bending tests to determine flexural stiffness is suggested (Mirnajafi et al., 2006). Only slight modifications would be needed to perform these experiments in our indentation set-up, possibly even combined with confocal imaging. Tests could be performed on the same tissue strips that are already being used for uniaxial tensile tests of the tissue engineered valves. In addition, Kortsmit et al. (2008) recently developed a method for non-invasive real-time assessment of global tissue mechanics based on volumetric deformation measured during pressurization of the valve, which can be performed *in situ* during tissue culture. Although this approach is currently limited to isotropic and homogenous material properties, it provides a powerful tool for real-time, non-destructive evaluation and control of the mechanical properties of the developing heart valve *in vitro*.

In conclusion, a generic numerical-experimental tool was developed for the local structural mechanical characterization of planar soft biological tissues. Application of this tool to native and tissue engineered heart valves has led to increased insight into the local structural mechanics of these valves. Results indicate that we should aim for a thickness reduction for the tissue engineered valves to increase flexibility in the *in vivo* strain regime. Future application of the proposed approach will allow quantification of the relationship between global mechanical conditioning and local structural tissue development, thus allowing further optimization and control of heart valve tissue engineering protocols.

---

## References

---

- Adamczyk, M.M., Lee, T.C., and Vesely, I. Biaxial strain properties of elastase-digested porcine aortic valves. *J. Heart Valve Dis.*, 9(3):445–453, 2000.
- Adamczyk, M.M. and Vesely, I. Biaxial strain distributions in explanted porcine bioprosthetic valves. *J. Heart Valve Dis.*, 11(5):688–695, 2002.
- Amouroux, N. and Leger, L. Effect of dangling chains on adhesion hysteresis of silicone elastomers, probed by jkr test. *Langmuir*, 19:1396–1401, 2003.
- Ankrom, M.A., Bennett, R.G., Sprigle, S., Langemo, D., Black, J.M., Berlowitz, D.R., and Lyder, C.H. Pressure-related deep tissue injury under intact skin and the current pressure ulcer staging systems. *Adv. Skin Wound Care*, 2005.
- Aoki, T., Ohashi, T., Matsumoto, T., and Sato, M. The pipette aspiration applied to the local stiffness measurement of soft tissues. *Ann. Biomed. Eng.*, 25:581–587, 1997.
- Baek, S., Rajagopal, K.R., and Humphrey, J.D. A theoretical model of enlarging intracranial fusiform aneurysms. *J. Biomech. Eng.*, 128:142–149, 2006.
- Balguid, A., Mol, A., van Vlimmeren, M.A.A., Baaijens, F.P.T., and Bouten, C.V.C. Hypoxia induces near-native mechanical properties in engineered heart valve tissue. *Circulation*, 119:290–297, 2009.
- Balguid, A., Rubbens, M.P., Mol, A., Bank, R.A., Bogers, A.J.J.C., van Kats, J.P., de Mol, B.A.J.M., Baaijens, F.P.T., and Bouten, C.V.C. The role of collagen cross-links in biomechanical behavior of human aortic valve leaflets: Relevance for tissue engineering. *Tissue Engineering*, 13(7):1501–1511, 2007.
- Bard, Y. *Nonlinear Parameter Estimation*. Academic Press Inc., London, UK, 1974.

- Barocas, V.H. and Tranquillo, R.T. An anisotropic biphasic theory of tissue-equivalent mechanics: the interplay among cell traction, fibrillar network deformation, fibril alignment and cell contact guidance. *J. Biomech. Eng.*, 119:137–145, 1997.
- Bechtel, J.F.M., Muller-Steinhardt, M., Schmidtke, C., Brunswik, A., Stierle, U., and Sievers, H. Evaluation of the decellularized pulmonary valve homograft (synergraft<sup>tm</sup>). *J. Heart Valve Dis.*, 12:734–740, 2003.
- Belytschko, T., Liu, W.K., and Moran, B. *Nonlinear Finite Elements for Continua and Structures*, chapter 10. Wiley and Sons Ltd, Chichester, England, 2000.
- Billiar, K.L. and Sacks, M.S. A method to quantify the fiber kinematics of planar tissues under biaxial stretch. *J. Biomech.*, 30(7):753–756, 1997.
- Billiar, K.L. and Sacks, M.S. Biaxial mechanical properties of the native and glutaraldehyde-treated aortic valve cusp - Part II: A structural constitutive model. *J. Biomech. Eng.*, 122:327–335, 2000a.
- Billiar, K.L. and Sacks, M.S. Biaxial mechanical properties of the natural and glutaraldehyde treated aortic valve cusp - Part I: Experimental results. *J. Biomech. Eng.*, 122:23–30, 2000b.
- Bischoff, J.E. Static indentation of anisotropic biomaterials using axially asymmetric indenters - a computational study. *J. Biomech. Eng.*, 126:498–505, 2004.
- Boerboom, R.A., Bouten, C.V.C., and Baaijens, F.P.T. Development of structural and mechanical anisotropy in engineered cardiovascular tissues. *J. Biomech. Eng.*, 2007a. To be submitted.
- Boerboom, R.A., Nash-Krahn, K., Megens, R.T.A., van Zandvoort, M.A.M.M.J., Merckx, M., and Bouten, C.V.C. High resolution imaging of collagen organisation and synthesis using a versatile collagen specific probe. *J. Struct. Biol.*, 159:392–399, 2007b.
- Boerboom, R.A., Rubbens, M.P., Driessen, N.J.B., Bouten, C.V.C., and Baaijens, F.P.T. Effect of strain magnitude on the tissue properties of engineered cardiovascular constructs. *Ann. Biomed. Eng.*, 36(2):244–253, 2008.
- Bouten, C.V.C., Knight, M.M., Lee, D.A., and Bader, D.L. Compressive deformation and damage of muscle cell subpopulations in a model system. *Ann. Biomed. Engineering*, 29:153–163, 2001.
- Breuls, R.G.L., Bouten, C.V.C., Oomens, C.W.J., Bader, D.L., and Baaijens, F.P.T. A theoretical analysis of damage evolution in skeletal muscle tissue with reference to pressure ulcer development. *J. Biomech. Eng.*, 125:902–909, 2003a.
- Breuls, R.G.M., Bouten, C.V.C., Oomens, C.W.J., Bader, D.L., and Baaijens, F.P.T. Compression induced cell damage in engineered muscle tissue: an in vitro model to study pressure ulcer etiology. *Annals in Biomedical Engineering*, 31:1357–1364, 2003b.

- Carew, E.O., Barber, J.E., and Vesely, I. Role of preconditioning and recovery time in repeated testing of aortic valve tissues: Validation through quasilinear viscoelastic theory. *Ann. Biomed. Eng.*, 28:1093–1100, 2000.
- Carr-White, G.S., Kilner, P.J., Hon, J.J.F., Rutledge, T., Edwards, S., Burman, E D Pennell, D., and Yacoub, M.H. Incidence, location, pathology and significance of pulmonary homograft stenosis after the ross operation. *Circulation*, 104:116–20, 2001.
- Ceelen, K.K., Oomens, C.W.J., and Baaijens, F.P.T. Microstructural analysis of deformation-induced hypoxic damage in skeletal muscle. *Biomech. Mod. Mechanobiol.*, 7(4):277–284, 2008.
- Chew, P.H., Yin, F.C.P., and Zeger, S.L. Biaxial stress-strain properties of canine pericardium. *J. Mol. Cell. Cardiol.*, 18:567–578, 1986.
- Christie, G.W. and Barratt-Boyes, B.G. Mechanical properties of porcine pulmonary valve leaflets: How do they differ from aortic leaflets? *Ann. Thorac. Surg.*, 60:S195–S199, 1995.
- Clark, R.E. Stress-strain characteristics of fresh and frozen human aortic and mitral leaflets and chordae tendinae. *J. Thorac. Card. Surg.*, 66(2):202–208, 1973.
- Costa, K.D., Lee, E.J., and Holmes, J.W. Creating alignment and anisotropy in engineered heart tissue: Role of boundary conditions in a model three-dimensional culture system. *Tissue Engineering*, 9(4):567–577, 2003.
- Costa, K.D. and Yin, F.C.P. Analysis of indentation: Implications for measuring mechanical properties with atomic force microscopy. *J. Biomech. Eng.*, 121:462–471, 1999.
- Cox, M.A.J., Driessen, N.J.B., Boerboom, R.A., Bouten, C.V.C., and Baaijens, F.P.T. Mechanical characterization of anisotropic planar biological soft tissues using finite indentation: experimental feasibility. *J. Biomech.*, 41(2):422–429, 2008.
- Cox, M.A.J., Driessen, N.J.B., Bouten, C.V.C., and Baaijens, F.P.T. Mechanical characterization of anisotropic planar biological soft tissues using large indentation: An experimental validation study. In H. Rodrigues, M. Cerrolaza, M. Doblare, J. Ambrosio, and M. Viceconti, editors, *Proceedings of ICCB 2005*, pp. 339–350. Lisbon, Portugal, 2005.
- Cox, M.A.J., Driessen, N.J.B., Bouten, C.V.C., and Baaijens, F.P.T. Mechanical characterization of anisotropic planar biological soft tissues using large indentation: A computational feasibility study. *J. Biomech. Eng.*, 128(3):428–436, 2006.
- Cox, M.A.J., Kortsmid, J., Driessen, N.J.B., Bouten, C.V.C., and Baaijens, F.P.T. Tissue engineered heart valves develop native-like structural properties. *Tissue Engineering Part A*, 2009. Submitted.
- David, H., Boughner, D.R., Vesely, I., and Gerosa, G. The pulmonary valve. is it mechanically suitable for use as an aortic replacement? *ASAIO J*, 40(2):206–212, 1994.

- Delalleau, A., Josse, G., Lagarde, J., Zahouani, H., and Bergheau, J. Characterization of the mechanical properties of skin by inverse analysis combined with the indentation test. *J. Biomech.*, 39:1603–1610, 2006.
- Doehring, T.C., Kahelin, M., and Vesely, I. Mesostructures of the aortic valve. *Journal of Heart Valve Disease*, 14:679–686, 2005.
- Dolk, H. Annual report to who 2004-5. Technical report, EUROCAT, <http://www.eurocat.ulster.ac.uk/pdf/EUROCAT-Annual-Report-2005-for-WHO.pdf>, 2005.
- Donnelly, J. Should we include deep tissue injury in pressure ulcer staging systems? The NPUAP debate. *J. Wound Care*, 2005.
- Driessen, N.J.B., Bouten, C.V.C., and Baaijens, F.P.T. Improved prediction of the collagen fiber architecture in the aortic heart valve. *J. Biomech. Eng.*, 127:329–336, 2005a.
- Driessen, N.J.B., Bouten, C.V.C., and Baaijens, F.P.T. A structural constitutive model for collagenous cardiovascular tissues incorporating the angular fiber distribution. *J. Biomech. Eng.*, 127(3):494–503, 2005b.
- Driessen, N.J.B., Cox, M.A.J., Bouten, C.V.C., and Baaijens, F.P.T. Remodeling of the angular collagen fiber distribution in cardiovascular tissues. *Biomech. Mod. Mechanobiol.*, 7:93–103, 2008.
- Driessen, N.J.B., Mol, A., Bouten, C.V.C., and Baaijens, F.P.T. Modeling the mechanics of tissue-engineered human heart valve leaflets. In H. Rodrigues, M. Cerrolaza, M. Doblare, J. Ambrosio, and M. Viceconti, editors, *Proceedings of ICCB 2005*, pp. 457–476. Lisbon, Portugal, 2005c.
- Driessen, N.J.B., Mol, A., Bouten, C.V.C., and Baaijens, F.P.T. Modeling the mechanics of tissue-engineered human heart valve leaflets. *J. Biomech.*, 40:325–334, 2007.
- Driessen, N.J.B., Peters, G.W.M., Huyghe, J.M., Bouten, C.V.C., and Baaijens, F.P.T. Remodelling of continuously distributed collagen fibers in soft connective tissues. *J. Biomech.*, 36:1151–1158, 2003.
- Ebenstein, D.M. and Pruitt, L.A. Nanoindentation of soft hydrated materials for application to vascular tissues. *J. Biomed. Mater. A*, 69(2):222–232, 2004.
- Elkins, R.C., Dawson, P.E., Goldstein, S., Walsh, S.P., and Black, K.S. Decellularized allografts. *Ann Thorac Surg*, 71:s428–s432, 2001.
- Erdemir, A., Viveiros, M.L., Ulbrecht, J.S., and Cavanagh, P.R. An inverse finite-element model of heel-pad indentation. *J. Biomech.*, 39(7):1279–1286, 2006.
- Fung, Y.C. Biorheology of soft tissues. *Biorheology*, 10(2):139–155, 1973.

- Gasser, T.C., Ogden, R.W., and Holzapfel, G.A. Hyperelastic modelling of arterial layers with distributed collagen fibre orientations. *J. Roy. Soc. Interface*, 3:15–35, 2006.
- Gawlitta, D., Li, W., Oomens, C.W.J., Baaijens, F.P.T., Bader, D.L., and Bouten, C.V.C. The relative contributions of compression and hypoxia to development of muscle tissue damage: an in vitro study. *Ann Biomed. Eng.*, 35(3):273–284, 2007.
- Geers, M.G.D., de Borst, R., and Brekelmans, W.A.M. Computing strain fields from discrete displacements in 2d-solids. *Int. J. Solids Structures*, 33:4293–4307, 1996.
- Gefen, A., Gefen, N., Linder-Ganz, E., and Margulies, S.S. In vivo muscle stiffening under bone compression promotes deep pressure sores. *J. Biomech. Eng.*, 127:512–524, 2005.
- Ghista, D.N. and Rao, A.P. Mitral-valve mechanics - stress/strain characteristics of excised leaflets, analysis of its functional mechanics and its medical application. *Med. Biol. Eng.*, 11(6):691–702, 1973.
- Gow, B.S., Castle, W.D., and Legg, M.J. An improved microindentation technique to measure changes in properties of arterial intima during atherogenesis. *J. Biomech.*, 16(6):451–458, 1983.
- Gow, B.S. and Vaishnav, R.N. A microindentation technique to measure rheological properties of the vascular intima. *J. Appl. Mech.*, 38(2):344–350, 1975.
- Green, A.E. and Zerna, W. *Theoretical elasticity*. Oxford University Press, London, 1968.
- Han, L., Noble, J.A., and Burcher, M. A novel ultrasound indentation system for measuring biomechanical properties of in vivo soft tissue. *Ultrasound in Med. Biol.*, 29(6):813–823, 2003.
- Haverich, A. Tissue engineering. *Eur. J. Cardiothorac. Surg.*, 26:59–61, 2004.
- Hayes, W.C., Keer, L.M., Hermann, G., and Mockros, L.F. A mathematical analysis for indentation tests of articular cartilage. *J. Biomech.*, 5:541–551, 1972.
- Hendriks, M.A.N., Oomens, C.W.J., Jans, H.W.J., Janssen, J.D., and Kok, J.J. A numerical experimental approach for the mechanical characterisation of composites and biological tissues by means of non-linear filtering. In V. Askegaard, editor, *Proc. 9th International Conference on Experimental Mechanics*, pp. 552–561. 1990.
- Hertz, H. Über die berührung fester elastischer körper (on the contact of elastic solids). *J. Reine Angew. Mathematik*, 92:156–171, 1881.
- Hoerstrup, S.P., Kadner, A., Breyman, C., Maurus, C.F., Gunter, C.I., Sodian, R., Visjager, J.F., Zund, G., and Turina, M.I. Living, autologous pulmonary artery conduits tissue engineered from human umbilical cord cells. *Ann. Thorac. Surg.*, 74:46–52, 2002.

- Hoerstrup, S.P., Sodian, R., Daebritz, S., Wang, J., Bacha, E.A., Martin, D.P., Moran, A.M., Guleserian, K.J., Sperling, J.S., Kaushal, S., Vacanti, J.P., Schoen, F.J., and Mayer Jr, J.E. Functional living trileaflet heart valves grown in vitro. *Circ.*, 102:III-44-III-49, 2000.
- Hoffman, J.I.E. and Kaplan, S. The incidence of congenital heart disease. *J. Am. Coll. Cardiol.*, 39(12):1890-1900, 2002.
- Holzapfel, G.A., Gasser, T.C., and Ogden, R.W. A new constitutive framework for arterial wall mechanics and a comparative study of material models. *J. Elast.*, 61(1-3):1-48, 2000.
- Hori, R.Y. and Mockros, L.F. Indentation tests of human articular cartilage. *J. Biomech.*, 9:259-268, 1976.
- Humphrey, J.D. *Cardiovascular solid mechanics : cells, tissues, and organs*. Springer, Berlin, Germany, 2002.
- Humphrey, J.D., Halperin, H.R., and Yin, F.C.P. Small indentation superimposed on a finite equibiaxial stretch: Implications for cardiac mechanics. *J. Appl. Mech.*, 58:1108-1111, 1991.
- Humphrey, J.D., Strumpf, R.K., and Yin, F.C.P. Determination of a constitutive relation for passive myocardium: I. a new functional form. *J. Biomech. Eng.*, 112(4):333-339, 1990.
- Jockenhoevel, S., Zund, G., Hoerstrup, S.P., Chalabi, K., Sachweh, J.S., Demircan, L., Messmer, B.J., and Turina, M. Fibrin gel - advantages of a new scaffold in cardiovascular tissue engineering. *Eur. J. Cardiothorac. Surg.*, 19(4):424-430, 2001.
- Johnson, K.L., Kendall, K., and Roberts, A.D. Surface energy and the contact of elastic solids. *Proc. R. Soc. Lond. A*, 324:301-313, 1971.
- Kadner, A., Zund, G., Maurus, C., Breymann, C., Yakarisik, S., Kadner, G., Turina, M., and Hoerstrup, S.P. Human umbilical cord cells for cardiovascular tissue engineering: a comparative study. *Eur. J. Card. Thor. Surg.*, 25:635-641, 2004.
- Karduna, A.R., Halperin, H.R., and Yin, F.C.P. Experimental and numerical analyses of indentation in finite-sized isotropic and anisotropic rubber-like materials. *Ann. Biomed. Eng.*, 25:1009-1016, 1997.
- Klieverik, L M Aand Takkenberg, J.J.M., Bekkers, J.A., Roos-Hesselink, J.W., Witsenburg, M., and Bogers, A.J.J.C. The ross operation: a trojan horse? *European Heart Journal*, 28(16):1993-2000, 2007.
- Kortsmit, J., Driessen, N.J.B., M, R.M.C., and Baaijens, F.P.T. Nondestructive and noninvasive assessment of mechanical properties in heart valve tissue engineering. *Tissue Engineering Part A*, 2008. Epub ahead of print.

- Kortsmit, J., Driessen, N.J.B., Rutten, M.C.M., and Baaijens, F.P.T. Real time, non-invasive assessment of leaflet deformation in heart valve tissue engineering. *Annals of Biomedical Engineering*, 37(3):532, 2009. Epub 2008.
- Kunzelman, K.S. and Cochran, R.P. Stress/strain characteristics of porcine mitral valve tissue: Parallel versus perpendicular collagen orientation. *J. Card. Surg.*, 7(1):71–78, 1992.
- Lanir, Y. Constitutive equations for fibrous connective tissues. *J. Biomech.*, 16:1–12, 1983.
- Lanir, Y. and Fung, Y.C. Two-dimensional mechanical properties of rabbit skin - I. experimental system. *J. Biomech.*, 7:29–34, 1974a.
- Lanir, Y. and Fung, Y.C. Two-dimensional mechanical properties of rabbit skin - II. experimental results. *J. Biomech.*, 7:171–182, 1974b.
- Lanir, Y., Lichtenstein, O., and Immanuel, O. Optimal design of biaxial tests for structural material characterization of flat tissues. *J. Biomech. Eng.*, 118:41–47, 1996.
- Lee, T.C., Midura, R.J., Hascall, V.C., and Vesely, I. The effect of elastin damage on the mechanics of the aortic valve. *J. Biomech.*, 34:203–210, 2001.
- Lei, F. and Szeri, A.Z. Inverse analysis of constitutive models: Biological soft tissues. *J. Biomech.*, 40(4):936–940, 2007.
- Li, J., Luo, X.Y., and Kuang, Z.B. A nonlinear anisotropic model for porcine heart valves. *J. Biomech.*, 34:1279–1289, 2001.
- Li, Z., Brokken-Zijp, J.C.M., and de With, G. Determination of the elastic moduli of silicone rubber coatings and films using depth-sensing indentation. *Polymer*, 45(5403-5406), 2004.
- Linder-Ganz, E. and Gefen, A. Mechanical compression-induced pressure sores in rat hindlimb: muscle stiffness, histology and computational models. *J. Appl. Physiol.*, 96:2034–2049, 2004.
- Lundkvist, A., Lilleodden, E., Siekhaus, W., Kinney, J., Pruitt, L., and Balooch, M. Viscoelastic properties of healthy human artery measured in saline solution by afm-based indentation technique. In W.W. Gerberich, H. Gao, J.E. Sundgren, and S.P. Baker, editors, *Thin Films: Stresses and mechanical properties VI*, volume 436, pp. 353–358. Materials Research Society, Boston, 1997.
- Matthewson, M.J. Axi-symmetric contact on thin compliant coatings. *J. Mech. Phys. Solids*, 29:89–113, 1981.
- May-Newman, K. and Yin, F.C.P. Biaxial mechanical behavior of excised porcine mitral valve leaflets. *Am. J. Physiol.*, 269:H1319–H1327, 1995.



- Merryman, W.D., Huang, H.Y.S., Schoen, F.J., and Sacks, M.S. The effect of cellular contraction on aortic valve leaflet flexural stiffness. *Journal of Biomechanics*, 39:88–96, 2006.
- Meuwissen, M.H.H. *An inverse method for the mechanical characterisation of metals*. Ph.D. thesis, Eindhoven University of Technology, <http://www.mate.tue.nl/mate/pdfs/53.pdf>, 1998.
- Meuwissen, M.H.H., Oomens, C.W.J., Baaijens, F.P.T., Petterson, R., and Janssen, J.D. Determination of elasto-plastic properties of aluminium using a mixed numerical-experimental method. *J. Mat. Proc. Techn.*, 75(1-3):204–211, 1998.
- Mirnajafi, A., Raymer, J., Scott, M.J., and Sacks, M.S. The effects of collagen fiber orientation on the flexural properties of pericardial heterograft biomaterials. *Biomat.*, 26:795–804, 2005.
- Mirnajafi, A., Raymer, J.M., McClure, L.R., and Sacks, M.S. The flexural rigidity of the aortic valve leaflet in the commissural region. *J. Biomech.*, 39:2966–2973, 2006.
- Mol, A., Bouten, C.V.C., Baaijens, F.P.T., Zund, G., Turina, M.I., and Hoerstrup, S.P. Tissue engineering of semilunar heart valves: current status and future developments. *J. Heart. Valve Dis.*, 13:272–280, 2004.
- Mol, A., Bouten, C.V.C., Zund, G., Gunter, C.I., Visjager, J.F., Turina, M.I., Baaijens, F.P.T., and Hoerstrup, S.P. The relevance of large strains in functional tissue engineering of heart valves. *Thor. Card. Surg.*, 51:78–83, 2003.
- Mol, A., Driessen, N.J.B., Rutten, M.C.M., Hoerstrup, S.P., Bouten, C.V.C., and Baaijens, F.P.T. Tissue engineering of human heart valve leaflets: a novel bioreactor for a strain-based conditioning approach. *Annals of Biomedical Engineering*, 33(12):1778–1788, 2005a.
- Mol, A. and Hoerstrup, S.P. Heart valve tissue engineering - where do we stand? *Int. J. Card.*, 95:S57–S58, 2004.
- Mol, A., van Lieshout, M.I., Dam, G.C., Hoerstrup, S.P., Baaijens, F.P.T., and Bouten, C.V.C. Fibrin as a cell carrier in cardiovascular tissue engineering applications. *Annals of Biomedical Engineering*, 26:3113–3121, 2005b.
- Mol, A., Rutten, M.C.M., Driessen, N.J.B., Bouten, C.V.C., Zund, G., Baaijens, F.P.T., and Hoerstrup, S.P. Autologous human tissue-engineered heart valves: Prospects for systemic application. *Circulation*, 114:152–158, 2006.
- Mooney, M. A theory of large elastic deformation. *J. Appl. Phys.*, 11:582–592, 1940.
- Nash-Krahn, K., Bouten, C.V.C., van Tuijl, S., van Zandvoort, M.A.M.J., and Merckx, M. Fluorescently labeled collagen binding proteins allow specific visualization of collagen in tissues and live cell culture. *Anal. Biochem.*, 350:177–185, 2006.

- Neidert, M.R., Lee, E.S., Oegema, T.R., and Tranquillo, R.T. Enhanced fibrin remodeling in vitro with tgf-beta1, insulin and plasmin for improved tissue-equivalents. *Biomaterials*, 23(17):3717–3731, 2002.
- Nielsen, P.M.F., Hunter, P.J., and Smaill, B.H. Biaxial testing of membrane biomaterials: Testing equipment and procedures. *J. Biomech. Eng.*, 113:295–300, 1991.
- Nielsen, P.M.F., Malcolm, D.T.K., Hunter, P.J., and Charette, P.G. Instrumentation and procedures for estimating the constitutive parameters of inhomogeneous elastic membranes. *Biomechan. Model. Mechanobiol.*, 1:211–218, 2002.
- Ohashi, T., Abe, H., Matsumoto, T., and Sato, M. Pipette aspiration technique for the measurement of nonlinear and anisotropic mechanical properties of blood vessel walls under biaxial stretch. *J. Biomech.*, 38:2248–2256, 2005.
- Ohashi, T., Matsumoto, T., Abe, H., and Sato, M. Intramural distribution of local elastic moduli in bovine thoracic aorta measured by pipette aspiration method. *Cell. Eng.*, 2(1):12–18, 1997.
- van Oijen, C.H.G.A. *Mechanics and design of fiber-reinforced vascular prostheses*. Ph.D. thesis, Eindhoven University of Technology, <http://www.mate.tue.nl/mate/pdfs/4006.pdf>, 2003.
- Oomens, C.W.J., Hendriks, M.A.N., van Ratingen, M.R., Janssen, J.D., and Kok, J.J. A numerical - experimental method for a mechanical characterization of biological materials. *J. Biomech.*, 26(4/5):617–621, 1993.
- Oswald, J.D. Acceptance and versatility of the ross procedure. *Curr. Opin. Cardiol.*, 14(2):90–94, 1999.
- Peeters, E.A., Oomens, C.W.J., Bouten, C.V.C., Bader, D.L., and Baaijens, F.P.T. Mechanical and failure properties of single attached cells under compression. *J. Biomech.*, 2005.
- Rabkin, E. and Schoen, F.J. Cardiovascular tissue engineering. *Cardiovasc. Pathol.*, 11:305–317, 2002.
- Ross, D.N. Replacement of aortic and mitral valves with a pulmonary autograft. *Lancet*, 2:956–958, 1967.
- Rubbens, M.P., Mol, A., Boerboom, R.A., Bank, R.A., Baaijens, F.P.T., and Bouten, C.V.C. Intermittent straining accelerates the development of tissue properties in engineered heart valve tissue. *Tissue Engineering Part A*, 2008. Available online, doi:10.1089/ten.tea.2007.0396.
- Sacks, M.S. A method for planar biaxial mechanical testing that includes in-plane shear. *J. Biomech. Eng.*, 121:551–555, 1999.
- Sacks, M.S. Biaxial mechanical evaluation of planar biological materials. *J. Elasticity*, 61:199–244, 2000.

- Sacks, M.S. Incorporation of experimentally-derived fiber orientation into a constitutive model for planar collagenous tissues. *J. Biomech. Eng.*, 125:280–287, 2003.
- Sacks, M.S. and Chuong, C.J. Orthotropic mechanical properties of chemically treated bovine pericardium. *Ann. Biomed. Eng.*, 26:892–902, 1998.
- Sacks, M.S., Smith, D.B., and Hiester, E.D. The aortic valve microstructure: effects of transvalvular pressure. *J. Biomed. Mater. Res.*, 41:131–141, 1998.
- Sacks, M.S. and Sun, W. Multiaxial mechanical behavior of biological materials. *Annu. Rev. Biomed. Eng.*, 5:251–284, 2003.
- Sauren, A.A.H.J. *The mechanical behavior of the aortic valve*. Ph.D. thesis, Technische Hogeschool Eindhoven, <http://alexandria.tue.nl/extra3/proefschrift/PRF3B/8105502.pdf>, 1981.
- Sauren, A.A.H.J., van Hout, M.C., van Steenhoven, A.A., Veldpaus, F.E., and Janssen, J.D. The mechanical properties of porcine aortic valve tissues. *J. Biomech.*, 16(5):327–337, 1983.
- Schnell, A.M., Hoerstrup, S.P., Zund, G., Kolb, S., Sodian, R., Visjager, J.F., Grunenfelder, J., Suter, A., and Turina, M. Optimal cell source for cardiovascular tissue-engineering: venous vs. aortic human myofibroblasts. *Thorac. Cardiovasc. Surg.*, 49(4):221–225, 2001.
- Schoen, F.J. and Levy, R.J. Tissue heart valves: Current challenges and future research perspectives. *J. Biomed. Mater. Res.*, 37(4):439–465, 1999.
- Scott, M. and Vesely, I. Aortic valve microstructure: the role of elastin. *Ann. Thorac. Surg.*, 60:S391–S394, 1995.
- Scott, M. and Vesely, I. Morphology of aortic valve cusp elastin. *J. Heart Valve Dis.*, 5:464–471, 1996.
- Segal, A. *SEPRAN user manual, standard problems and programmer's guide*. Ingenieursbureau SEPRAN, Leidschendam, the Netherlands, 1984.
- Shinoka, T., Breuer, C., Tanel, R.E., Zund, G., Miura, T., Ma, P.X., Langer, R., Vacanti, J.P., and Mayer Jr, J.E. Tissue engineering heart valves: Valve leaflet replacement study in a lamb model. *Ann. Thorac. Surg.*, 60:S513–S516, 1995.
- Shull, K.R. Contact mechanics and the adhesion of soft solids. *Mat. Sci. Eng. R*, 36:1–45, 2002.
- Simon, P., Kasimir, M.T., Seebacher, G., Weigel, G., Ullrich, R., Salzer-Muhar, U., Rieder, E., and Wolner, E. Early failure of the tissue engineered porcine heart valve synergraft<sup>tm</sup> in pediatric patients. *Eu. J. Card. Vasc. Surg.*, 23:1002–1006, 2003.
- Sodian, R., Hoerstrup, S.P., Sperling, J.S., Daebritz, S.H., Martin, D.P., Schoen, F.J., Vacanti, J.P., and Mayer Jr, J.E. Tissue engineering of heart valves: In vitro experiences. *Ann. Thorac. Surg.*, 70:140–144, 2000.

- Stamm, C. and Steinhoff, G. When less is more: go slowly when repopulating a decellularized valve *in vivo!* *J. Thorac. Cardiovasc. Surg.*, 132:735–737, 2006.
- Stekelenburg, A., Strijkers, G.J., Parusel, H., Bader, D.L., Nicolay, K., and Oomens, C.W.J. Role of ischemia and deformation in the onset of compression-induced deep tissue injury: MRI-based studies in a rat model. *J. Appl. Physiol.*, 102:2002–2011, 2007.
- Stradins, P., Lacis, R., Ozolanta, I., Purina, B., Ose, V., Feldmane, L., and Kasyanov, V. Comparison of biomechanical and structural properties between human aortic and pulmonary valve. *Eur. J. Card. Thorac. Surg.*, 26:634–639, 2004.
- Sutton, M., Wolters, W., Peters, III, W., Ranson, W., and McNeill, S. Determination of displacements using an improved digital correlation method. *Im. Vis. Comp.*, 1:133–139, 1983.
- Takkenberg, J.J.M., Klieverik, L.M.A., Schoof, P.H., van Suylen, R., van Herwerden, L.A., Zondervan, P.E., Roos-Hesselink, J.W., Eijkemans, M.J., Yacoub, M.H., and Bogers, A.J. The ross procedure: a systematic review and meta-analysis. *Circulation*, 119(2):222–228, 2009.
- Thomopoulos, S., Fomovsky, G.M., and Holmes, J.W. The development of structural and mechanical anisotropy in fibroblast populated collagen gels. *J. Biomech. Eng.*, 127(5):742–750, 2005.
- Thubrikar, N. *The aortic valve*. Boca Raton CRC Press, 1990.
- Trowbridge, E.A. Mechanical characteristics of pericardial tissue and their relevance to bio-prosthetic design. *Crit. Rev. Biocomp.*, 5(2):105–172, 1989.
- Vaenkatesan, V., Li, Z.L., and Vellinga, W.P. Adhesion and friction behaviours of polydimethylsiloxane - a fresh perspective on JKR measurements. *Polymer*, 47(25):8317–8325, 2006.
- Vandenburgh, H., Del Tatto, M., Shansky, J., Lemaire, J., Chang, A., Payumo, F., Lee, P., Goodyear, A., and Raven, L. Tissue-engineered skeletal muscle organoids for reversible gene therapy. *Human Gene Therapy*, 7:2195–2200, 1996.
- Vanderwee, K., Clark, M., Dealey, C., Gunningberg, L., and Defloor, T. Pressure ulcer prevalence in Europe: a pilot study. *J. Eval. Clin. Pract.*, 13(2):227–235, 2007.
- Vara, D.S., Salacinski, H.J., Kannan, R.Y., Bordenave, L., Hamilton, G., and Seifalian, A.M. Cardiovascular tissue engineering: state of the art. *Pathol. Biol.*, 53(10):599–612, 2005.
- Vesely, I. and Noseworthy, R. Micromechanics of the fibrosa and the ventricularis in aortic leaflets. *J. Biomech.*, 25(1):101–113, 1992.
- Vito, R.P. The mechanical properties of soft tissues - I: A mechanical system for biaxial testing. *J. Biomech.*, 13:947–950, 1980.

- Yacoub, M.H. and Takkenberg, J.J. Will heart valve tissue engineering change the world? *Nat. Clin. Pract. Cardiovasc. Med.*, 2(2):60–61, 2005.
- Zheng, Y.P. and Mak, A.F. An ultrasound indentation system for biomechanical properties assessment of soft tissues in-vivo. *IEEE Trans. Biomed. Eng.*, 43(9):912–918, 1996.
- Zioupos, P. and Barbenel, J.C. II. a structure based model for the anisotropic material behavior of the tissue. *Biomat.*, 15(5):374–382, 1994.
- Zulliger, M.A., Fridez, P., Hayashi, K., and Stergiopoulos, N. A strain energy function for arteries accounting for wall composition and structure. *J. Biomech.*, 37:989–1000, 2004.

---

## Samenvatting

---

Alleen al in Europa worden jaarlijks 6000 kinderen geboren met een hartklepafwijking, waardoor een hartklepvervanging noodzakelijk is. Aangezien de in de kliniek beschikbare hartkleppen bestaan uit niet-levend materiaal, kunnen deze niet meegroeien met de patiënt. Hierdoor zijn over de levensduur van de patiënt verschillende heroperaties nodig om de hartklep te vervangen door een groter exemplaar.

Tissue engineering is een veelbelovend alternatief voor de bestaande strategieën voor hartklepvervanging. Hartklep tissue engineering richt zich op de productie van een levende hartklep, gemaakt met cellen van de patiënt. Hierdoor is de klep wèl in staat om te groeien, herstellen en remodelleren met de groeiende behoefte van de patiënt. Kort samengevat worden de cellen van de patiënt *in vitro* op een biologisch afbreekbare mal gezaaid, die de vorm heeft van een hartklep. Het aldus verkregen construct wordt in een bioreactor geplaatst, waar mechanische en biochemische conditioneringsprotocollen worden gebruikt om de ontwikkeling van hartklepweefsel te stimuleren. Na enkele weken in de bioreactor is de oorspronkelijke biologisch afbreekbare mal vervangen door weefsel dat is geproduceerd door de eigen cellen van de patiënt. De tissue engineered hartklep is dan klaar voor implantatie in de patiënt.

Eén van de belangrijkste uitdagingen bij het tissue engineeren van hartkleppen is om een klep te maken die sterk genoeg is om de hoge drukken te weerstaan die in het menselijk lichaam op-treden. De mechanische sterkte van een natuurlijke hartklep wordt grotendeels bepaald door een sterk georganiseerd netwerk van collageenvezels. Onderzoekers aan de Technische Universiteit Eindhoven hebben met computermodellen aangetoond dat de natuurlijk collageen architectuur is te voorspellen als gevolg van de lokale spanningen in de hartklep tijdens de diastole fase van de hartcyclus (als de klep gesloten is). Op basis van deze resultaten is een Diastolic Pulse Duplicator ontwikkeld waarmee de diastole drukken *in vitro* kunnen worden nagebootst in een bioreactor voor het kweken van hartkleppen. Het bleek vervolgens inderdaad mogelijk om sterke hartkleppen te kweken met de DPD. Bij *in vitro* tests bleken deze kleppen zelfs in

staat om de hoge drukken te weerstaan die relevant zijn voor het *in vivo* functioneren van de klep. Hoewel dit een belangrijke stap is in de goede richting, is het nog niet duidelijk of, en zo ja in welke mate, deze tissue engineered hartkleppen zich ontwikkelen richting de collageen architectuur in natuurlijke kleppen.

Het doel in dit proefschrift is om het antwoord te vinden op deze vraag door de lokale vezelarchitectuur te meten in natuurlijke en tissue engineered hartkleppen. Aangezien de bestaande methodes voor mechanische karakterisatie niet voldoen voor het meten van de volledige lokale mechanische eigenschappen, is hiervoor een nieuwe methode ontwikkeld en gevalideerd. In deze innovatieve benadering wordt lokale indentatie toegepast terwijl weefseldeformatie wordt gemeten met een confocaal microscoop. Hierna wordt een computersimulatie vergeleken met de experimentele resultaten door middel van parameterschatting. Op deze manier worden zowel de lokale vezelarchitectuur als het lokale mechanische gedrag van het weefsel gemeten.

Na toepassing van deze methode op natuurlijke en tissue engineered hartkleppen is gebleken dat de tissue engineered hartkleppen zich inderdaad ontwikkelen richting de natuurlijke vezelarchitectuur, hoewel organisatie en oriëntatie meer uitgesproken zijn in het natuurlijke weefsel. Het belangrijkste verschil tussen natuurlijke kleppen en de huidige tissue engineered kleppen is dat de laatstgenoemden veel stijver lijken in het *in vivo* rekgebied. Gebaseerd op experimentele observaties beschreven in dit proefschrift is het mijn hypothese dat dit verschil wordt veroorzaakt door een verschil in de spanningsloze configuratie van de individuele collageenvezels.

Hoewel de nieuwe methode specifiek is ontworpen voor de mechanische karakterisatie van hartkleppen, moet worden benadrukt dat de methode algemeen toepasbaar is voor de lokale mechanische karakterisatie van vlakke, zachte biologische weefsels.

---

## Dankwoord

---

Terugkijkend op ruim 4 jaar promotieonderzoek schiet er van alles door je heen: kameretentjes, pizzameetings, koffiepauzes, ze droegen allemaal bij aan de gezellige atmosfeer op vloer 4. Het eerste artikel dat met succes door de review-molen kwam, want er werd natuurlijk ook hard gewerkt. Congressen en cursussen op allerlei interessante locaties, al ben ik vreemd genoeg nog nooit in Lunteren geweest. De verschillende tripjes naar Zwitserland zijn een schoolvoorbeeld van hoe je het nuttige met het aangename kunt verenigen. Heel wat uren heb ik doorgebracht in het lab, zij het niet met afwassen dan wel met turen door de microscoop, gevolgd door uitgebreide sessies achter de Aramis. En na nog een paar weken Matlab en Sepran was het resultaat dan daar. Gelukkig was er in de tussentijd genoeg te doen. Niet te vergeten de vele activiteiten en borrels van Hora Est, waar dat ene pilsje er vaak toch een paar meer werden. Het lustrumgala was zeker één van de hoogtepunten. Al met al heb ik de afgelopen jaren veel geleerd, veel gezien en vooral veel gelachen, en daar wil ik graag een paar mensen voor bedanken.

Frank, de basis voor mijn onderzoek was jouw idee en je goed geplaatste opmerkingen hebben me gedurende de rit regelmatig aan het denken gezet. Carlijn, door allerlei omstandigheden ben je minder intensief bij mijn onderzoek betrokken geweest dan je waarschijnlijk had gewild. Desondanks ben je altijd goed op de hoogte gebleven en je waardering voor mijn werk heeft me zeker gemotiveerd. Niels, ik heb erg veel van je geleerd, maar we hebben samen ook veel gezien en nog veel meer gelachen. Onze uitgebreide discussies zijn me zeker bijgebleven, zowel de wetenschappelijke als de minder wetenschappelijke. Ook na je carrière-switch ben je altijd betrokken gebleven. Het is een prettig gevoel dat de sterke arm der wet zijn goedkeuring over mijn werk heeft uitgesproken.

Anthal, Bart, Marijke en Ana, bedankt voor jullie bijdrage aan mijn onderzoek, hopelijk hebben jullie ook iets van mij opgestoken. Vidya, Nederlands zal inmiddels geen probleem meer zijn, ik heb prettig met je samengewerkt tijdens het begin van mijn promotie. Verder wil ik Jeroen, Debby, Ralf, Debbie, Mirjam en Imo bedanken. Zonder jullie samples had ik heel wat minder



hoofdstukken gehad. Jeroen, vooral dankzij jouw vrijgevigheid tijdens het kleppen snijden heb ik veel van mijn belangrijkste metingen kunnen doen.

Vele kamergenoten hebben bijgedragen aan de gezellige sfeer in kamer 4.11, vooral met Karlien, Rolf, Lisette, Mirjam en Juliënne heb ik veel tijd doorgebracht. Onze kameretentjes zijn natuurlijk legendarisch, en het wordt hoog tijd voor het volgende! Sinds kort heb ik 4.11 veruuld voor de QTIS/e kamer. Hoewel het lastig wordt om de kameretentjes van 4.11 te evenaren, was ons eerste bedrijfsuitje al zeer geslaagd. Ik ga er van uit dat er vele zullen volgen.

Niels, Ralf en Jeroen, vooral het avondprogramma van de congressen was altijd zeer geslaagd; de München-reünie moeten we er zeker in houden. Roel, Ewout, Rolf, Kristel, Rudi, Famke en Arjen, het organiseren van de Hora Est activiteiten was bijna net zo leuk als de activiteiten zelf. Vooral de beleidsvergadering na de cocktailborrel staat mij nog helder voor de geest. Het is eigenlijk wel weer eens tijd voor Mundial. Uiteraard zijn er nog veel meer collega's die hebben bijgedragen aan de gezellige werksfeer de afgelopen jaren, ook jullie bedankt!

Sander, dankjewel dat ik me al 4 jaar lang verzekerd weet van tenminste één paranimf, dat scheelt toch al weer de helft. Lieke, iedereen weet natuurlijk dat ik jouw grote voorbeeld ben, maar jouw kritische kijk op de zaken heeft mij ook scherper leren formuleren. Ik vertrouw erop dat jij het 2 juni indien nodig probleemloos van me overneemt.

Hoewel de meesten van de club waarschijnlijk geen flauw idee hebben waar ik mee bezig ben, kan CV de Zuipschuiten in dit lijstje niet ontbreken. Uitgerekend in ons jubileumjaar had ik erg weinig tijd, bedankt dat jullie geen artikel 4 procedure tegen me zijn gestart. Hopelijk ben ik er volgend jaar weer wat vaker bij. Huub en Mien, jullie belangstelling heb ik altijd erg leuk gevonden. Pap en mam, jullie steun beperkt zich natuurlijk niet tot het smeren van mijn boterhammen, en jullie nuchtere kijk op de dingen houdt me met beide benen op de grond. Pap, erg leuk dat je mijn proefschrift al hebt gelezen voordat de Nederlandse samenvatting af was. En last but not least, Anouk, we zijn in een voor mij erg drukke periode gaan samenwonen, en dat heb je prima opgevangen! Misschien wordt het nu toch eens tijd dat je me uitlegt hoe de wasmachine werkt...

Allemaal bedankt!

Martijn, 8 april 2009

---

## Curriculum vitae

---

Martijn Cox is geboren op 18 januari 1982 in Budel-Dorplein. In 1999 behaalde hij zijn VWO diploma aan het Bisschoppelijk College in Weert. Aansluitend is hij Biomedische Technologie gaan studeren aan de Technische Universiteit Eindhoven. Als onderdeel van deze studie liep hij stage in de onderzoeksgroep van prof. Raymond Vito aan het Georgia Institute of Technology in Atlanta, waar hij onderzoek deed aan atherosclerose. Zijn afstudeerwerk was onderdeel van het decubitus-onderzoek van dr.ir. Cees Oomens en richtte zich op de relatie tussen spierschade en locale vervormingen tijdens langdurig belasten. In 2004 besloot hij tot een promotieonderzoek binnen het Tissue Engineering onderzoek aan de faculteit Biomedische Technologie van de Technische Universiteit Eindhoven, resulterend in dit proefschrift. Sinds september 2007 combineert hij zijn onderzoek met het management van QTIS/e, een spin-off bedrijf van de Technische Universiteit Eindhoven dat zich richt op de commercialisatie van het tissue engineering onderzoek.